ARL-RR-9

AR-008-367

AD-A274 870

②

DEPARTMENT OF DEFENCE

DEFENCE SCIENCE AND TECHNOLOGY ORGANISATION

AERONAUTICAL RESEARCH LABORATORY

MELBOURNE, VICTORIA

Research Report 9

LOW-SPEED PRESSURE DISTRIBUTION MEASUREMENTS
OVER THE AFT-FUSELAGE, FINS AND STABILATORS OF A 1/9th SCALE
F/A-18 WIND-TUNNEL MODEL

by

L.D. MacLAREN
H.A. QUICK

94-02039

Approved for public release.

OCTOBER 1993

94 1 24 011

DISCLAIMER NOTICE

THIS DOCUMENT IS BEST QUALITY AVAILABLE. THE COPY FURNISHED TO DTIC CONTAINED A SIGNIFICANT NUMBER OF COLOR PAGES WHICH DO NOT REPRODUCE LEGIBLY ON BLACK AND WHITE MICROFICHE.

DEPARTMENT OF DEFENCE
DEFENCE SCIENCE AND TECHNOLOGY ORGANISATION
AERONAUTICAL RESEARCH LABORATORY

Research Report 9

LOW-SPEED PRESSURE DISTRIBUTION MEASUREMENTS OVER THE AFT-FUSELAGE, FINS AND STABILATORS OF A 1/9th SCALE F/A-18 WIND-TUNNEL MODEL

by

L.D. MacLAREN

H.A. QUICK

SUMMARY

The steady-state aerodynamic pressure distribution over the aft fuselage, fin and stabilator of a 1/9th scale F/A-18 model has been measured for varying conditions at low speeds. Pressure distributions are presented in the form of a parametric study and the integration of the pressures to obtain total loads is included to indicate the overall effects of angle of attack, sideslip, stabilator deflection and the LEX fence. The results from these wind tunnel tests have illustrated the degree to which vortical flow dominates the conditions over the aft end of the aircraft, due to the presence of the primary LEX vortex and to local separations from sharp edged surfaces.

DSTO
A U S T R A L I A

Accesion For	
NTIS CRA&I	
DTIC TAB	
Unannounced	
Justification	
By	
Distribution /	
Availability Codes	
Dist	Avail and / or Special
A-1	

Contents

List of Tables

List of Figures

Notation

$\bar{c}$	Wing mean aerodynamic chord (m)
C_{BM}	Bending moment coefficient
C_L	Lift force coefficient normal to chord plane of surface
C_M	Pitching moment coefficient
C_p	Pressure coefficient
Hx	Spanwise station on full scale stabilator (inches)
S	Wing area (m²)
V	Airspeed (m/s)
X	Longitudinal aircraft axis
Y	Lateral aircraft axis
Z	Vertical aircraft axis
Zv	Spanwise station on full scale fin (inches)
α	Angle of attack (degrees)
β	Angle of sideslip (degrees)
δ	Stabilator deflection (degrees)
LEX	Leading edge extension
LEF	Leading edge flap
TEF	Trailing edge flap

Angular Sign Conventions

α is positive when the freestream velocity vector is below the nose

β is positive when the freestream velocity vector is right of the nose

δ is positive when the stabilator leading edge is deflected up

Reference Area and Length

Reference area   = 37.16 m²   (Full scale theoretical wing area)

Reference length   = 3.51 m   (Full scale wing mean aerodynamic chord)

Note: Aircraft stations defined by the manufacturer in inches are not
converted to SI units.

1 Introduction

The high angle of attack capability of the McDonnell-Douglas F/A-18 aircraft is achieved through the generation of large vorticies from the Leading Edge Extensions (LEX). At high angles of attack, the vortical nature of this flow breaks down or 'bursts' and becomes highly turbulent. This phenomenon results in significant problems within the aircraft structure and a subsequent reduction in the manufacturers predicted fatigue life of the airframe.

Due in part to the multi-role capability of the aircraft, Australian and Canadian operational useage of the F/A-18 differs from that of the U.S. Navy, with Australian and Canadian aircraft recording a proportionately higher number of operational hours at high angles of attack. This has resulted in the need to redetermine the fatigue life of the aircraft under more representative conditions than the manufacturers original fatigue tests.

The Royal Australian Air Force (RAAF), through the Airframes and Engines Division (AED) of the Defence Science and Technology Organisation (DSTO), is collaborating with the Canadian Forces through the Institute for Aeronautical Research (IAR) and the Canadian Aeronautical Industry to conduct a fatigue test on the F/A-18 aircraft. This collaboration, which is aimed at re-evaluating the aircraft's structural fatigue life, based on measured operational loading conditions, is designated the International Follow-On Structural Test Project (IFOSTP). Canada is responsible for the testing of the wing and centre fuselage of the aircraft while AED will test the rear fuselage, fins and stabilators.

The total loads which will be applied to the structure during the fatigue test are those corresponding to the parameters recorded by the onboard Maintenance Status Display and Recording System (MSDRS) during normal operational conditions.

Because little information was available on the F/A-18 aerodynamic loading distributions from the original equipment manufacturer, Air Operations Division (AOD) of DSTO agreed to supply these data for the aft end of the aircraft using the existing aerodynamic facilities at the Aeronautical Research Laboratory (ARL).

2 Aim

The objective of the wind-tunnel tests was to obtain a data-base of steady-state aerodynamic pressure distributions that could be used during the F/A-18 fatigue test to represent manoeuvre loading on the aircraft in normal operational conditions both with and without the 'fence' attached to the LEX. It is intended to superimpose buffet loads onto the steady-state aerodynamics at a later stage.

Because the F/A-18 aircraft is capable of flying at high Mach numbers and at high angles of attack, AOD was required to use both the Transonic Wind Tunnel (TWT) and the Low Speed Wind Tunnel (LSWT) facilities as well as computational techniques where appropriate to obtain the best possible coverage of the flight envelope. The TWT would have solely been used to obtain this data base but the use of a 1/24th scale half-model restricted the tests to the zero sideslip condition (Reference [1]). For this reason the LSWT and a 1/9th scale complete model was employed to determine the effects of sideslip. The results presented in this report are those from the LSWT tests.

1

3 Test Facility

The facility used for these pressure measurement tests was the ARL LSWT. This is a closed return circuit wind tunnel with a total installed drive power of 660 kW. An eight bladed fan of diameter 3.96 m allows speeds of up to 100 m/s to be reached in the working section which is an irregular octagon in shape, measuring 2.743 m × 2.134 m. The model was mounted via a sting to a pitch/roll rig for the setting of model attitudes.

4 Models

Prior to the requirement for steady aerodynamic loads data for the F/A-18 aircraft, a substantial amount of research had already been completed at ARL on the problem of fin buffet at high angle of attack. This work (Reference [2]) was done using a 1/9th scale model made from aluminium and carbon fibre. The major dimensions of this model are shown in Figure 1. Because this model was originally used for testing in the high angle of attack regime (greater than 25°), a wing was made with a fixed leading edge flap (LEF) setting of 34° which corresponds to the condition set by the aircraft flight control system. Since this wing would only be of use at angles of attack greater than or equal to 25°, a task was initiated to build a wing with variable flap settings that could be remotely actuated from the LSWT control room. While the fully actuated wing was under development a second wing was constructed with a fixed LEF setting of 0°. This wing would give valid information at angles of attack less than or equal to 0° and could also be used to investigate the trends of load behaviour at low positive angles of attack even though the flap settings would not be entirely correct. The mid range angles of attack were not investigated during this first stage. For ease of discussion, the series of tests involving the fixed LEF wings (both 0° and 34°) will be denoted as Test A.

Manual adjustment of the stabilators was possible although this was limited to a finite selection of discrete setting angles due to the mechanical design of the model. The carbon fibre construction allowed easy drilling of pressure tappings in the model surface. Seventy five ports were distributed over the the rear starboard fuselage as shown in Figure 2. The upper side of the port stabilator and the lower side of the starboard stabilator were each tapped with 60 pressure ports although a maximum of only 22 ports per stabilator could be utilised due to the physical limitations of the stabilator hinge design. The distribution of the ports on the stabilator is shown in Figure 3. All of these pressures were measured simultaneously using a Pressure Systems International[1] (PSI) electronic pressure scanning system with the model in the LEX-fence-off configuration and the stabilators in both the symmetric and asymmetric arrangement. The measurements from the upper surface of the port stabilator for a given α, δ and β were mirrored to the starboard stabilator for the same α and δ with a β of the opposite sign. The starboard fin was tapped with 60 ports on each side as in Figure 4.

A second series of LSWT tests was made with the actuated wing and new stabilators which will be denoted as Test B. This model featured the following characteristics.

- Actuated stabilators. These can be operated asymmetrically although for this test, the stabilators were kept in a symmetric configuration. The justification for this came from

---

[1]Pressure Systems International, 34 Research Drive, Hampton, Va. 23666, U.S.A.

2

the results obtained in Test A. The number of ports on the tail surfaces was increased to provide more points for the pressure distributions.

- Actuated leading edge flap. The port and starboard leading edge flaps must operate symmetrically.

- Actuated trailing edge flaps. Each flap may be operated independently of the other.

- Actuated ailerons. These can be adjusted to a given angle in general but for this series of tests, they were mechanically locked into place at a deflection of 0°.

- All control surfaces mentioned above can be controlled remotely via a micro-VAX computer (Reference [3]).

The model is pictured in Figure 1 and is described in detail in Reference [4]. Sixty static pressure ports were distributed over the fuselage in a pattern that closely resembled the distribution used on the model in Test A (Figure 5). The stabilator, being an important contributor to the total load, was re-tested for all angles of attack using the appropriate flap settings and with a larger number of pressure ports. The density of ports was increased to that shown in Figure 6. The fin port distribution was not altered from that used in Test A.

A preliminary investigation showed that the effect of an individual stabilator deflection on the opposite stabilator was negligible, therefore making extensive asymmetric stabilator tests unnecessary. Although there is a small but noticeable effect on the fuselage pressure distribution, these fuselage effects are of secondary importance relative to the fin and stabilator distributions. Tests were carried out with and without the LEX fence which was easily attached and removed.

In general, the results from Test A were regarded as preliminary only and were used as a guide for planning Test B both in terms of the test programme and the distribution of ports on the model. Although the results from Test A are referred to in this report, only the results from Test B are presented in detail.

5 Test Programme

5.1 Test A: Fixed Flap Wings

The limited number of scanners available at the time required the Test A programme to be completed in two phases. The first phase was conducted with the fuselage and stabilator pressure ports connected as in Figures 2 and 3 and the second phase was conducted with only the fin ports connected as shown in Figure 4. It was only necessary to investigate the effect of the LEX fence on the fin pressure distributions as this was where the major effect was expected to occur. Also as noted in Section 3, to reduce the length of the test programme, it was decided, based on the Phase I results, to use only symmetric stabilator settings during the Phase II tests. The tunnel airspeed was kept nominally at 50 m/s which equates to a Reynolds number of 1.34×10^6 based on the wing mean aerodynamic chord. The Test A programme is presented in Table 1.

Table 1: LSWT Test Programme for 1/9th-Scale F/A-18 with Fixed Flaps

α	Flaps		β	δ	Phase I	Phase II
(deg)	LEF	TEF	(deg)	(deg)	Stabs/Fuse	Starboard Fin
0	0.0	0.0	sweep	sweep	Asym. Stabs LEX fence off	Sym. Stabs LEX fence off/on
5	0.0	0.0	sweep	sweep	Asym. Stabs LEX fence off	Sym. Stabs LEX fence off/on
10	0.0	0.0	sweep	sweep	Asym. Stabs LEX fence off	Sym. Stabs LEX fence off/on
25	34.0	0.0	sweep	sweep	Asym. Stabs LEX fence off	Sym. Stabs LEX fence off/on
30	34.0	0.0	sweep	sweep	Asym. Stabs LEX fence off	Sym. Stabs LEX fence off/on
35	34.0	0.0	sweep	sweep	Asym. Stabs LEX fence off	Sym. Stabs LEX fence off/on

Note: β sweep is -10, -5, 0, +5, +10 degrees
δ sweep is -23, -11, +1, +9 degrees.

5.2   Test B: Actuated Control Surfaces

The aim of this test programme was to obtain a complete set of aerodynamic load distributions using the wing with actuated control surfaces which included the repetition of many Test A points. This provided a useful check on the results.

The availability of the adjustable surface wing meant that the complex system of flap movement on the aircraft could be more realistically simulated. The scheduling of flap positions on the F/A-18 aircraft is controlled by the onboard computer and is primarily a function of angle of attack and Mach number. The flap deflections are also limited by dynamic pressure to prevent structural overload, and when deflected asymmetrically, the flaps assist the ailerons in achieving high aircraft roll rates. The details of the flap schedule are given in Reference [5].

For these tests, steady manoeuvre loads only were considered. The effects of roll-rate are to be estimated later and used as an incremental change to the steady-state wind tunnel results. The effect of compressibility will be applied to the Test B data using an appropriate scaling technique up to a Mach number no greater than 0.8. For this reason, it was necessary to test the aircraft with the flaps positioned for each particular combination of angle of attack and Mach number where the LSWT results might be considered representative of F/A-18 operational usage.

The density of pressure ports on the stabilators and fuselage was increased for Test B as two more PSI scanners became available. Figures 5 and 6 illustrate the distribution of the ports for this test. The fin was instrumented in the same manner as in Test A (see Figure 4). Again the test programme was completed in two phases. Phase I was conducted with the stabilator pressure ports connected. This was primarily completed with the LEX fence in place although some check points were measured with the LEX fence removed to determine the influence of the fence on the stabilator pressure distribution. Phase II involved the measurement of pressures

4

on the surface of the starboard fin and the aft fuselage. This phase was conducted both with the LEX fence on and off. Symmetric stabilators were used throughout Test B as the effect of asymmetric settings from Test A results was found to be minimal. This greatly reduced the length of the test programme. As in Test A, the tunnel airspeed was kept nominally at 50 m/s corresponding to a Reynolds number of 1.34×10^6. The Test B programme is presented in Table 2.

Table 2: LSWT Test Programme for 1/9th-Scale F/A-18 with Actuated Control Surfaces

α (deg)	Effective Mach no.	LEF (deg)	TEF (deg)	δ (deg)	β (deg)	Phase I Stabilators	Phase II Fin/Fuselage
-10	0.0 - 0.8	0.0	0.0	sweep	sweep	LEX fence on	LEX fence on/off
-5	0.0 - 0.8	0.0	0.0	sweep	sweep	LEX fence on	LEX fence on/off
0	0.0 - 0.8	0.0	0.0	sweep	sweep	LEX fence on	LEX fence on/off
5	0.0 - 0.7	6.6	7.0	sweep	sweep	LEX fence on	LEX fence on/off
	0.8	5.1	7.0	sweep	sweep		
10	0.0 - 0.7	13.3	14.0	sweep	sweep	LEX fence on	LEX fence on/off
	0.8	11.8	12.2	sweep	sweep		
15	0.0 - 0.6	19.9	14.8	sweep	sweep	LEX fence on	LEX fence on/off
	0.7	19.9	12.6	sweep	sweep		
	0.8	18.4	9.8	sweep	sweep		
20	0.0 - 0.6	26.6	7.8	sweep	sweep	LEX fence on	LEX fence on/off
	0.7	26.6	5.6	sweep	sweep		
	0.8	25.0	2.8	sweep	sweep		
25	0.0 - 0.6	33.2	0.8	sweep	sweep	LEX fence on	LEX fence on/off
	0.7	33.2	0.0	sweep	sweep		
	0.8	31.7	0.0	sweep	sweep		
30	0.0 - 0.8	34.0	0.0	sweep	sweep	LEX fence on	LEX fence on/off
35	0.0 - 0.8	34.0	0.0	sweep	sweep	LEX fence on	LEX fence on/off

Note: δ sweep is -20, -10, -5, 0, +5 degrees (symmetrical stabilators only).
β sweep is -10, -5, 0, +5, +10 degrees
The ailerons were mechanically set at the neutral angle of 0°.

6 Data Reduction

The pressure information was gathered using a PSI 8400 electronic pressure measurement and data acquisition system. Four PSI scanners with range of ±34.5 kPa were used with each scanner capable of measuring 32 differential pressures. A further two scanners with a range of ±6.9 kPa became available during Test B. The software that controls the system was rewritten at ARL in the 'C' programming language. A detailed description of features of the system is given in Reference [6].

The software controlling the data acquisition allows the user to specify the sampling parameters. The time between each data frame, consisting of many measurement points, was set to

5

the maximum possible of 65000 μs. This defined a sampling frequency of 15.4 Hz that was sufficiently below the fundamental frequency within the vortex core (of the order of 100 Hz for this model and nominal tunnel speed as in Reference [2]) to avoid buffeting effects. The scanners are capable of sampling at frequencies of up to 20 kHz and each was calibrated over the range of pressures expected to be found during the tests (i.e. ±6.9 kPa).

A specified number of frames is sampled after which a mean pressure is calculated and recorded. The number of frames was set to the maximum value of 127. The procedure was repeated 5 times with a 5 sec delay between each sampling period.

This produced a data file at each test point, containing five mean differential pressure measurements for every port. The consistency of the mean pressures over the 5 sampling periods was examined for each test point to determine its acceptability. The mean of the five recorded pressures was then used in the further computation of pressure coefficients and load distributions.

6.1 Data Accuracy

Each of the scanners had the wind-tunnel total and static pressures connected to the first two ports respectively and every port was referenced to the tunnel static pressure. This results in tunnel dynamic pressure on port 1 and zero pressure on port 2. The measurements from each of these ports on all scanners were closely monitored and used to indicate when a recalibration of the scanners was necessary and to ensure that the peak pressure oscillations did not go outside the range of the transducers. Between calibrations, small drifts in the pressure measurements sometimes occurred due to temperature effects but these were minimised by frequent re-calibration.

As part of the data gathering routine used during Test B, a specified test point was repeated many times at regular intervals to provide a means to check on the repeatability of the test technique. This method takes into account errors induced by the pitch/roll mechanism and the setting of control surfaces as well as the pressure measuring equipment. Post test analysis of the data indicated that a mean pressure coefficient could be calculated for each port with a standard deviation of 0.02. A further test was made to check on the quality of data from the PSI system in isolation. For this test, a single test point was chosen again but this time, many mean pressure data points were taken without adjusting the model configuration at all. Analysis of these points indicated that the standard deviation of the pressure coefficients was less than 0.02.

6.2 Interpolation

In order to maximise the surface area of the aircraft covered by pressure information, an interpolation/extrapolation technique was implemented. This transformed the data from a set of pressure coefficients at discrete points on the aircraft to pressure information at panel centroids of a three dimensional Computational Fluid Dynamics (CFD) grid describing the geometry of the F/A-18. The computer program 'f18int9', which performs the calculations, is written in FORTRAN. This method enabled direct comparison with results from the CFD code VSAERO[2] and allowed for simple integration of pressure data to obtain total loads on the structure.

---

[2]Analytical Methods, Inc. 2133 - 152nd Avenue N.E., Redmond, Washington 98052, U.S.A.

The calculation procedure, shown schematically in Figure 7, was as follows:

1. Compute pressure coefficient at each of the discrete pressure port locations.

2. Estimate the pressure coefficient at intermediate or "missing" ports in the irregular grid of port locations using the software routine BIVAR (Reference [7]) to complete a rectangular grid of pressure coefficient data.

3. Fit a surface to the rectangular grid using the surface interpolation routine SURF1 (Reference [8]) and interpolate/extrapolate the pressure information to the centroids of the appropriate VSAERO panels.

4. Integrate over surface to obtain total loads.

The interpolation of the data on the fins and stabilators was carried out by converting the spatial coordinates locating the pressure ports to percentage chords and spanwise lengths, thus forming a rectangular grid. Each particular VSAERO panel centroid was converted in the same manner and a pressure coefficient calculated for that location. The pressure distributions were constrained to zero at the fin and stabilator tips and the root pressure distribution was taken as a duplication of the nearest outboard row of chordwise pressure ports.

The fuselage was slightly more complex. Due to the presence of the fins and the stabilators, and the consequent 'step change' in the pressure across them, it was felt that an interpolation using the aft fuselage as a whole was unjustified. The fuselage was therefore considered in separate patches. Information from positive and negative sideslip cases was combined to complete an interpolation grid that extended over both sides of the aircraft. Pressure ports along the aircraft centreline were assigned an average value of the results from the two sideslip cases (theoretically these should be identical on a symmetrical model). The distribution of ports allowed for an interpolation grid on the top of the fuselage in between the fins and extending slightly aft, another on the underside of the fuselage forward of the stabilator leading edge and a third patch that extended from the underside of the port stabilator to the underside of the starboard stabilator. The definition of the grid for this third patch required the conversion of the 3-dimensional cartesian coordinates of the pressure ports to a system of cylindrical coordinates.

6.3 Integration of Surface Pressures

After the interpolation of the wind tunnel data to the VSAERO grid, the results were integrated to produce total load coefficients for fins and stabilators. This technique significantly reduces the amount of information, provides a means by which to check the data for corrupt points and enables comparisons with results obtained from external sources. The load coefficients, C_L, C_M and C_{BM}, are all based on wing area and wing mean aerodynamic chord where applicable. For the stabilator, the moment coefficients are defined about the hinge point. The torsion moment axis is about the spindle and the bending moment axis is the root chord line. The fin moments are defined about the quarter chord point of the fin root. The bending moment axis is the root chord line and the torsion moment axis is perpendicular to this and is at a cant angle of 20° through the span of the fin. The sign convention used is given in Figure 8.

7

7 Results

The final results are a set of ASCII data files with each file representing a particular aircraft configuration and test condition (see Appendix A). The files contain two columns of data, these being a VSAERO panel number and the corresponding calculated pressure coefficient. A file containing the geometry of the VSAERO grid is required to make use of the pressure information. This arrangement allows the data to be presented graphically on a Silicon Graphics Workstation. An example of the graphical output is given in Figure 9 which also indicates the coverage of the aft fuselage and empennage achieved using this technique.

7.1 Pressure Distributions

Because of the large amount of data obtained during these tests, it is impractical to present pressure distributions for every case. For the purpose of this report, the necessary features of the data can be illustrated in the form of a parametric study. Pressure distributions for the starboard side of the aircraft over both sides of the fin, stabilator and also the top and bottom of the aft fuselage are presented for a given configuration defined by angle of attack, sideslip angle, stabilator angle and LEX fence condition. The effect of varying each of these parameters is described in the following sections. It should be noted that the data presented here are for the starboard side of the aircraft and for the flaps set according to the schedule for Mach numbers less than or equal to 0.6.

7.1.1 Effect of Angle of Attack

To illustrate the effect of angle of attack, the angle of sideslip and stabilator deflection were set to zero and the LEX fence was on. Figures 10a - 10j contain the pressure distributions for angles of attack from $-10°$ to $35°$ respectively in $5°$ increments.

For the F/A-18 aircraft, increasing aircraft angle of attack results in the formation of the LEX primary vortex. The effect of this vortex is most noticeable on the fin pressure distribution. Flow visualisation studies of this phenomenon were made in the ARL water tunnel and are fully documented in Reference [9]. The effect is seen in the fin pressure distributions, particularly at angles of attack greater than $10°$. By examining the difference between the inboard and outboard pressures, the helical nature of the LEX vortex is confirmed by evidence of a change in local angle of attack along the fin from root to tip. This means that some flight conditions experience very high loading near the fin tip and consequently high root bending moments.

The pressure distributions over the stabilator show little change up to an angle of attack of around $10°$. The changes above $10°$, unlike the fins, are not due to the LEX vortex, but to the separation of the flow from the stabilator leading edge. Surface flow visualisation evidence of this leading edge separation is available in Reference [10]. Because the stabilator has a high leading edge sweep angle of $47.16°$, the pressure distribution at high angles of attack resembles that seen on delta wing configurations.

As expected, the main effect of increasing angle of attack on the fuselage is to increase the pressure on the lower side and decrease the pressure on the top.

7.1.2 Effect of Sideslip

As indicated previously, the flowfield over the aircraft differs dramatically between low and high angles of attack. For this reason, the effect of sideslip will be presented in both angle of attack regions. The stabilator deflection is set to zero for all of these cases and the LEX fence is on.

At 0° angle of attack (Figures 11a - 11e), the major effect of sideslip occurs on the fins. As mentioned in the previous section with regard to the stabilator, a leading edge separation is apparent on the leeward side of the fin which begins at a sideslip of around 5° and is fully developed into a vortex by 10°. Again, visual evidence of this is given in Reference [10].

The pressure distributions on the stabilators at low angle of attack are like those expected for attached flow.

For low angle of attack, there seems to be a reasonable degree of similarity between the distributions on a given side of the fin or stabilator in positive sideslip, to those on the opposite side in negative sideslip.

Sideslip effects on the fuselage seem to be limited to the row of ports on the upper side that are located closest to the root of the fin.

At 25° angle of attack (Figures 12a - 12e), the sideslip effects on the fin are primarily due to the lateral movement of the LEX vortex trajectory and also the change in vortex burst position. Flow visualisation studies show that at −10° sideslip, the starboard LEX vortex passes outboard of the fin and the burst is located approximately at the fin mid-chord. A reduction in sideslip angle to −5° brings the vortex slightly inboard and the helical nature of the vortex flow becomes evident in the fin pressure distribution. The burst position also moves forward to a point just ahead of the fin. As sideslip increases in the positive direction, a similar trend is apparent. The vortex continues to move inboard of the fin and the burst moves further forward.

7.1.3 Effect of Stabilator deflection

As part of the Test A programme, the pressure distributions were measured both with symmetric and asymmetric stabilators. The results from the asymmetric stabilator tests were checked to determine the necessity of re-testing the asymmetric stabilators in Test B. It was found that the effect of one stabilator on the opposing stabilator and fin was minimal and that further asymmetric measurements would not be required. This also meant that the Test B programme could be kept to an acceptable length.

An angle of attack of 10° was chosen to illustrate the effect of stabilator deflection. At this angle, an aircraft in flight is likely to be subject to large pitch demands from a pilot during a pull-up manoeuvre. The sideslip angle is 0° and the LEX fence is on. Figures 13a - 13e are for stabilator deflections of +5° to −20° respectively.

The stabilator pressure distribution varies greatly with deflection. Inspection of Figure 13b (i.e. $\delta = 0°$) indicates that there may be a vortex impinging on the stabilator that has been generated from some point upstream. This could possibly be from the outboard end of the trailing edge flap. Larger deflections of the stabilator result in the generation of a vortex from the sharp leading edge and as the stabilator is deflected even further ($\delta = -20°$), the pressure distribution shows signs of tip stall.

The fin pressure distribution is virtually unaffected by the deflections of the stabilator. This is also true for the upper and lower surfaces of the fuselage. The side of the fuselage is likely to be affected by stabilator deflection especially near the stabilator leading edge.

7.1.4 Effect of LEX Fence

The LEX fence was fitted to the F/A-18 to reduce the severity of the fin buffet problem experienced at high angles of attack. The fence creates a secondary vortex (Reference [9]) that interacts with the primary LEX vortex to alter the flow field seen by the fins. As the fence was designed to alter the vortex flow in the high angle of attack region only, comparisons of the effect of the fence are provided for angles of attack of 10°, where the LEX vortex begins to develop, and for 25°, where the vortex is fully developed.

Figures 14a and 14b show that the LEX fence has a small effect on the pressure distribution over the stabilator. However, it was judged that the differences were not sufficient to justify the testing of the stabilators with the fence both on and off.

Figures 15a and 15b show how the LEX fence affects the pressure distributions on the fin. At 10° angle of attack, the effect is small relative to that at 25°. At the higher angle of attack, the pressure distribution is affected more at the fin tip with no real change at the root. This is to be expected since flow visualisation studies (Reference [9]) show that, at this angle of attack, the LEX vortex core is closer to the fin tip than the root.

7.1.5 Effect of Flap Deflection

As specified previously, the flap deflections used in the test programme were calculated using the flight control system logic which is primarily based on angle of attack and Mach number. However, the flap settings used in flight are also a function of dynamic pressure, and pilot roll-rate demand. Providing pressure information for every combination of flap setting, angle of attack, sideslip, etc. would be prohibited by time constraints. For this reason, only the major parameters affecting the flap deflections (angle of attack and Mach number) were used and an indication of the sensitivity to flap deflection of the fin and stabilator pressure distributions is given.

Preliminary data from Test A were compared with data obtained from a similar test series on a 1/24th scale F/A-18 half model in the ARL Transonic wind tunnel (Reference [1]). At angles of attack where both models had the same flap settings (0° and 25°), the data agreed reasonably well. At 10° angle of attack, the flap settings from the two tests differed by 5° and this difference was reflected in the integrated loads results. This was the angle of attack where the highest discrepancy in the loads occurred. For this reason, an angle of attack of 10° was chosen for the flap sensitivity tests. During the second phase of Test B (measurement of fin and fuselage pressures) some higher angle of attack measurements were made also.

At an angle of attack of 10° (and Mach numbers less than 0.6), the LEF deflection was calculated to be 13.3° and the TEF deflection was calculated to be 14.0°. With the TEF set at 14.0°, the LEF was swept from 0° to 35° in 5° increments and the pressures over the stabilator, fin and fuselage measured. Similarly, with the LEF set at 13.3°, the TEF was swept from 0° to 20° in 4° increments.

Pressure distributions are presented for the starboard fin and stabilator, indicating the effect of deflecting the LEF from 10° to 20° (Figures 16a and 16b) and the TEF from 12° to 20° (Figures 17a and 17b). The figures illustrate that the effect of LEF deflection is almost unnoticable. The TEF effect is more prominent. As the TEF is deflected down, the increase in downwash causes a reduction in the inward loading on the fin and also the upward loading on the stabilator.

7.1.6 Effect of Fuel Tank

An investigation was carried out to determine the effect on the stabilator pressure distribution of a '330 gallon' fuel tank mounted on the inboard wing pylon. Tests were conducted using the model configured as in Test A with the fixed undeflected flaps, as this wing had been manufactured with attachment holes for fitting a wing pylon. The investigation was therefore limited to low angles of attack which was considered acceptable since the major effect was expected to be due to the tank wake impinging on the stabilator.

The two cases presented here in Figures 18a and 18b represent $\alpha = 5°$, $\beta = 0°$, $\delta = +1°$, and $\alpha = 0°$, $\beta = 5°$, $\delta = -11°$ respectively with the LEX fence off for both. These figures indicate that the carriage of a fuel tank on the inboard wing pylon has a relatively minor effect on the stabilator pressure distribution.

Figure 18b was included in particular as it shows the greatest change in the pressure distribution with the tank fitted. A slight decrease in pressure coefficient is observed at the leading edge on the lower side of the stabilator with the tank in place.

7.2 Integrated Loads

The amount of data gathered in this test programme makes it impractical to present all measured pressure distributions in this report. Integration of the pressure distributions to obtain total surface loads allows every test point to be presented in a form that clearly illustrates how the aerodynamic loads change over the whole of the test envelope. The load information also provides a useful reference for other F/A-18 studies. Force and moment coefficients are presented for the starboard fin and stabilator.

7.2.1 Fin Loads

The loads derived from integration of the fin pressure distributions provide an overall indication of the major steady-state aerodynamic effects. Figures 19a to 19e, 20a to 20e and 21a to 21e represent the lift (or normal force), pitching moment (or root torsion) and bending moment coefficients respectively on the starboard fin for varying sideslip and stabilator angles.

At low angle of attack, the flow over the fins is attached. As the angle of attack increases, the inboard loading on the fin increases in a relatively linear fashion due to the fin cant angle of 20°, until the formation of the LEX vortex occurs. The integrated fin load results show that, at high angle of attack, the fin is dominated by the presence of the LEX vortex. This is evident by noting the change in the fin loads with the attachment of the LEX fence, which

11

alters the structure and trajectory of the primary LEX vortex. The flow visualisation studies in Reference [9] illustrate that angle of attack alters both the vertical position of the vortex relative to the fin and also the streamwise location of the burst.

At low angle of attack (less than about 10°) the difference in fin loading between LEX fence on and off is minor. From $\alpha = 10°$ to 35°, the fin loads are dominated by the LEX vortex and therefore, any change in this vortical flow (i.e. due to the LEX fence) is more easily recognised. At $\alpha = 35°$, the effect of the fence begins to be less pronounced. This is due to the the trajectory of the vortex passing above the fin tip. In general, the attachment of the LEX fence results in increased inboard loading on the fin.

The fin normal force results show that there is a linear change in fin loading with sideslip at low angles of attack. At high angles of attack, this gradient reduces and non-linear behaviour occurs at negative sideslip angles. Flow visualisation tests show that the starboard vortex burst point moves forward and inboard with positive sideslip and aft and outboard with negative sideslip. This means that the effect of the LEX fence on the starboard fin will be evident at lower angles of attack for positive sideslip cases and at higher angles of attack for negative sideslip cases. This effect is observed in the integrated loads results.

The effect of stabilator deflection on the steady state fin loads is negligible over the whole angle of attack and sideslip range.

7.2.2 Stabilator Loads

Figures 22a to 22e, 23a to 23e and 24a to 24e represent the lift (or normal force), pitching moment (or hinge torsion) and bending moment coefficients respectively on the starboard stabilator for varying stabilator and sideslip angles.

The most noticeable trend in the stabilator load data (Figures 22a to 22e) is the nonlinear behaviour with aircraft angle of attack. At angles of attack less than 10°, deflection of the stabilator results in a considerably larger change in the stabilator load than does a change in incidence of similar magnitude. This indicates that although the aircraft incidence may change, the local angle of attack at the stabilator changes to a much lesser degree. This effect is almost reversed at aircraft angles of attack greater than 10°. Here, the change in load from a stabilator deflection is less than that obtained from a change in incidence. The strengthening of the primary LEX vortex in the high angle of attack range and the consequential alteration to the flow field in the vicinity of the stabilator is most likely to be the cause of this effect.

Though not entirely obvious from the manner in which the data are presented here, inspection of Figures 22a to 22e shows that the variation of stabilator load with stabilator deflection is approximately linear. The effect of sideslip is also relatively small by comparison.

Minor exceptions to the general trends are evident. Firstly, at a combination of high angle of attack and positive sideslip angles, a positive increase in the stabilator deflection from the 0° position actually results in a decrease in lift. Secondly, at low angle of attack and large sideslip angles (mainly negative but also positive), an increase in angle of attack does not always produce an increase in upward loading on the stabilator. This may be an effect due to separated flow from the modified fuselage contours located just forward of the stabilators for mounting the Sparrow Missile. Specific tests to identify the causes of these variations were not made.

12

The effect of the LEX fence on the stabilator was checked for a limited number of cases (i.e. 0° sideslip and 0° stabilator deflection). As discussed previously with regard to the pressure distributions, the LEX fence is shown to have a small effect on the stabilator loads but given the magnitude of the changes due to other parameters, it is considered negligible.

7.2.3 Variations in Fin and Stabilator Loads Due to Flap Deflections

Deflection of the flaps, within the vicinity of the calculated trim position, results in a reasonably linear change in the fin and stabilator loading. Figures 25, 26 and 27 present the aerodynamic loads measured using the trim flap settings to provide a clear indication of the relative effect of flap deflection in these regions.

Although the flap positions, in particular those of the trailing edge flap, do affect the pressure distributions and consequently the total loads on the fins and stabilators, the effect of angle of attack, angle of sideslip and stabilator angle is significantly larger. As discussed, the trim flap settings used in these tests are an estimate of the operational flap deflections, and as shown in Figures 25 to 27, small deviations from these settings produce a minor effect on the fin and stabilator loads.

Conclusions

The steady aerodynamic load distributions over the aft fuselage, fins and stabilators have been measured using a 1/9th scale wind-tunnel model for a wide range of operational flight conditions. The results are presented for a range of angles of attack, sideslip angles and stabilator deflections with the LEX fence on and off. The wing flap settings are scheduled as a function of angle of attack as defined by the aircraft flight control system.

In this report, a selection of the pressure distributions has been presented to illustrate the changes due to the major parameters. The integration of the surface pressures has been carried out and these results are presented to show the major changes in the aerodynamic loads on the aircraft.

Due to the fin cant angle and the LEX vortex flow, aircraft angle of attack has a major effect on the steady state loads on the fins as well as on the stabilators. As expected, sideslip has a large effect on the fin loading but has a relatively minor influence on the stabilator loading. Stabilator deflection has a large effect on the stabilator load distribution as expected but has a negligible effect on fin loads. At low angles of attack, stabilator deflection produces considerably greater changes in stabilator lift than the equivalent change in aircraft incidence, but the reverse is true at high angles of attack. Variations in the TEF angle have a larger effect on the fin and stabilator loads than does the LEF although these are still relatively small.

Neither the attachment of the LEX fence nor mounting the '330 gallon' fuel tank on the inboard wing pylon had much effect on the stabilator loads. However, the fins were affected by the LEX fence at angles of attack greater than around 10° where the LEX vortex begins to form and dominate the fin flow field.

13

Acknowledgements

The work presented in this report is the culmination of effort from many people. The authors would like to thank the major contributors on an individual basis and indicate the area of the project where their input was invaluable.

Colin Martin   - Task Manager

Mike Glaister   - Manager of model design and manufacture

Peter Malone, Alberto Gonzales, Dennis Carnell and John Clayton
          - Test operation and model preparation

Shane Austin, John Williams, Sam Burrows and George Millers
          - Model design

John Winter, Graeme Precious, Tom Knaub, Gary Windsor and Jeff Spencer
          - Model manufacture

John Harvey and Stephen Kent
          - Hardware for control of actuated surfaces

Stephen Lam and Yoel Link
          - Software for control of actuated surfaces

Shane Hill   - Pressure measurement software

References

[1] Glaister, M.K., MacLaren, L.D. and Pierens, D.A., 'Transonic Pressure Distribution Measurements Over the Aft-Fuselage, Fin and Stabilator of a 1/24th Scale F/A-18 Wind-Tunnel Half-Model', Research Report 11, Aeronautical Research Laboratory, Melbourne Australia, (in preparation).

[2] Martin, C.A., Glaister, M.K., MacLaren, L.D., Meyn, L.A. and Ross, J., 'F/A-18 1/9th Scale Model Tail Buffet Measurements', Flight Mechanics Report 188, Aeronautical Research Laboratory, Melbourne Australia, June 1991.

[3] Lam, S.S.W. and Link, Y.Y., 'Development and Operation of the F/A-18 Model Control Surface Actuators', Technical Note 29, Aeronautical Research Laboratory, Melbourne Australia, 1993.

[4] Glaister, M.K., 'The Design of a 1/9th Scale F/A-18 Wind Tunnel Model', Technical Note (in preparation), Aeronautical Research Laboratory, Melbourne Australia.

[5] 'F/A-18A Flight Control System Design Report', MDC A7813 Vol.I, McDonnell Aircraft Company, St Louis Missouri U.S.A., December 1982.

[6] Glaister, M.K. and Hill, S.D., 'Electronic Pressure Scanning Experience and Software Development', Proceedings of the Commonwealth Advisory Aeronautical Research Council (CAARC) specialists meeting on Experimental Aerodynamics and Test Techniques, Defence Research Agency, Farnborough U.K., September 1992.

[7] Akima, H., 'BIVAR - Interpolation Package, NCAR Public Software Libraries', National Center for Atmospheric Research, Boulder Colorado U.S.A., January 1985.

[8] Cline, A.K. and Renka, R.J., 'SURF1 - Interpolation Routine, NCAR Graphics Routines', Dept. of Computer Sciences, University of Texas, Austin Texas U.S.A, undated.

[9] Thompson, D.H., 'Water Tunnel Flow Visualisation of Vortex Breakdown over the F/A-18', Flight Mechanics Report 179, Aeronautical Research Laboratory, Melbourne Australia, October 1990.

[10] Thompson, D.H., 'Surface Flow Visualisation over the F/A-18', Technical Note (in preparation), Aeronautical Research Laboratory, Melbourne Australia.

Appendix A - Archiving of Test Results

The data from this series of tests have been stored on a 150 Mbyte tape in 'tar' format using a Silicon Graphics 4D/310 GTX computer. The tape contains all raw data from the tunnel tests, the source code for the computer programs used in the analysis of the data and the final results. The tape has been registered in the Applied Aerodynamics data storage facility at ARL.

A.1 Geometry file

The root directory provided by ARL contains the geometry data file 'f18panel.out'. This file contains data describing the surface geometry of the F/A-18 aircraft as obtained from the ARL F/A-18 VSAERO CFD model. The data included in the file are panel number, panel area, x, y and z co-ordinates of the panel centroids, and the components of the unit normal vector of each panel in the x, y, and z directions. All control surfaces on the panel model are in the undeflected position.

A.2 Pressure coefficient files

Each of these files contains a list of panel numbers and the corresponding pressure coefficients as obtained from the tunnel tests and subsequent interpolation. The file naming system takes the form 'a6b1d3t2f0.out'. The results are presented as interpolated pressure coefficients for a given VSAERO panel. Each data file represents a single test point in the programme and is coded in the following manner.

a - code for angle of attack, α
b - code for angle of sideslip, β
d - code for stabilator deflection, δ
t - code for flap deflection, LEF and TEF
f - code for LEX fence condition.

The code used to name the files is as in Table A1. For example, the file 'a6b1d3t2f0.out' would contain data for the case:

$\alpha = 20°$
$\beta = -5°$
$\delta = 0°$
LEF=26.6°, TEF=7.8°
LEX fence off.

A.3 Integrated loads files

Files 'fin.out' and 'tail.out' contain the results of the pressure coefficient integration over the fin and stabilator respectively for all tested combinations of α, β, δ, flap deflection and fence. The pressure coefficients have been integrated to obtain a lift force coefficient acting normal to the chord plane of each flying surface, a torsion moment coefficient about the quarter chord point at the root of the fin and the pivot point on the tailplane as described in section 6.3, and a bending moment coefficient for both fin and tailplane. Note that this is the order in which the integrated loads appear in the data files. All coefficients have been non-dimensionalised using the wing area and also the wing mean aerodynamic chord where appropriate. The sign convention used is provided in Figure 8.

Table A1: Coding of file names for pressure distribution results

'a'		't'		
code	α (deg)	code	LEF (deg)	TEF (deg)
0	-10	0	0.0	0.0
1	-5	0	0.0	0.0
2	0	0	0.0	0.0
3	5	0	5.0	5.0
		1	6.6	7.0
		2	5.1	7.0
4	10	0	15.0	15.0
		1	10.0	10.0
		2	13.3	14.0
		3	11.8	12.2
5	15	0	20.0	15.0
		1	20.0	10.0
		2	19.9	14.8
		3	19.9	12.6
		4	18.4	9.8
6	20	0	25.0	10.0
		1	25.0	5.0
		2	26.6	7.8
		3	26.6	5.6
		4	25.0	2.8
7	25	0	35.0	0 0
		1	33.2	0.8
		2	33.2	0.0
		3	31.7	0.0
8	30	0	34.0	0.0
9	35	0	34.0	0.0

	'b'	'd'	'f'
code	β (deg)	δ (deg)	LEX Fence
0	-10	-20	off
1	-5	-10	on
2	0	-5	
3	5	0	
4	10	5	

Wing Area	0.459 sq m (400 sq ft, full scale)
Fin Area	0.060 sq m (52.12 sq ft each, full scale)
Stabilator Area	0.051 sq m (44.05 sq " each, full scale)

1268 mm

390 mm
MAC

1896 mm
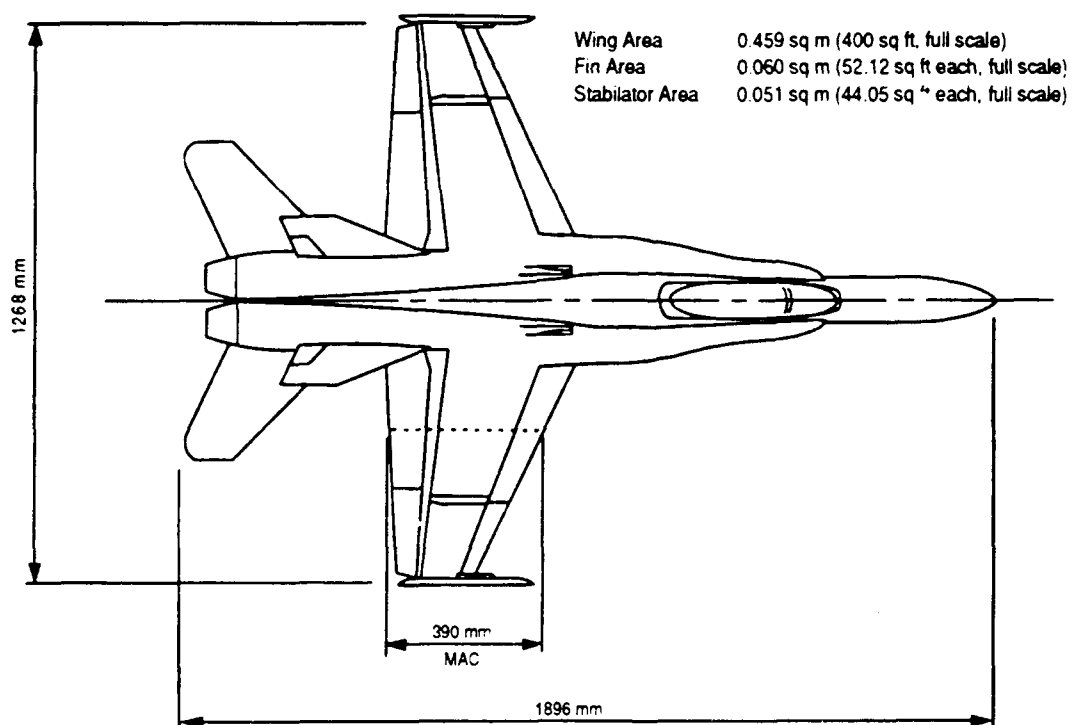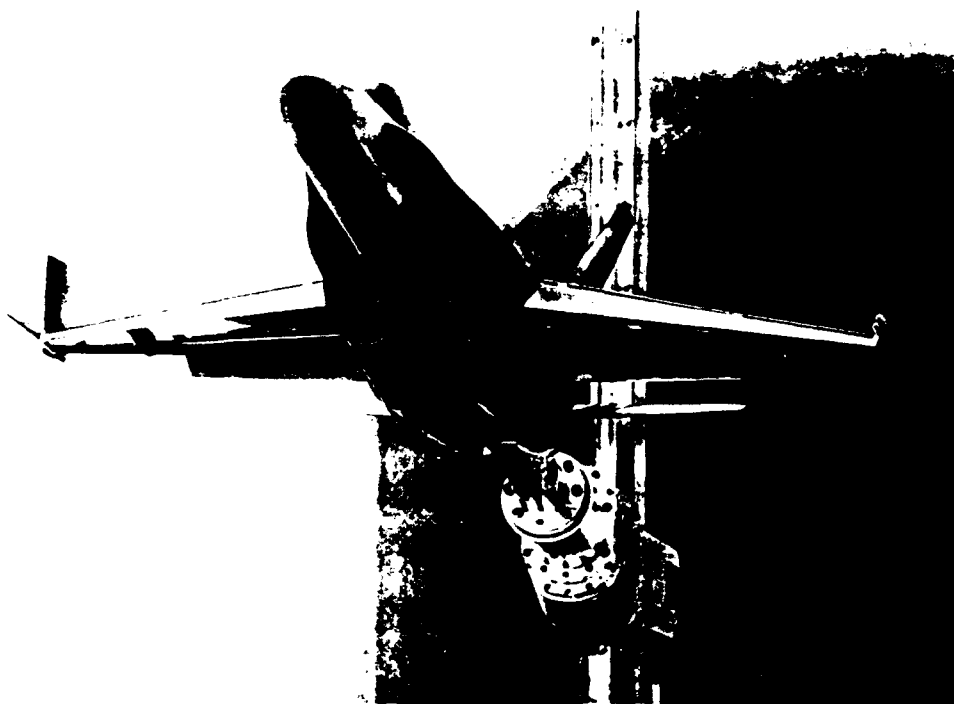
Figure 1 :   1/9th Scale F/A-18 Wind-Tunnel Model
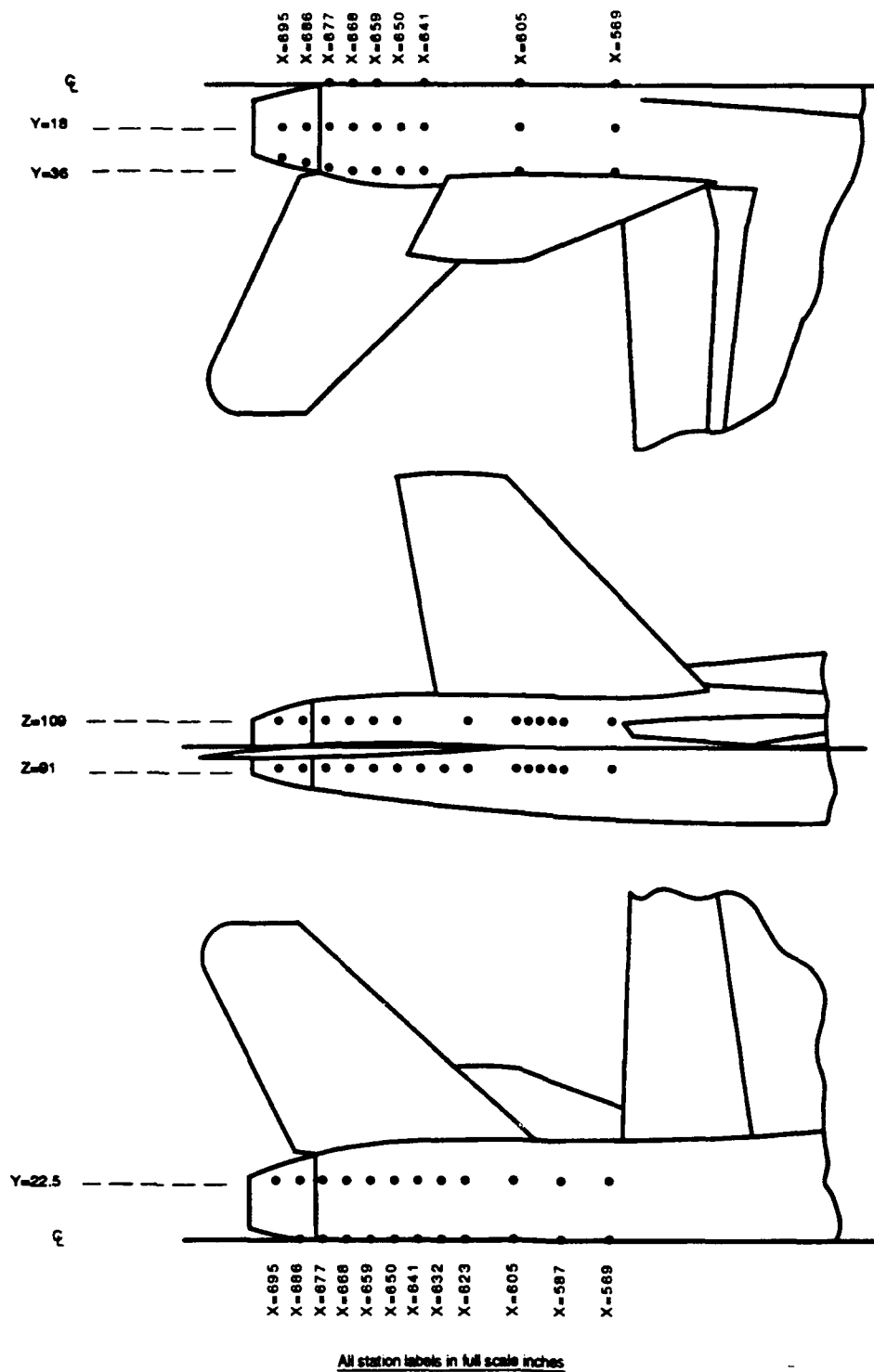
Figure 2 : Fuselage Pressure Ports for Test A

All station labels in full scale inches

20

% Chord

1.0 %
2.5 %
5.0 %

15.0 %

30.0 %

50.0 %

70.0 %

95.0 %

Hx=0   Hx=20   Hx=40   Hx=60   Hx=80   Hx=88

Station on full scale aircraft (inches)
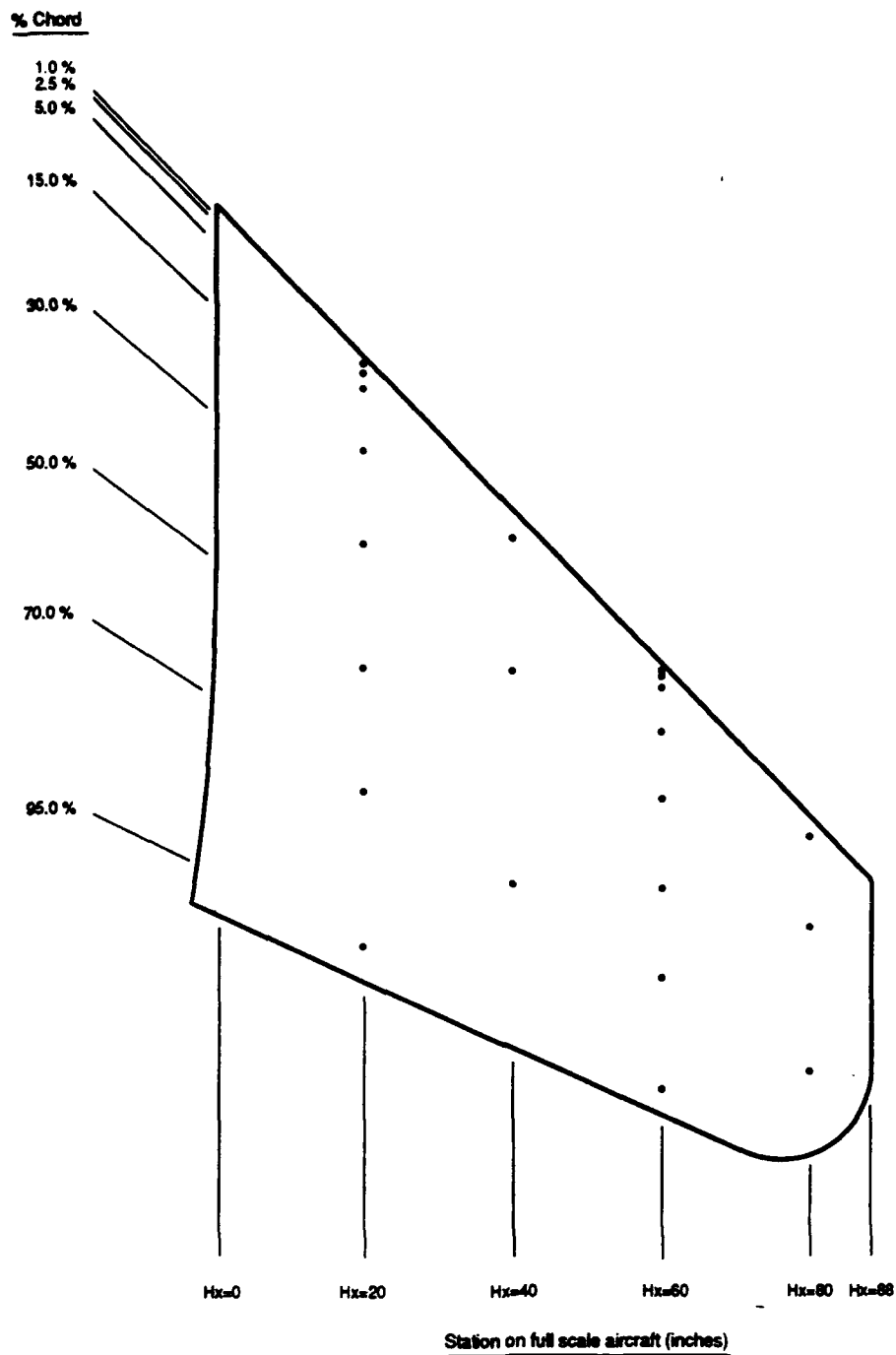
Figure 3 :   Stabilator Pressure Ports for Test A
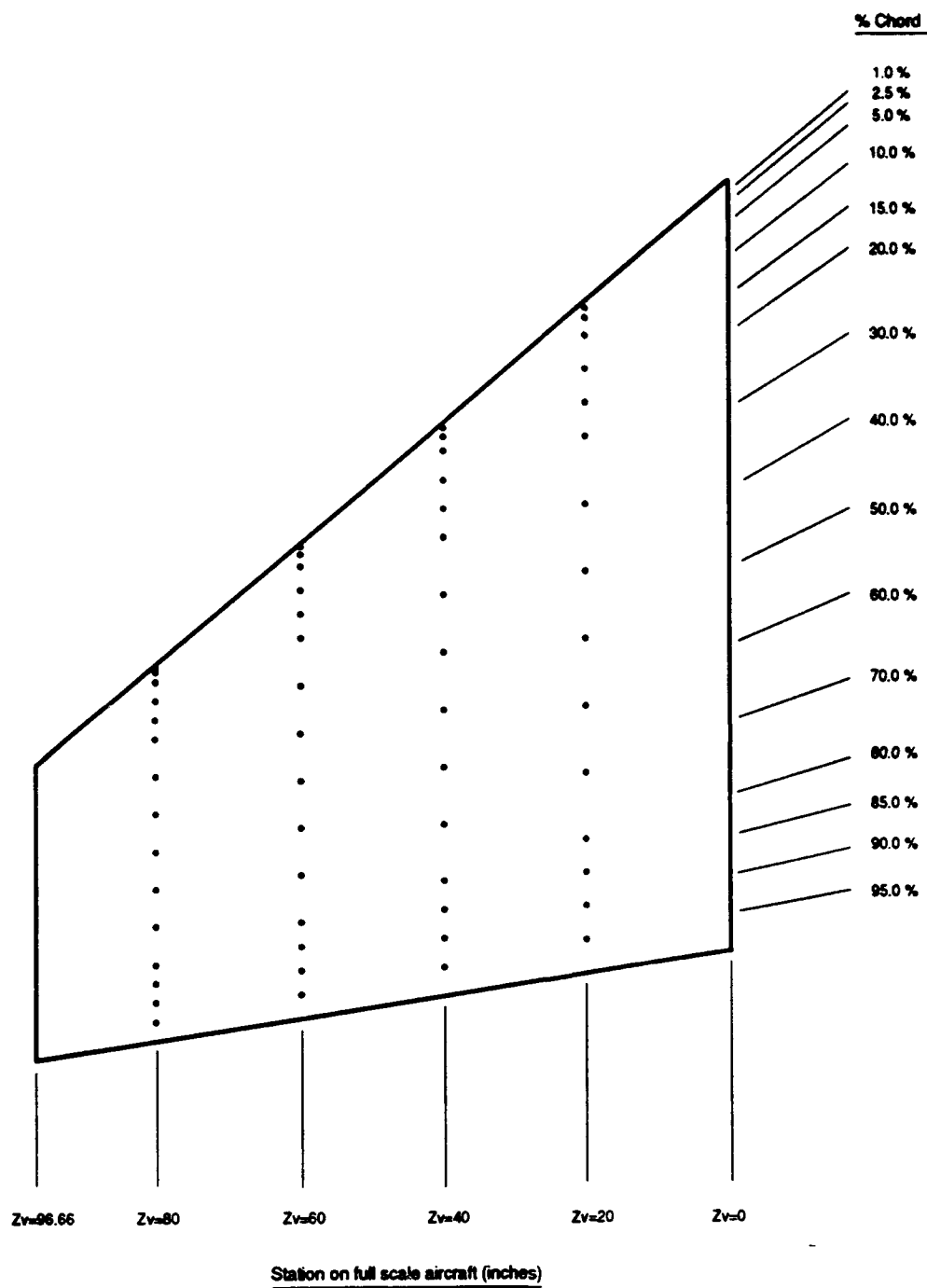
Figure 4 : Fin Pressure Ports for Tests A and B

22

Figure 5 : Fuselage Pressure Ports for Test B
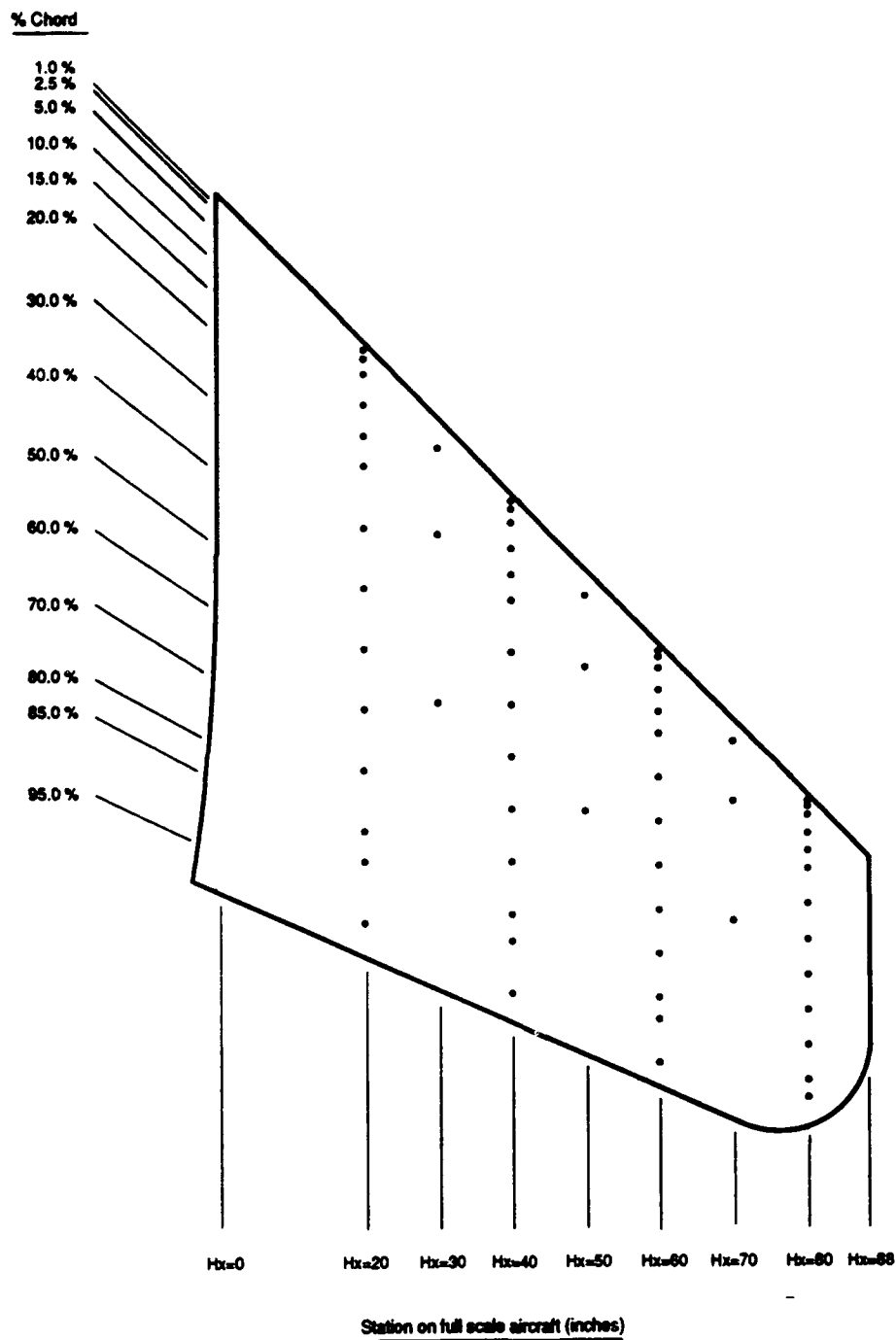
Figure 6 :   Stabilator Pressure Ports for Test B

24
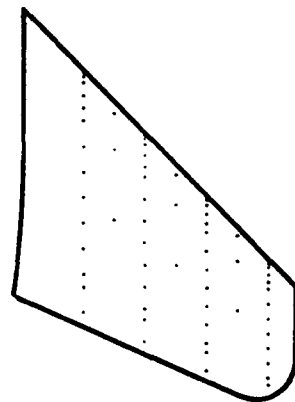
1. Measure pressure at each port using PSI instrumentation and convert to pressure coefficients.
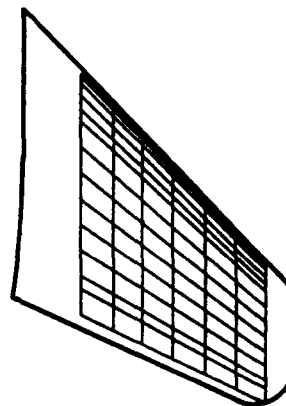
2. Complete rectangular grid of pressure coefficients at missing or unusable ports using the BIVAR routines.
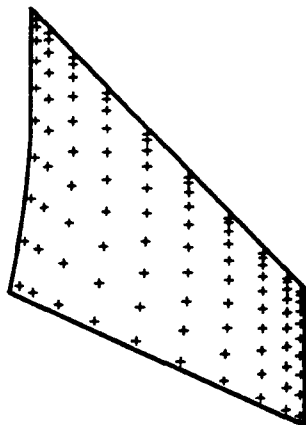
3. Perform 3-dimensional surface interpolation/extrapolation using the routine SURF to obtain pressure coefficients at VSAERO panels and integrate for total loads.

Figure 7 :   Post-Processing Data Analysis Procedure
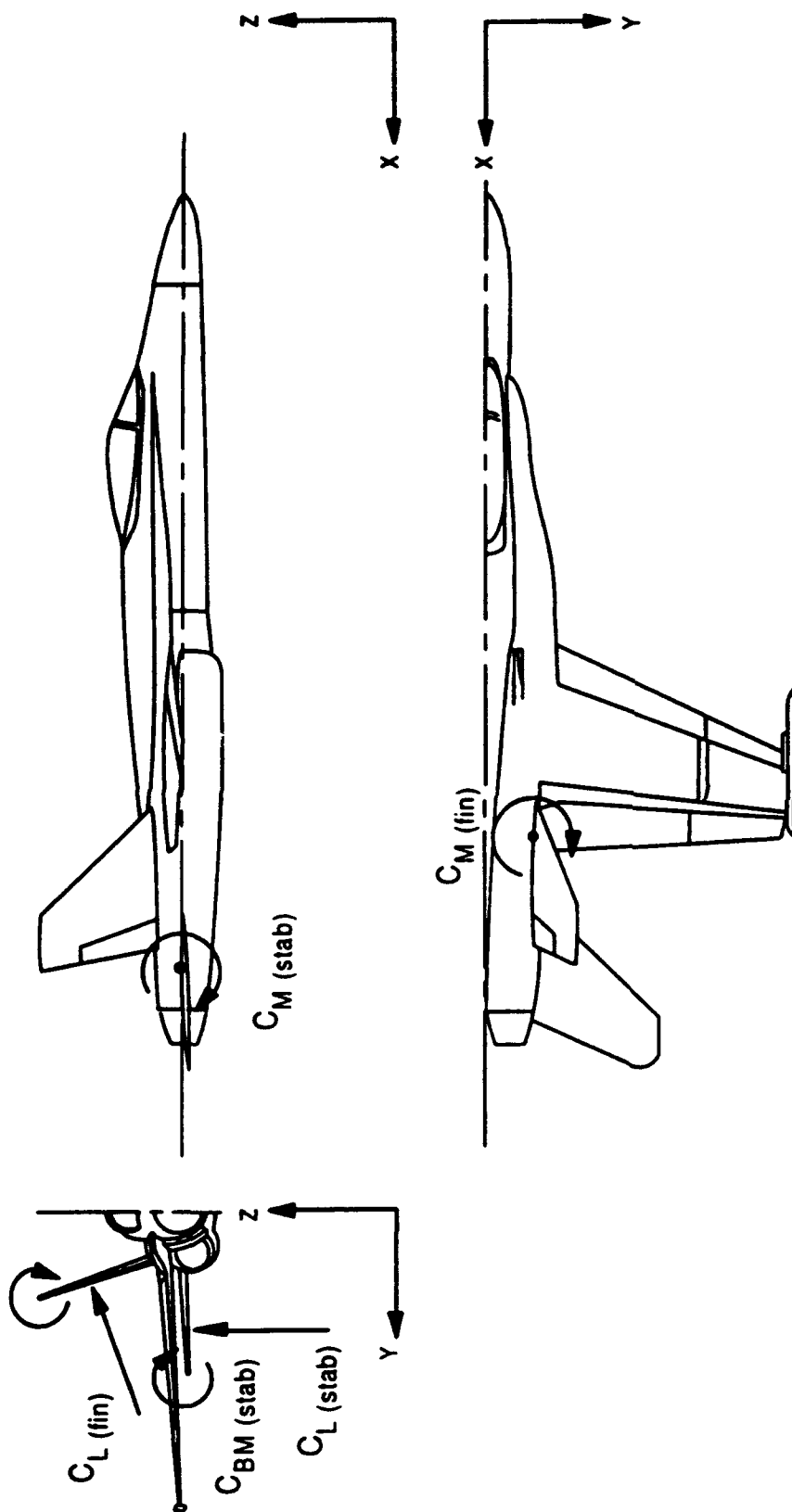
Figure 8 : Positive Sign Convention for Total Loads on Fins and Stabilators

Angle of Attack	25°
Angle of Sideslip	0°
Stabilator Deflection	0°
Leading Edge Flap	33.2°
Trailing Edge Flap	0.8°
LEX Fence	off

Cp Values

0.5000
0.4000
0.3000
0.2000
0.1000
0.0000
-.1000
-.2000
-.5000
-.6000
-.7000
-.8000
-.9000
-1.000
-1.100
-1.200
-1.300
-1.400
-1.500
-1.600
-1.700
-1.800
-1.900
-2.000
-2.100
-2.200
-2.300
-2.400
-2.500
-2.600
-2.700
-2.800
-2.900
-3.000
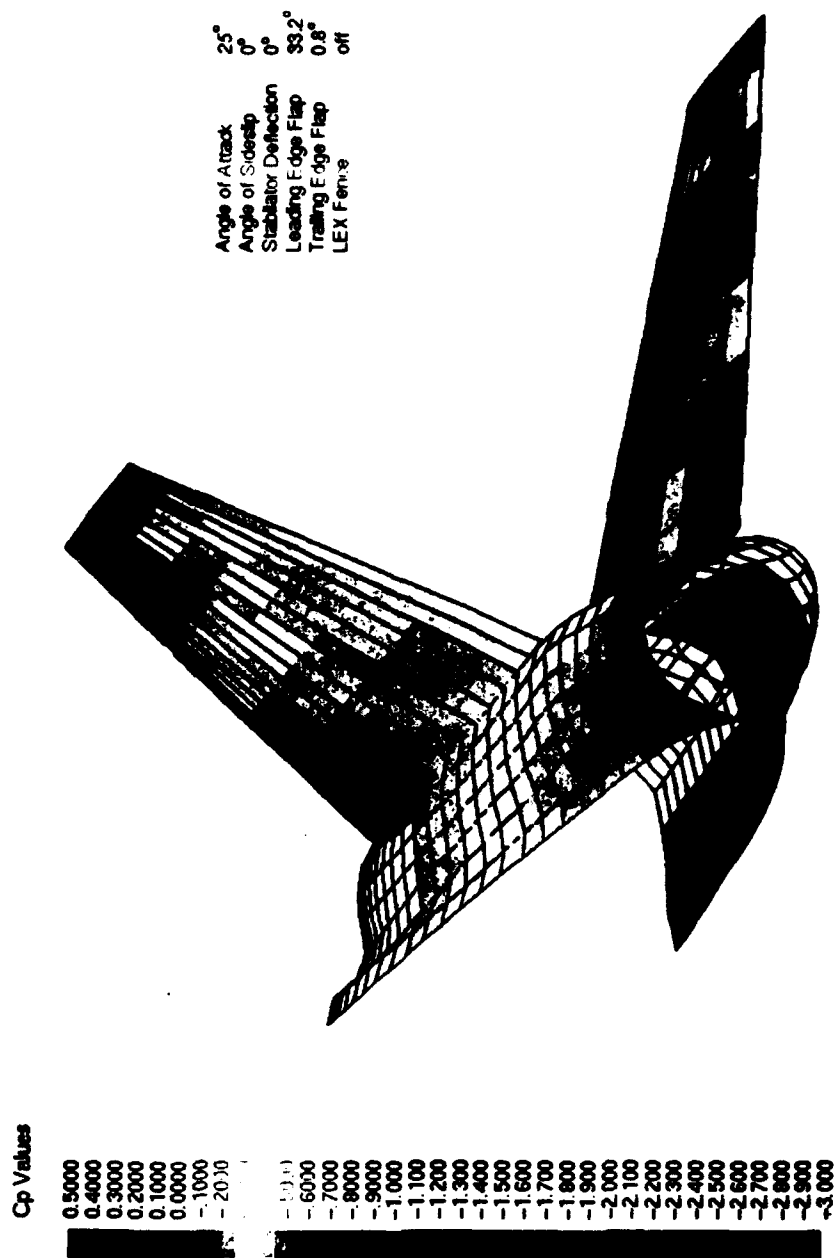
Figure 9 : Example of Graphical Output of Pressure Contours
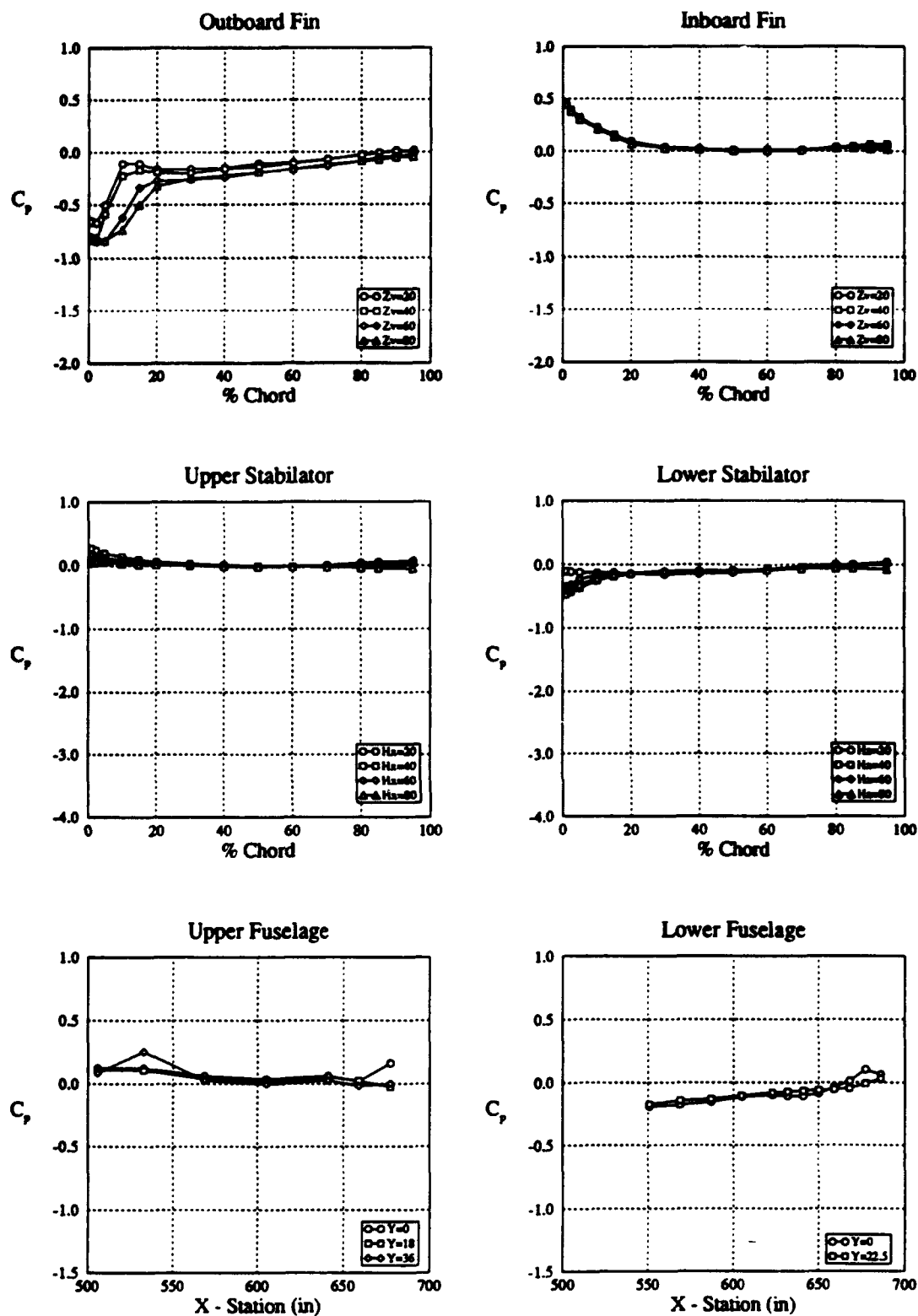
Figure 10 a :   Starboard Side Surface Pressure Distribution for Varying Angle of Attack
$\alpha = -10°, \beta = 0°, \delta = 0°$, LEF= 0.0°, TEF= 0.0°, LEX fence on

29
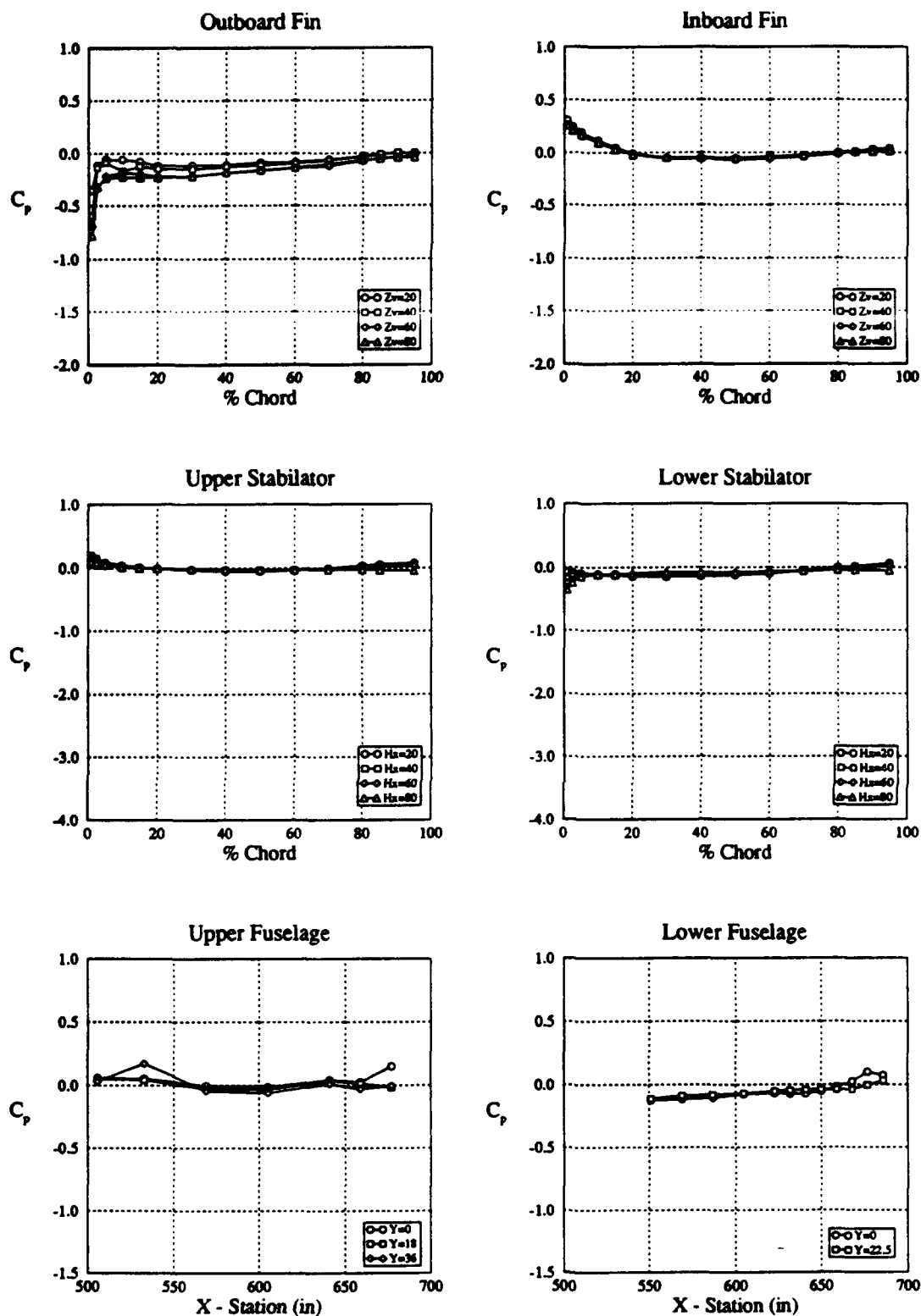
Figure 10 b : Starboard Side Surface Pressure Distribution for Varying Angle of Attack
$\alpha = -5°, \beta = 0°, \delta = 0°$, LEF= 0.0°, TEF= 0.0°, LEX fence on

Outboard Fin

C_p

% Chord

Legend: Z=20, Z=40, Z=60, Z=80

Inboard Fin

C_p

% Chord

Legend: Z=20, Z=40, Z=60, Z=80

Upper Stabilator

C_p

% Chord

Legend: Hx=20, Hx=40, Hx=60, Hx=80

Lower Stabilator

C_p

% Chord

Legend: Hx=20, Hx=40, Hx=60, Hx=80

Upper Fuselage

C_p

X - Station (in)

Legend: Y=0, Y=18, Y=36

Lower Fuselage

C_p

X - Station (in)

Legend: Y=0, Y=22.5
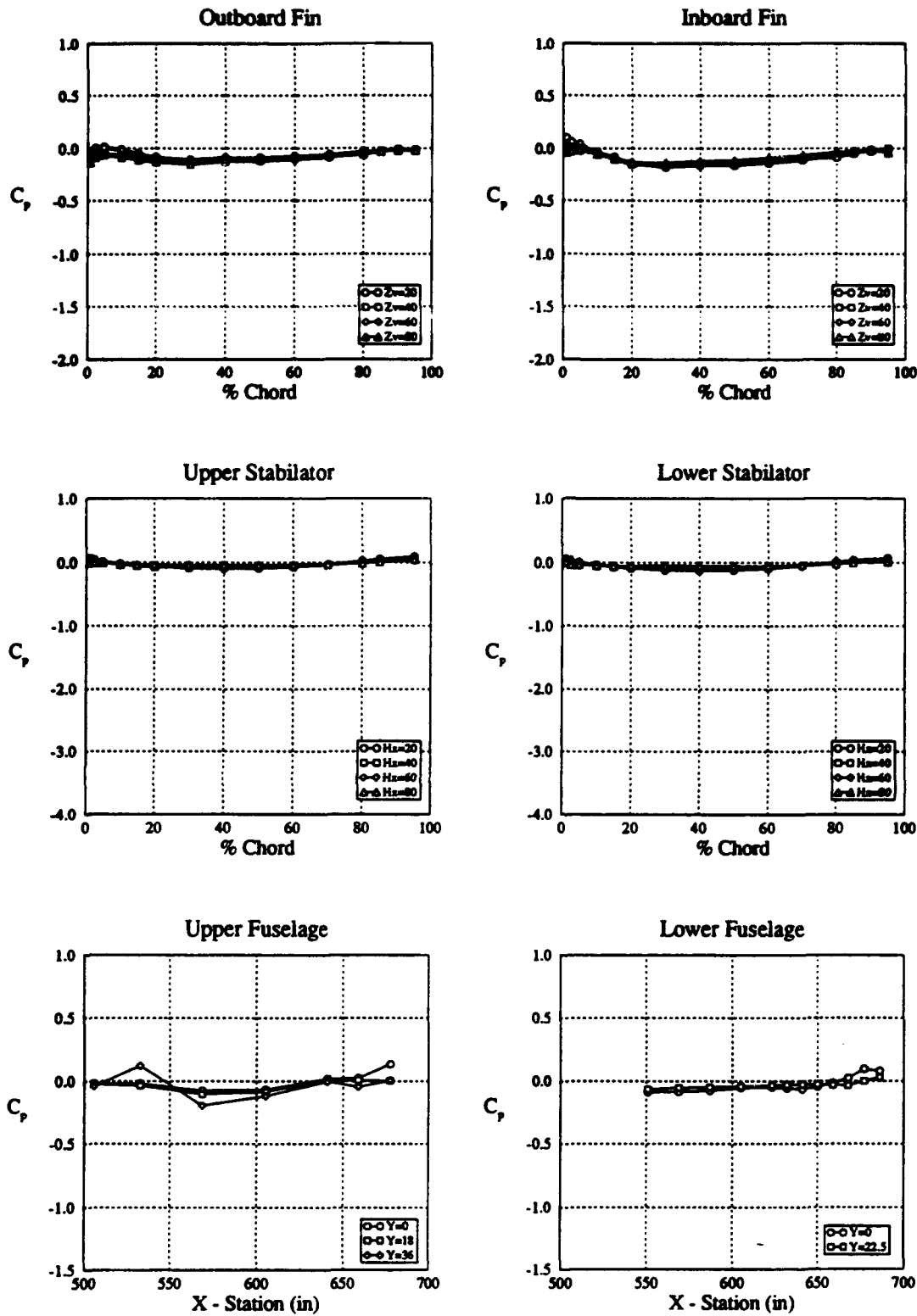
Figure 10 c :   Starboard Side Surface Pressure Distribution for Varying Angle of Attack
$\alpha = 0°, \beta = 0°, \delta = 0°$, LEF= 0.0°, TEF= 0.0°, LEX fence on

31

Outboard Fin

Inboard Fin

Upper Stabilator

Lower Stabilator

Upper Fuselage

Lower Fuselage
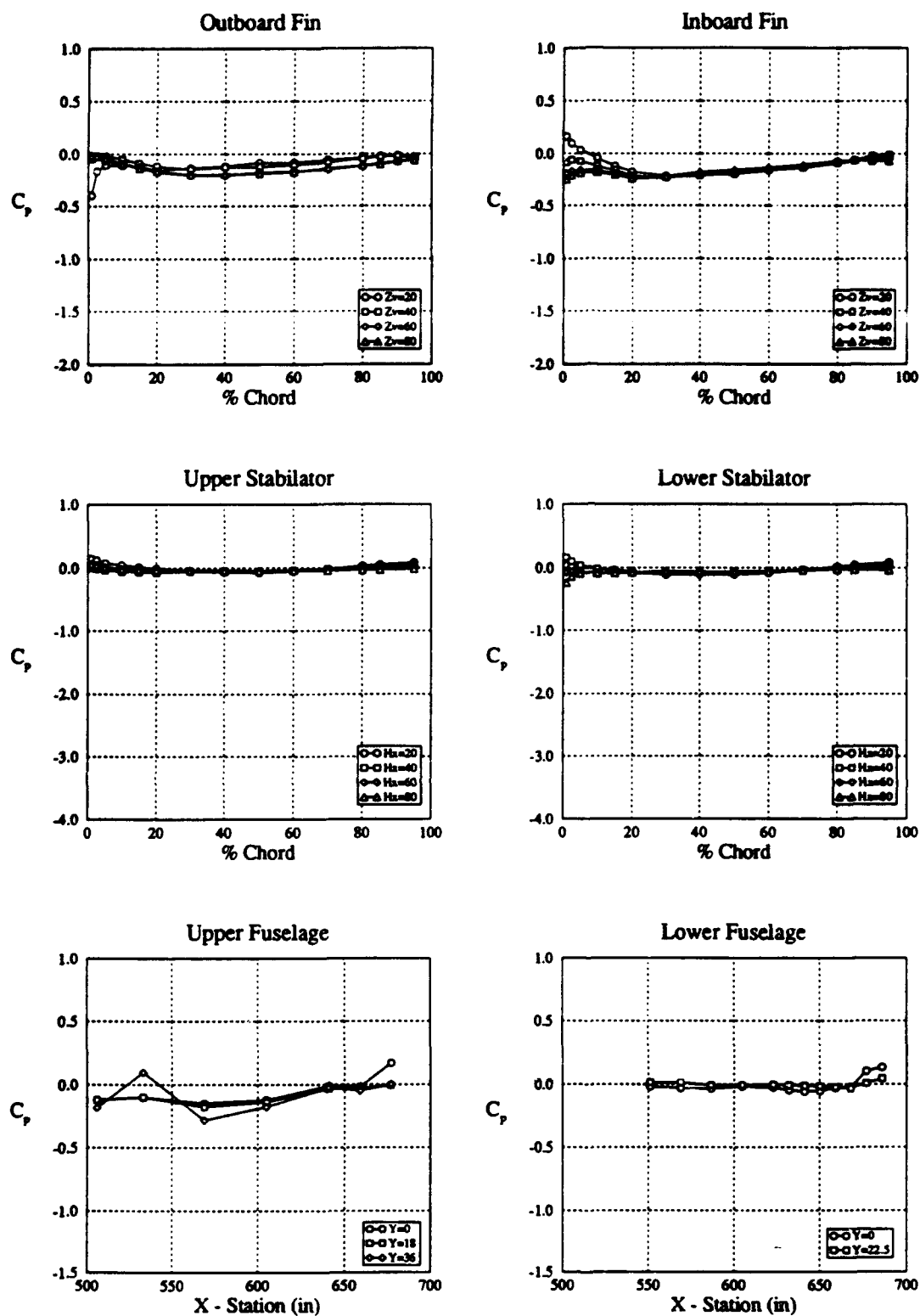
Figure 10 d : Starboard Side Surface Pressure Distribution for Varying Angle of Attack
$\alpha = 5°, \beta = 0°, \delta = 0°$, LEF= 6.6°, TEF= 7.0°, LEX fence on

32
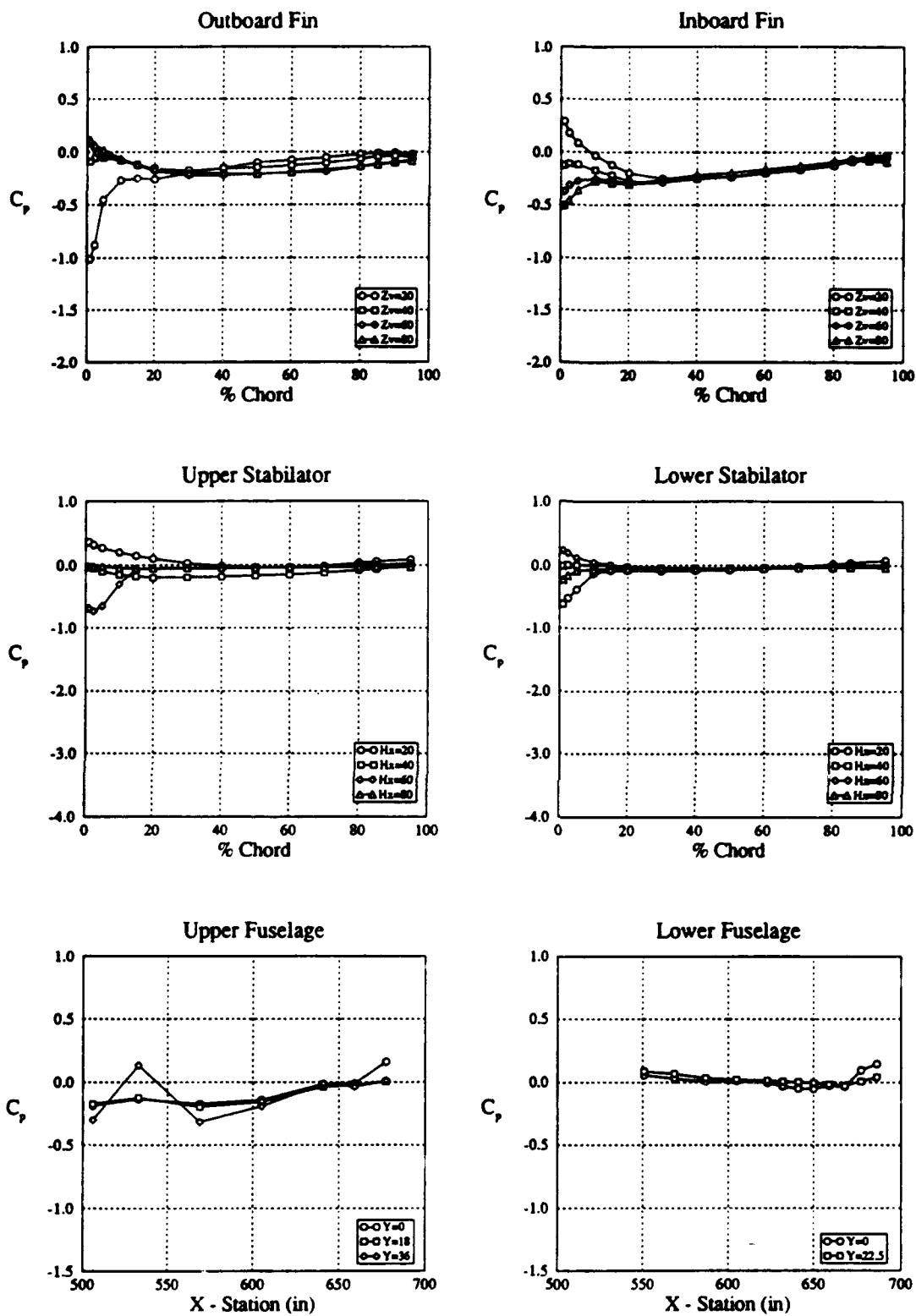
Figure 10 e : Starboard Side Surface Pressure Distribution for Varying Angle of Attack
$\alpha = 10°, \beta = 0°, \delta = 0°$, LEF= 13.3°, TEF= 14.0°, LEX fence on

33
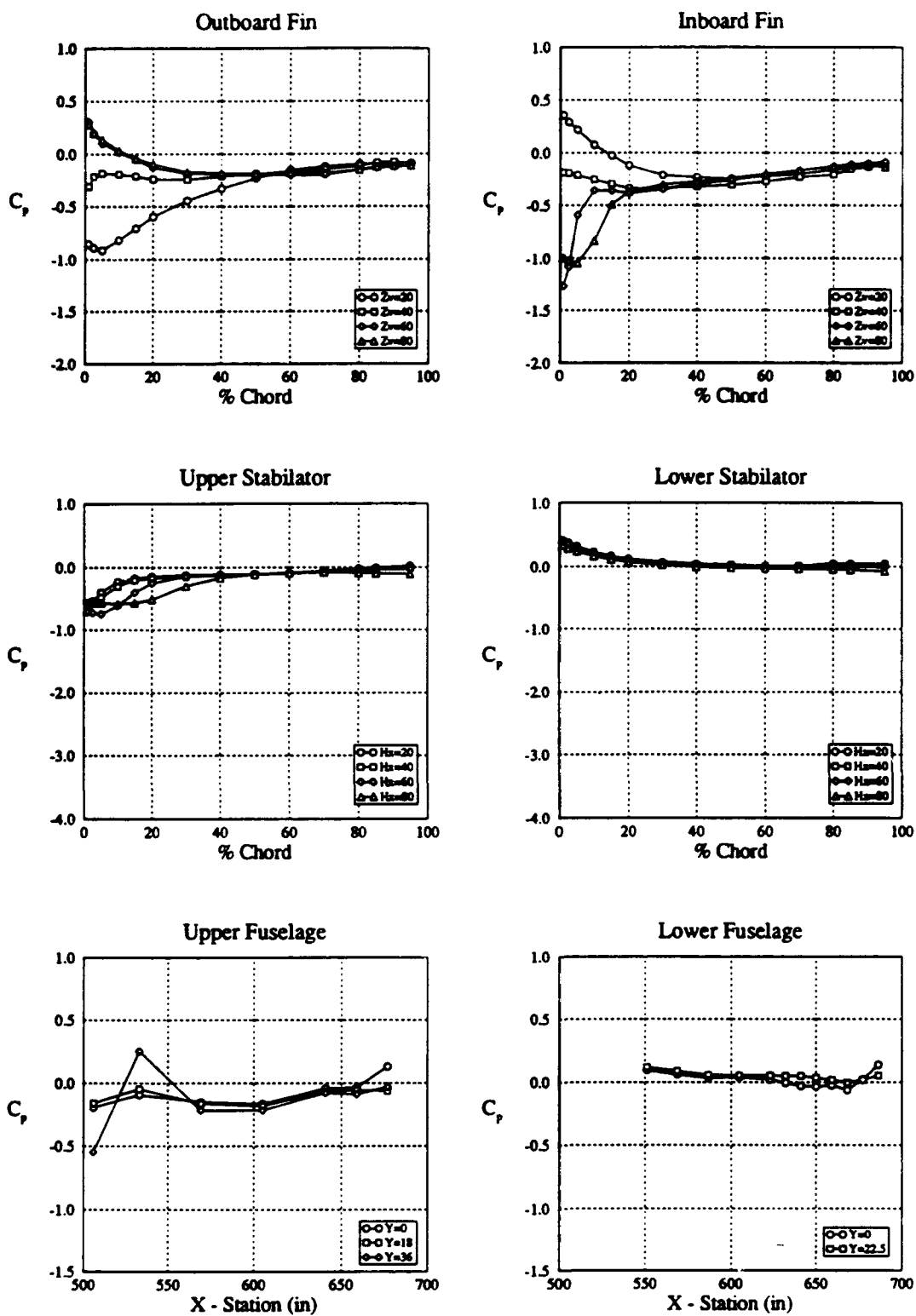
Figure 10 f : Starboard Side Surface Pressure Distribution for Varying Angle of Attack
$\alpha = 15°, \beta = 0°, \delta = 0°$, LEF= 19.9°, TEF= 14.8°, LEX fence on

34
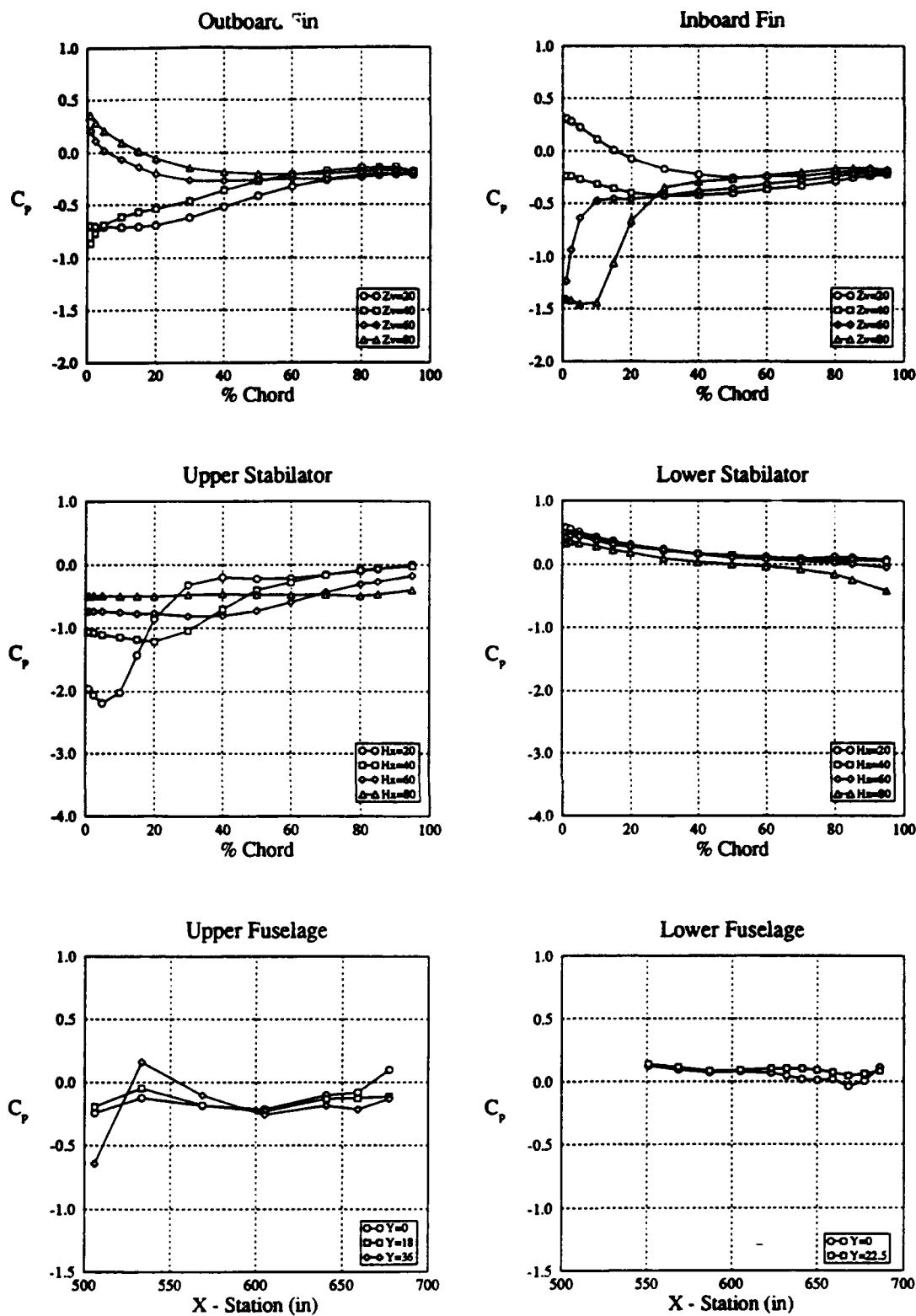
Figure 10 g : Starboard Side Surface Pressure Distribution for Varying Angle of Attack
$\alpha = 20°, \beta = 0°, \delta = 0°$, LEF= 26.6°, TEF= 7.8°, LEX fence on
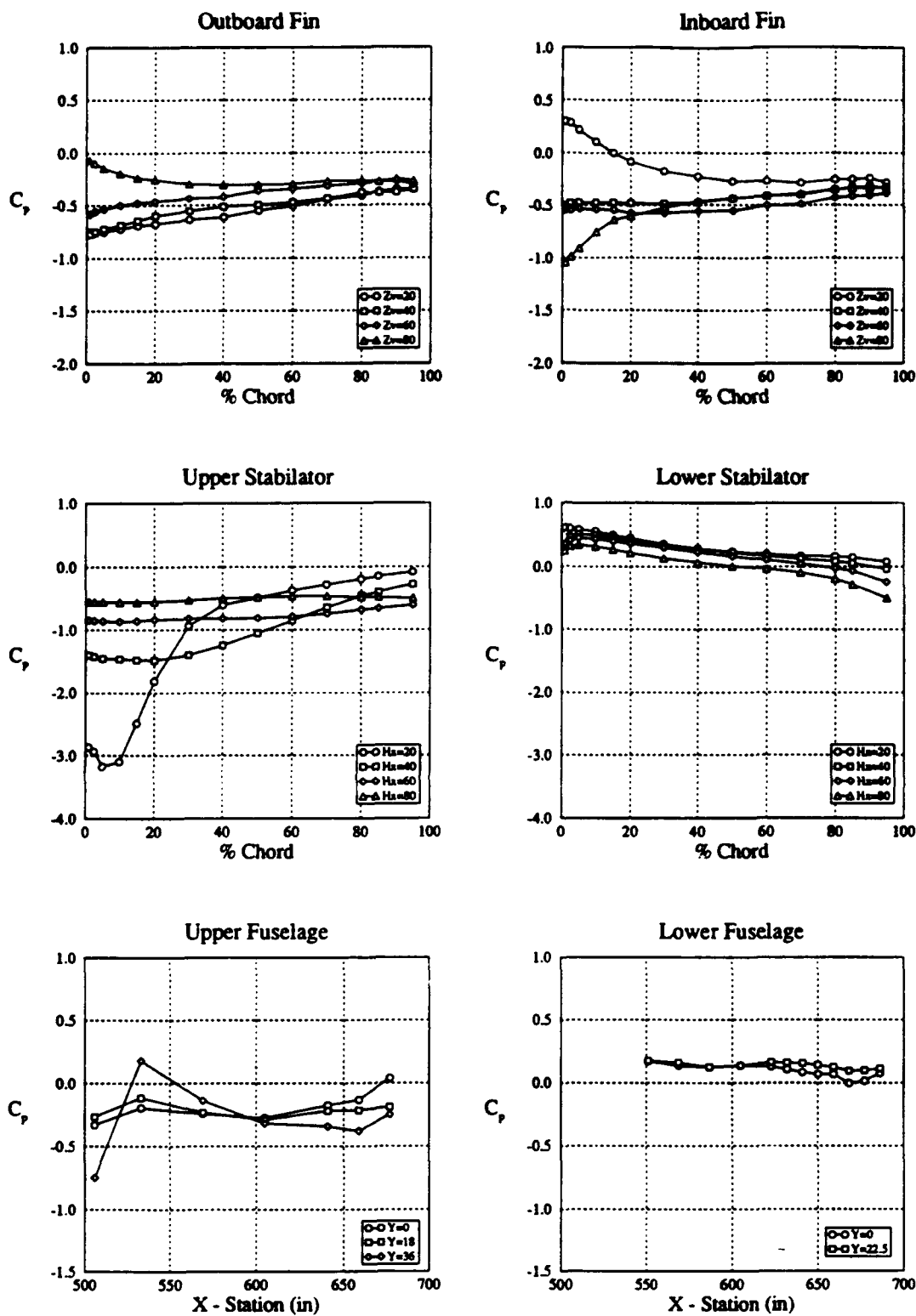
Figure 10 h :   Starboard Side Surface Pressure Distribution for Varying Angle of Attack
$\alpha = 25°, \beta = 0°, \delta = 0°$, LEF= 33.2°, TEF= 0.8°, LEX fence on

36
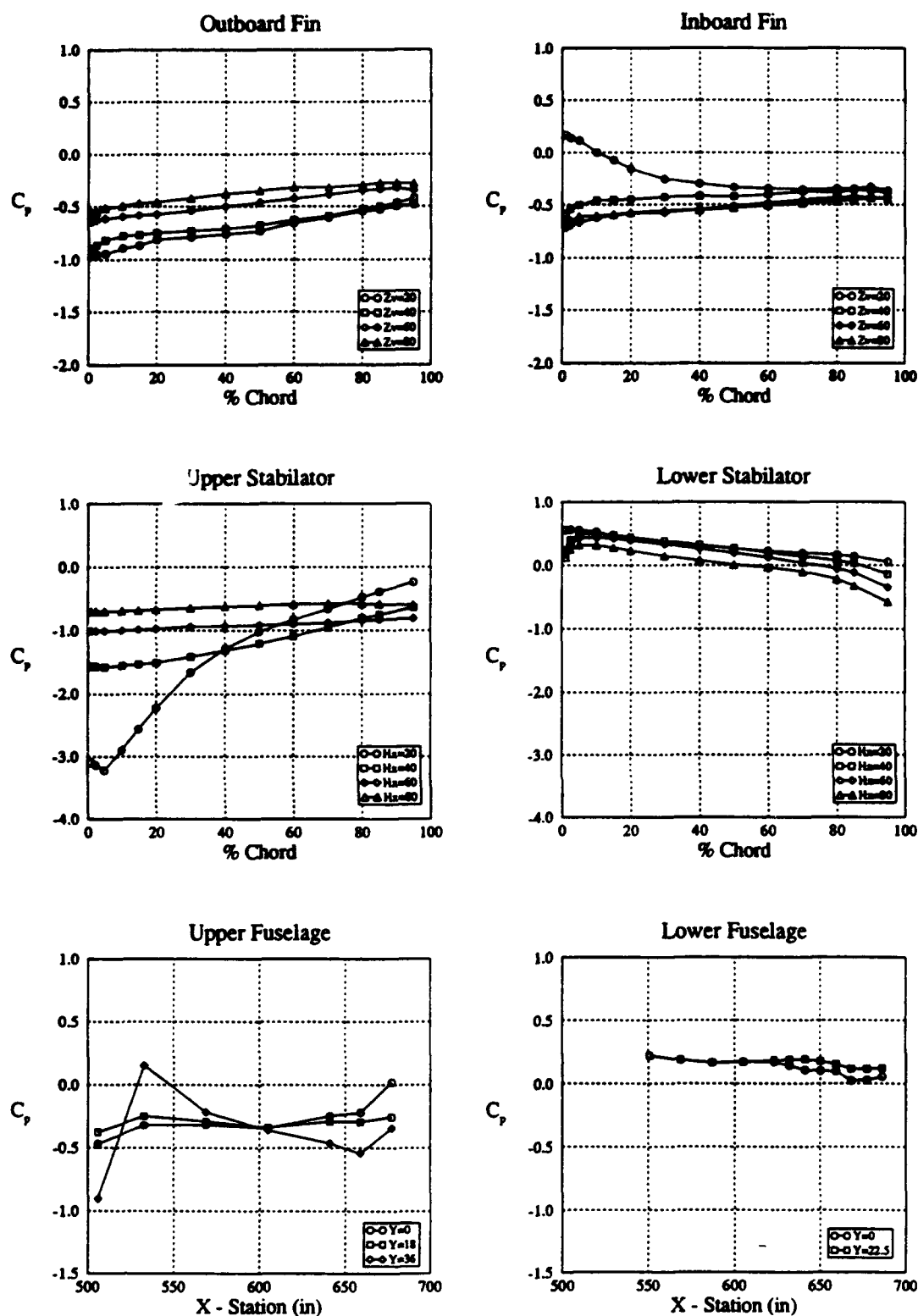
Figure 10 i : Starboard Side Surface Pressure Distribution for Varying Angle of Attack
$\alpha = 30°, \beta = 0°, \delta = 0°$, LEF= 34.0°, TEF= 0.0°, LEX fence on

37
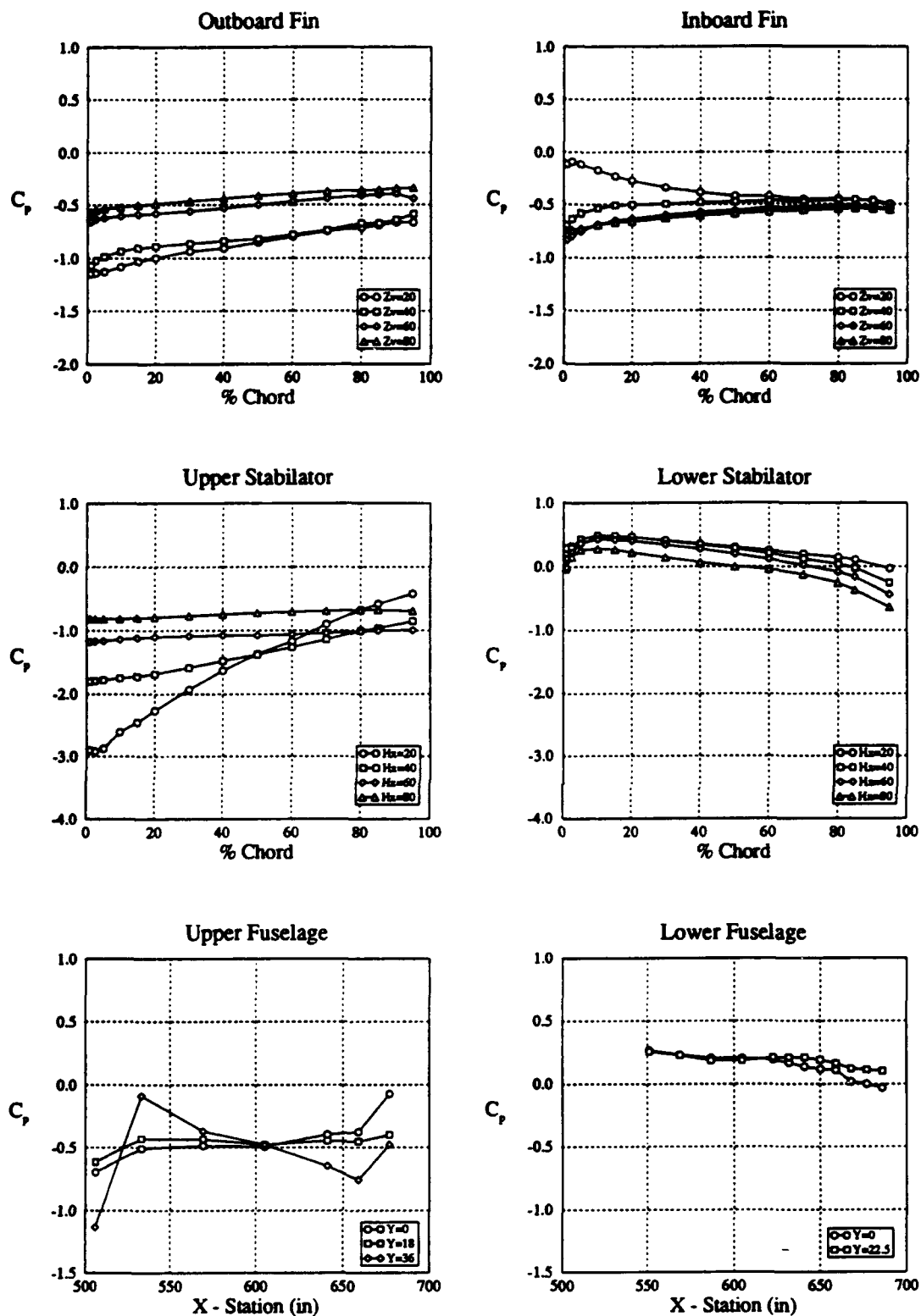
Figure 10 j : Starboard Side Surface Pressure Distribution for Varying Angle of Attack
$\alpha = 35°, \beta = 0°, \delta = 0°$, LEF= 34.0°, TEF= 0.0°, LEX fence on

38
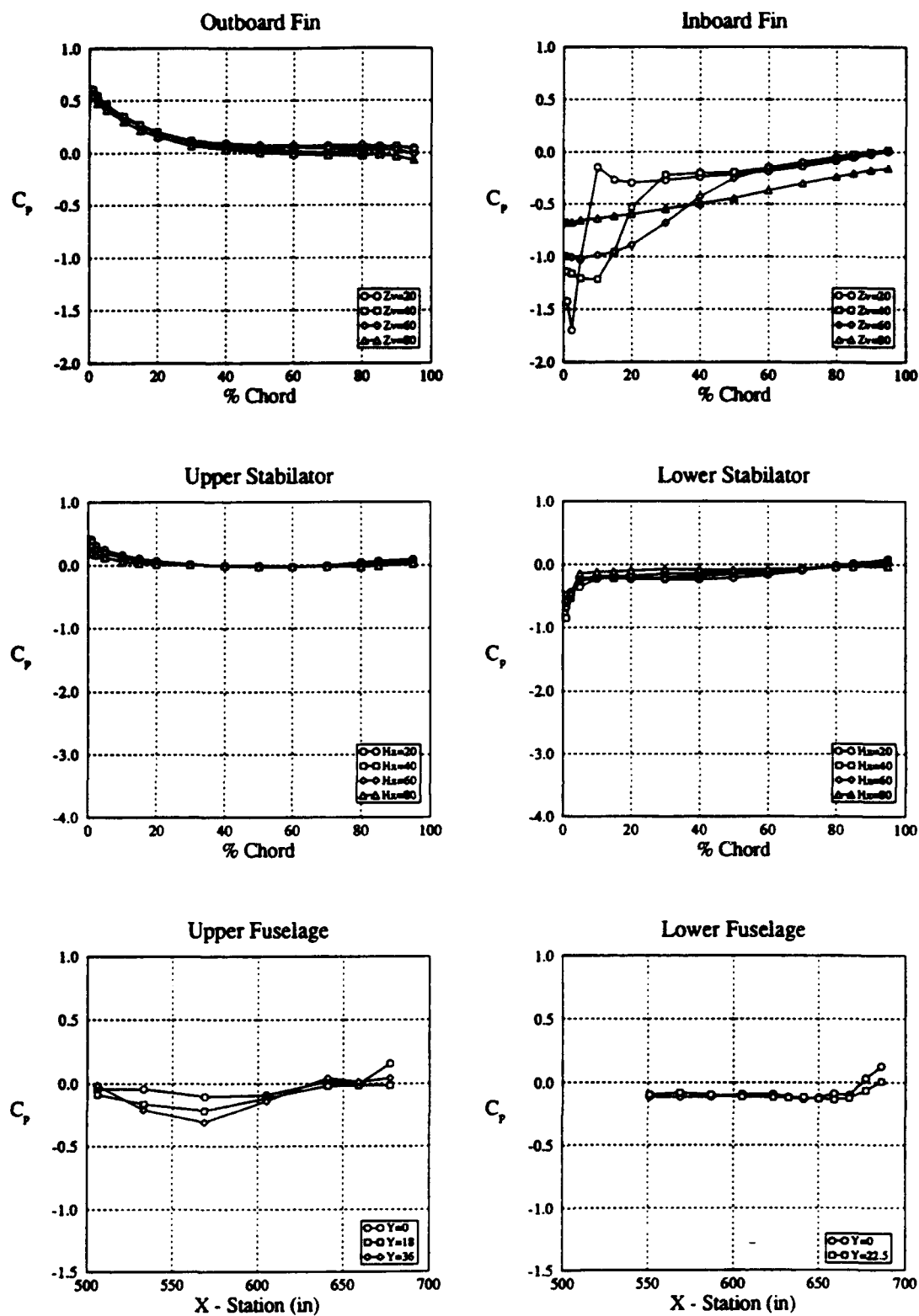
Figure 11 a : Starboard Side Surface Pressure Distribution for Varying Angle of Sideslip
$\alpha = 0°, \beta = 10°, \delta = 0°$, LEF= 0.0°, TEF= 0.0°, LEX fence on
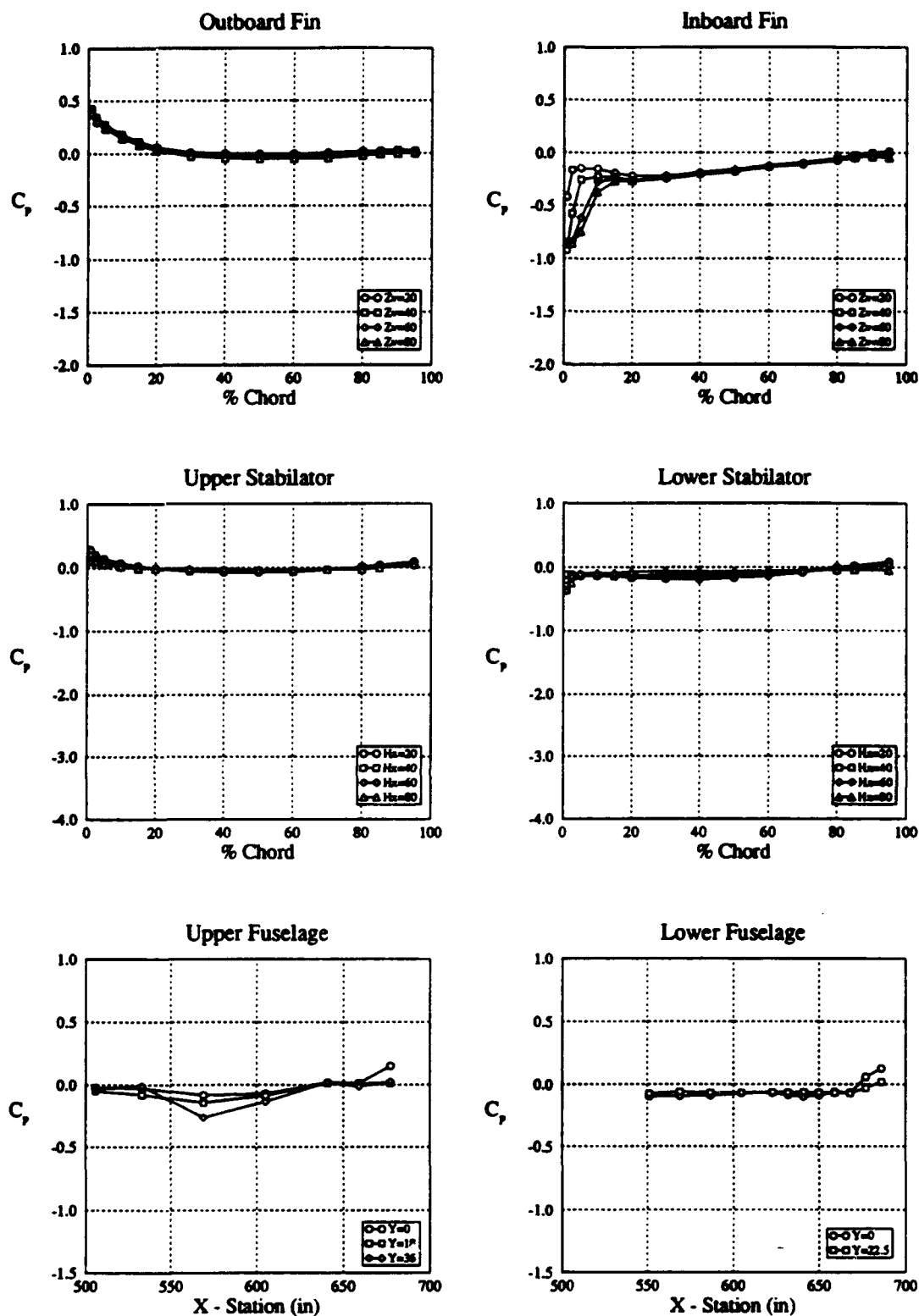
Figure 11 b :   Starboard Side Surface Pressure Distribution for Varying Angle of Sideslip
$\alpha = 0°, \beta = 5°, \delta = 0°$, LEF= 0.0°, TEF= 0.0°, LEX fence on

40
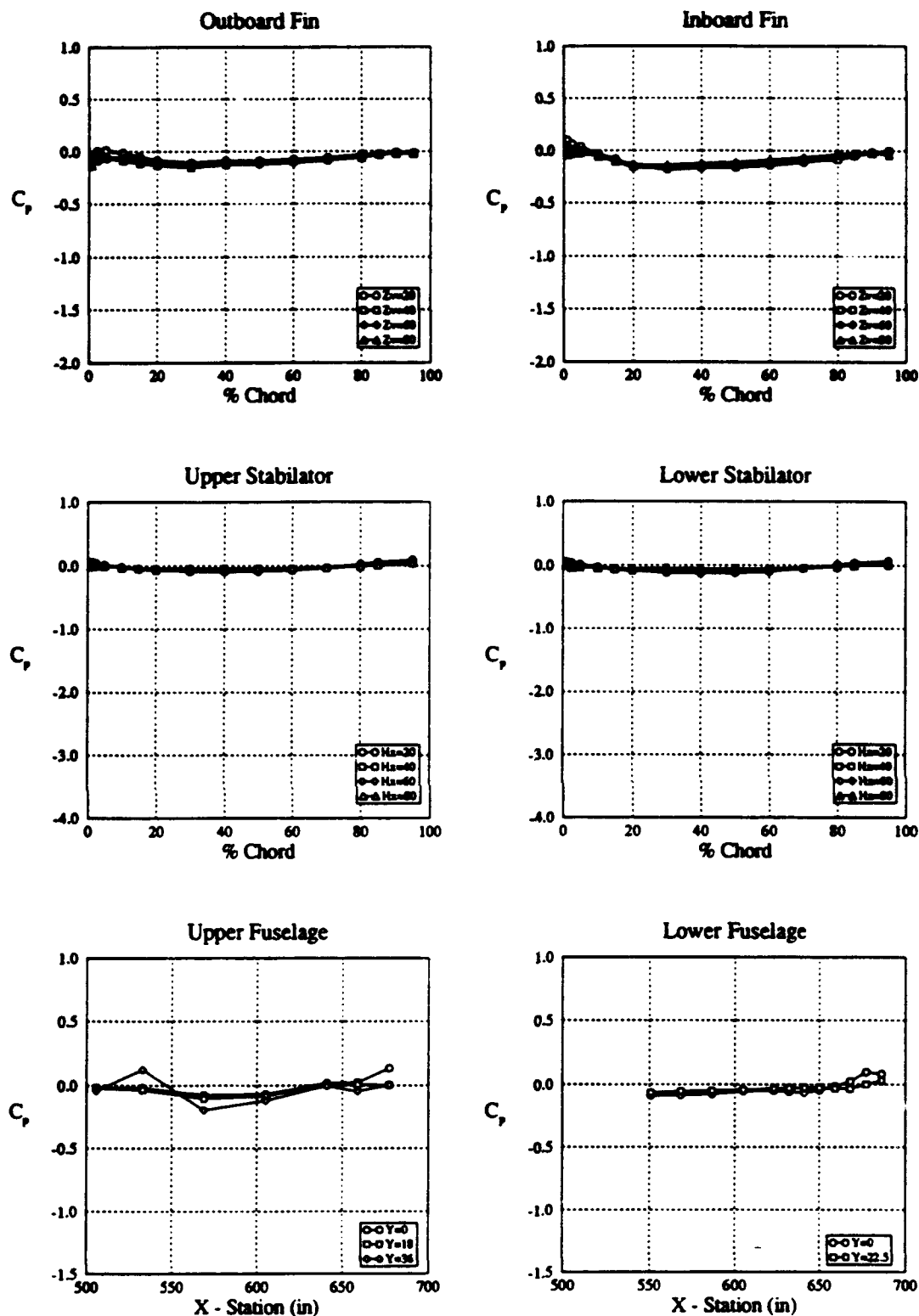
Figure 11 c :   Starboard Side Surface Pressure Distribution for Varying Angle of Sideslip
$\alpha = 0°, \beta = 0°, \delta = 0°$, LEF= 0.0°, TEF= 0.0°, LEX fence on

41

Outboard Fin

Inboard Fin

Upper Stabilator

Lower Stabilator

Upper Fuselage

Lower Fuselage
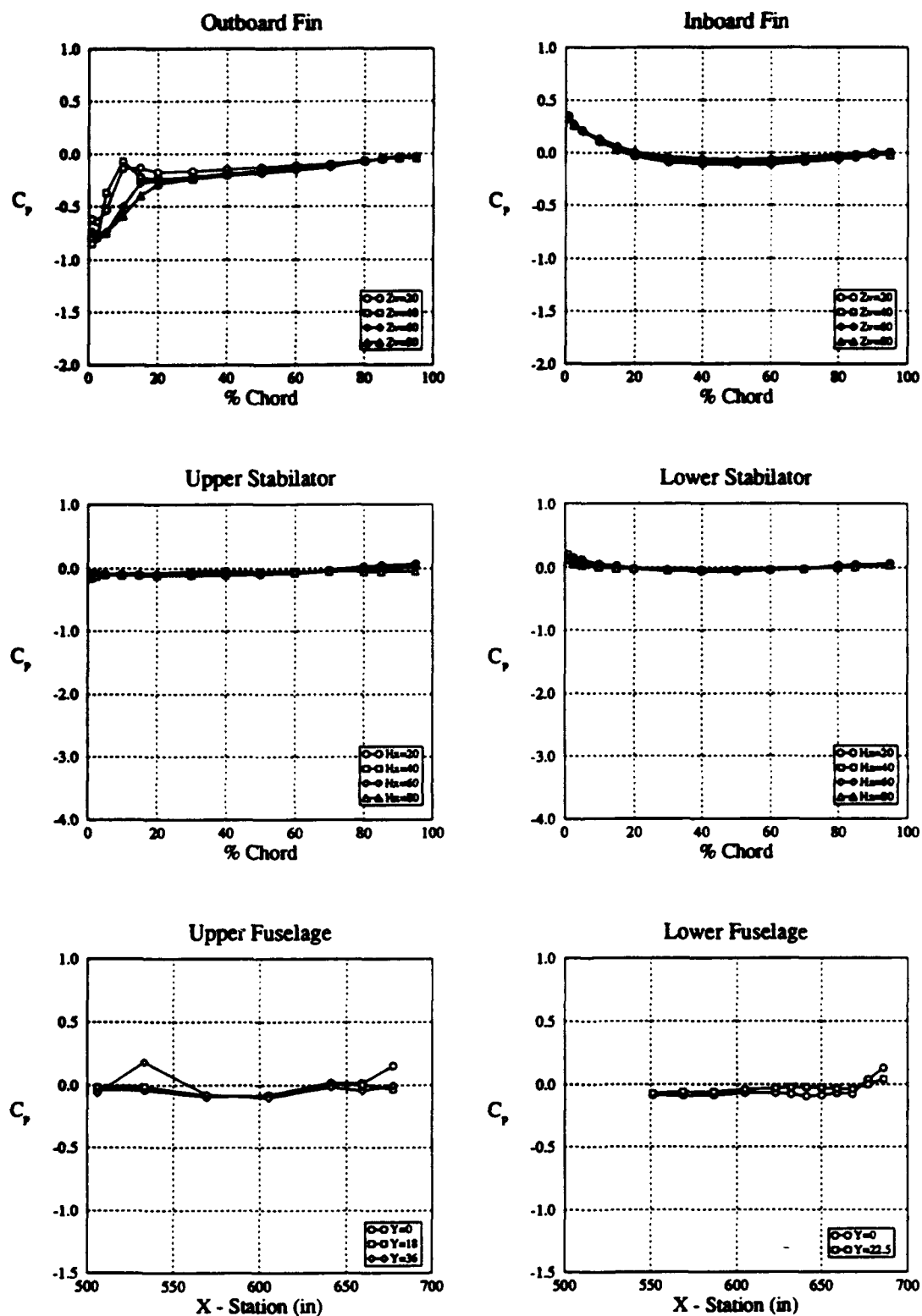
Figure 11 d :   Starboard Side Surface Pressure Distribution for Varying Angle of Sideslip
$\alpha = 0°, \beta = -5°, \delta = 0°$, LEF= 0.0°, TEF= 0.0°, LEX fence on
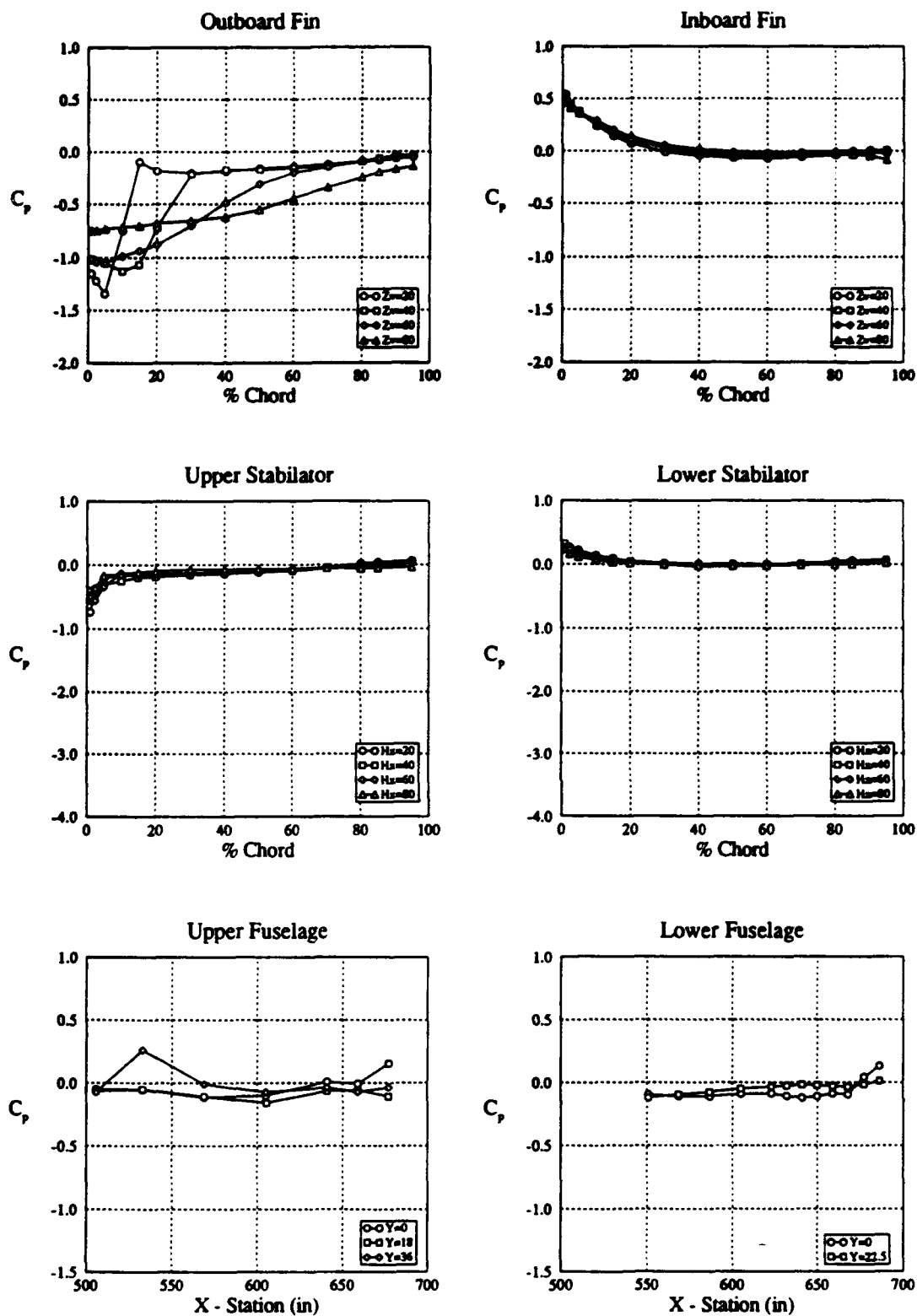
Figure 11 e : Starboard Side Surface Pressure Distribution for Varying Angle of Sideslip $\alpha = 0°, \beta = -10°, \delta = 0°$, LEF= 0.0°, TEF= 0.0°, LEX fence on

43
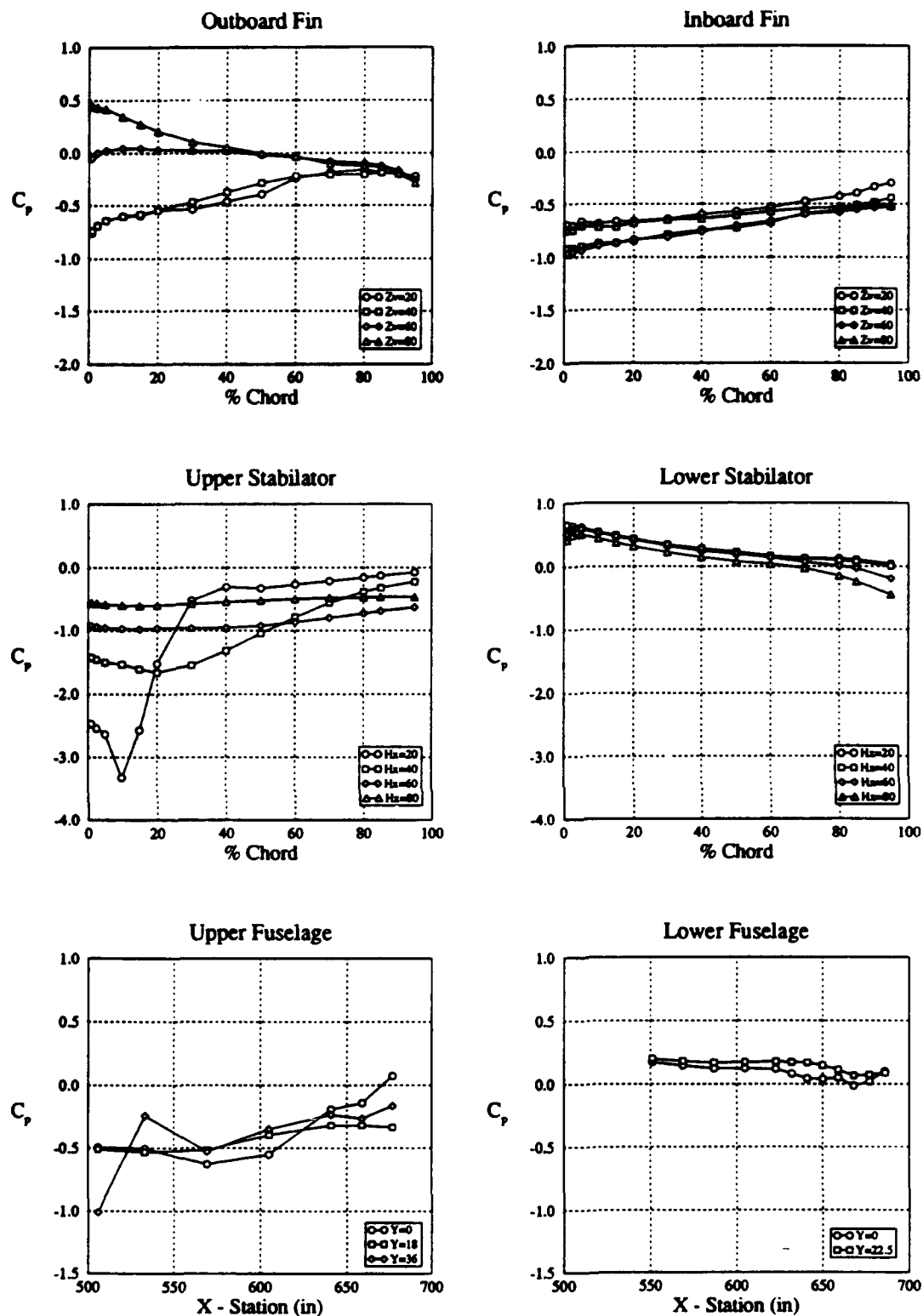
Figure 12 a : Starboard Side Surface Pressure Distribution for Varying Angle of Sideslip
$\alpha = 25°, \beta = 10°, \delta = 0°$, LEF= 33.2°, TEF= 0.8°, LEX fence on

44
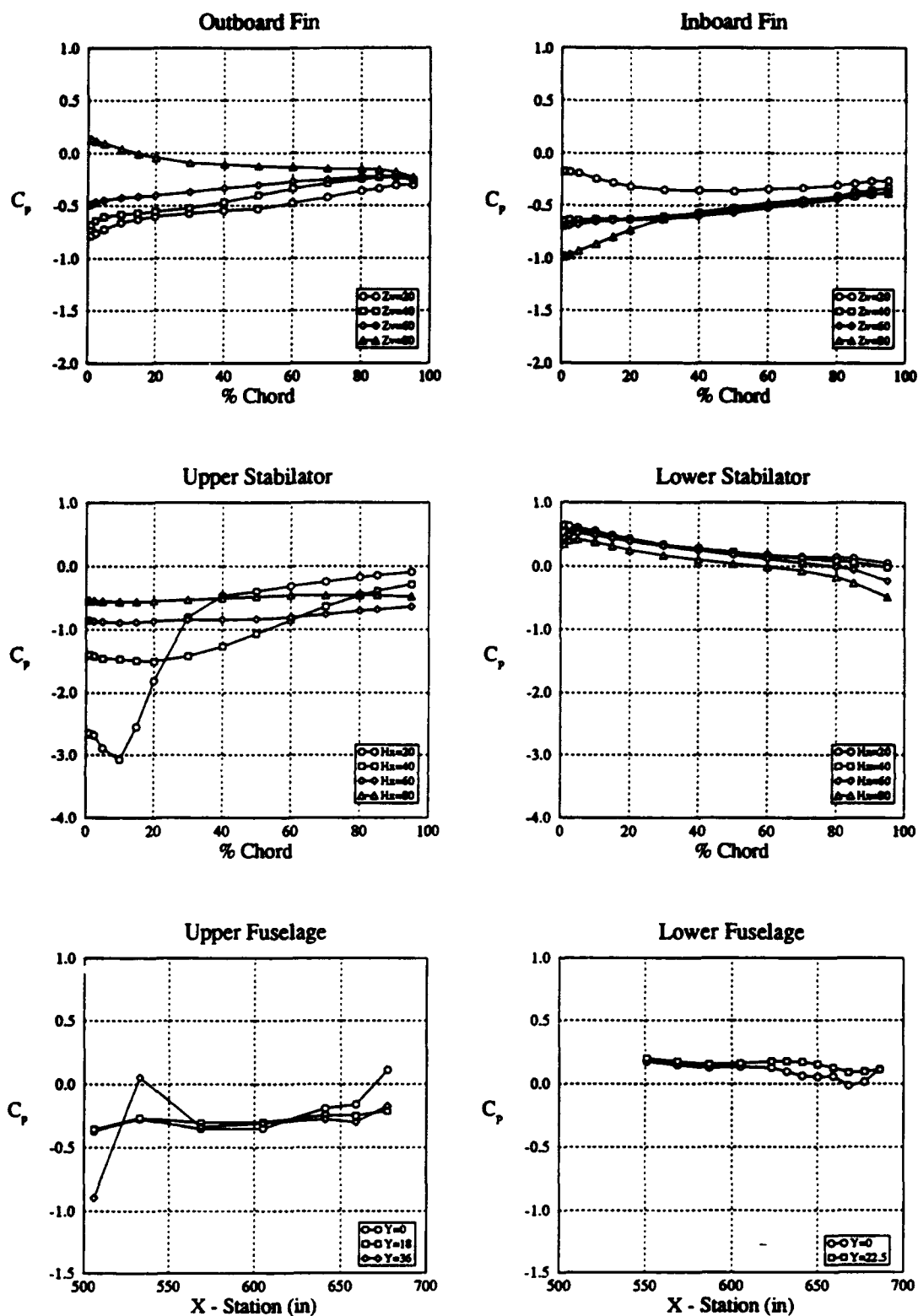
Figure 12 b : Starboard Side Surface Pressure Distribution for Varying Angle of Sideslip
$\alpha = 25°, \beta = 5°, \delta = 0°$, LEF= 33.2°, TEF= 0.8°, LEX fence on

45
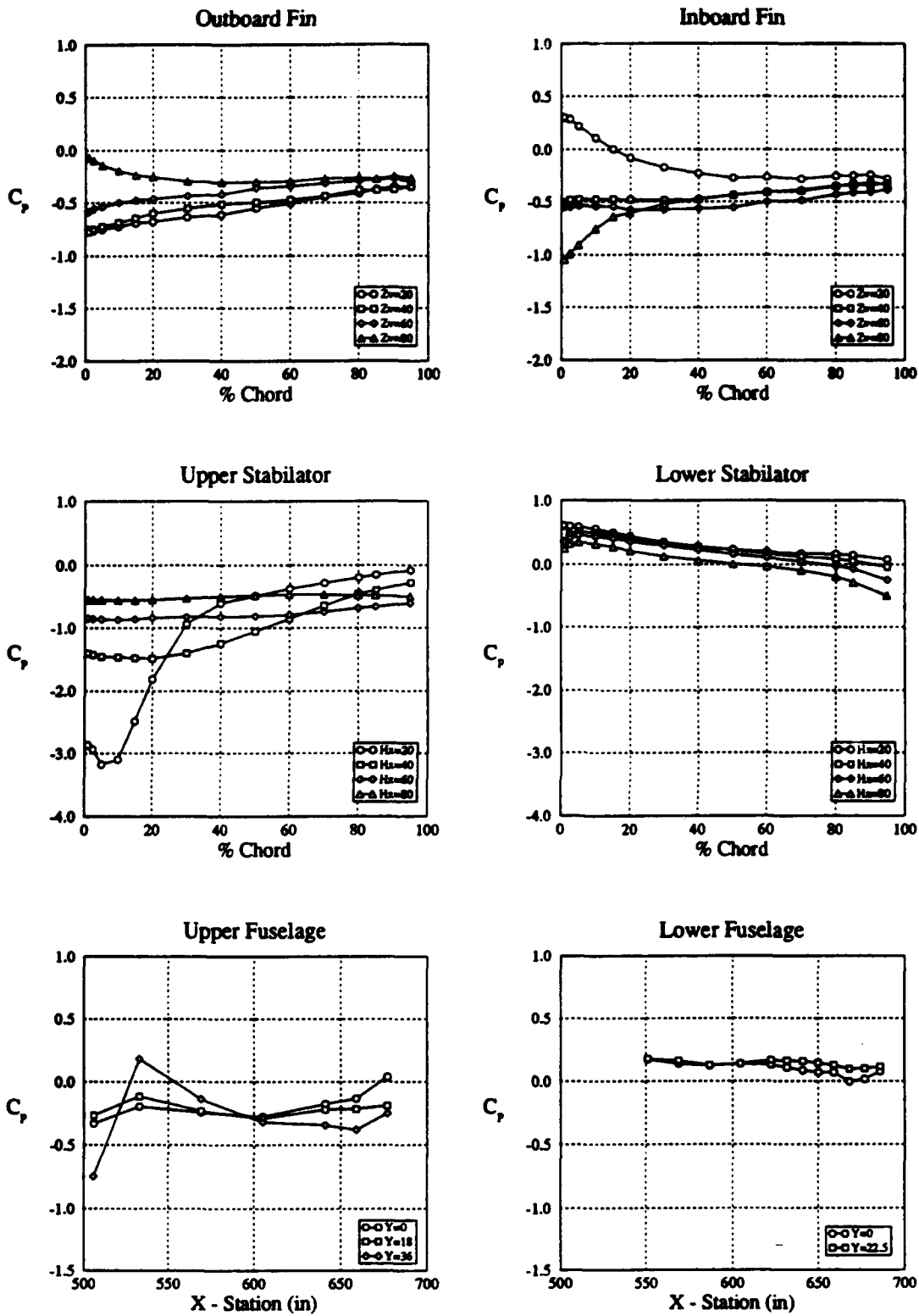
Figure 12 c :   Starboard Side Surface Pressure Distribution for Varying Angle of Sideslip
$\alpha = 25°, \beta = 0°, \delta = 0°$, LEF= 33.2°, TEF= 0.8°, LEX fence on

46
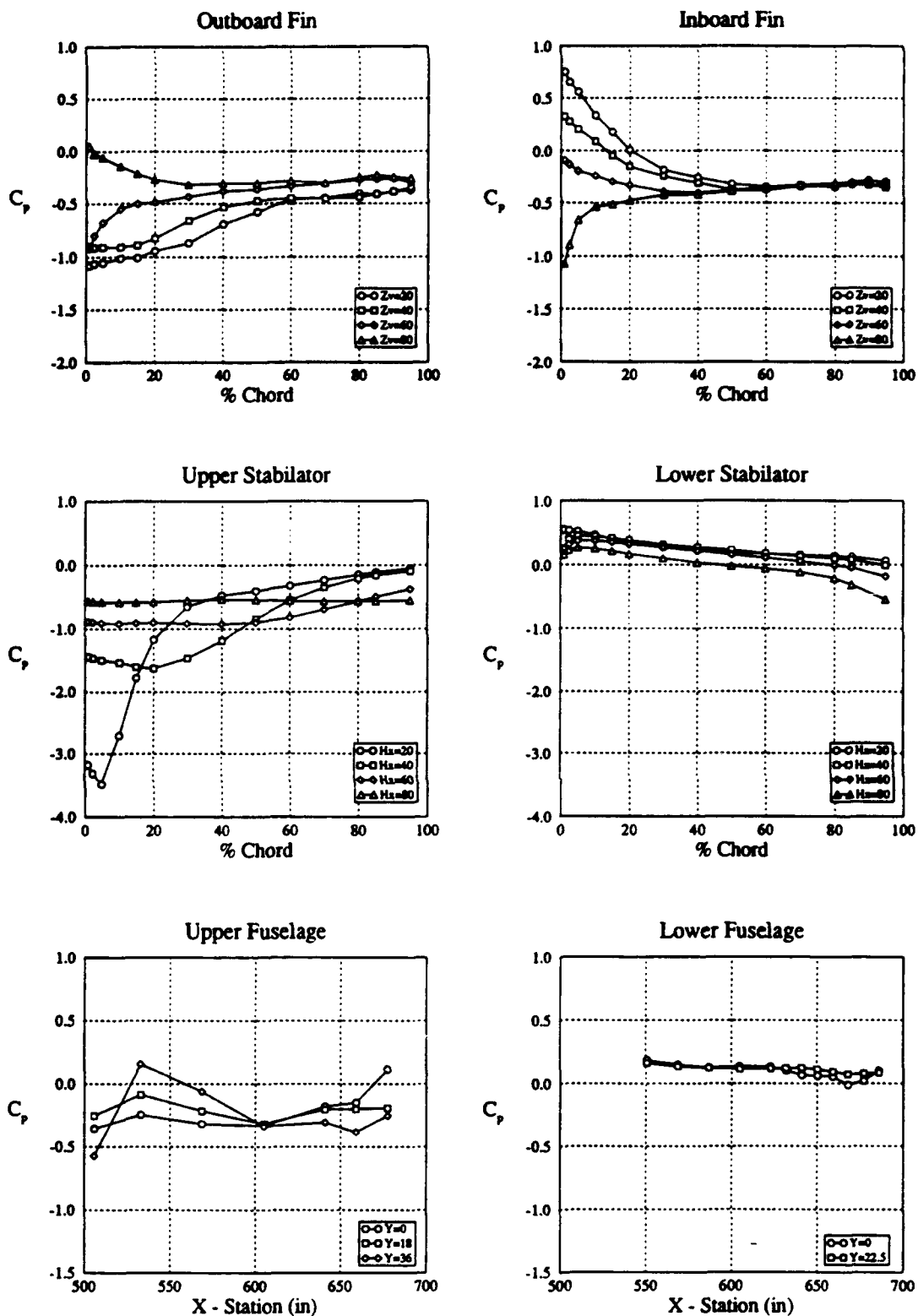
Figure 12 d :   Starboard Side Surface Pressure Distribution for Varying Angle of Sideslip
$\alpha = 25°, \beta = -5°, \delta = 0°$, LEF= 33.2°, TEF= 0.8°, LEX fence on
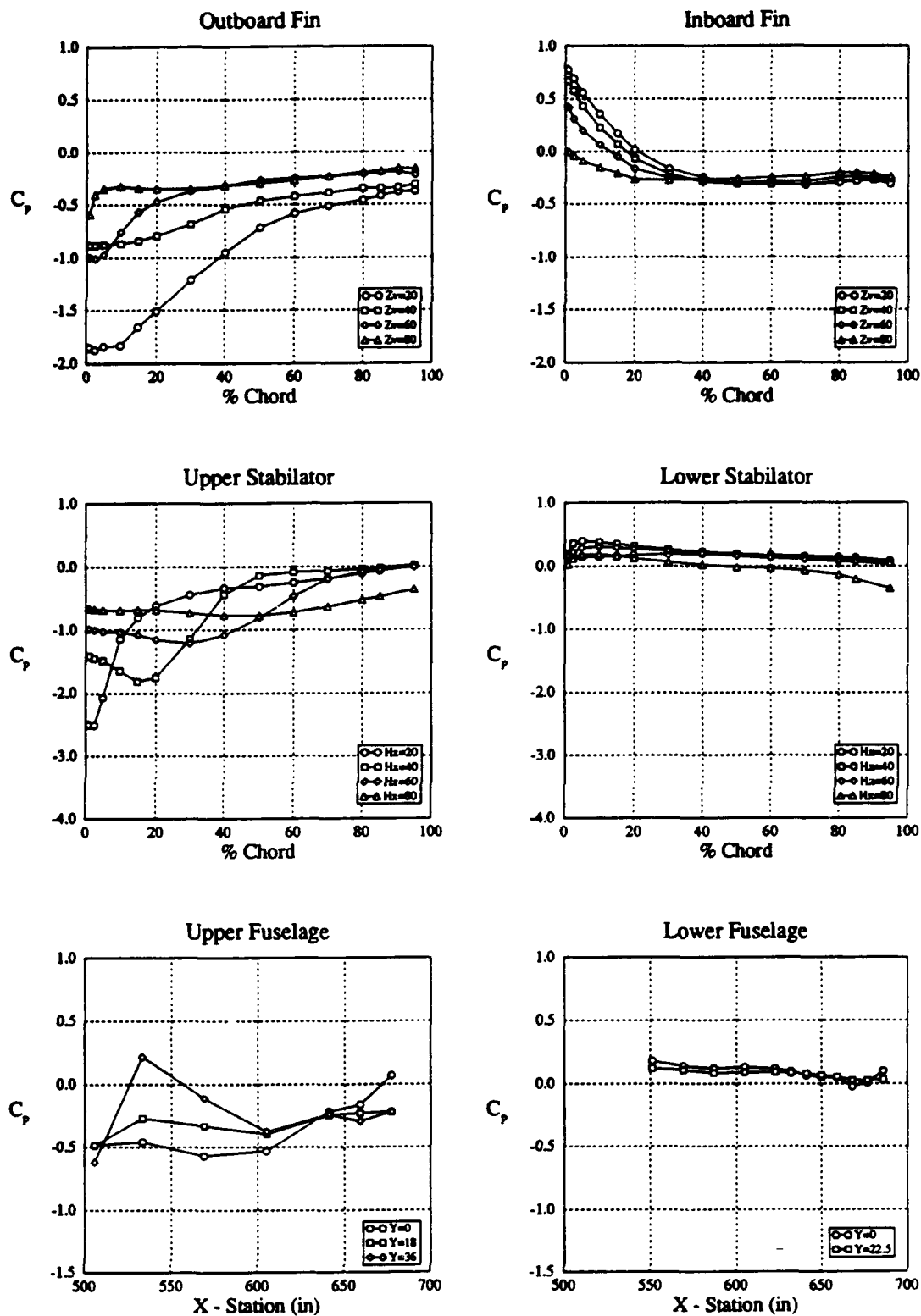
Figure 12 e :   Starboard Side Surface Pressure Distribution for Varying Angle of Sideslip
$\alpha = 25°, \beta = -10°, \delta = 0°$, LEF= 33.2°, TEF= 0.8°, LEX fence on
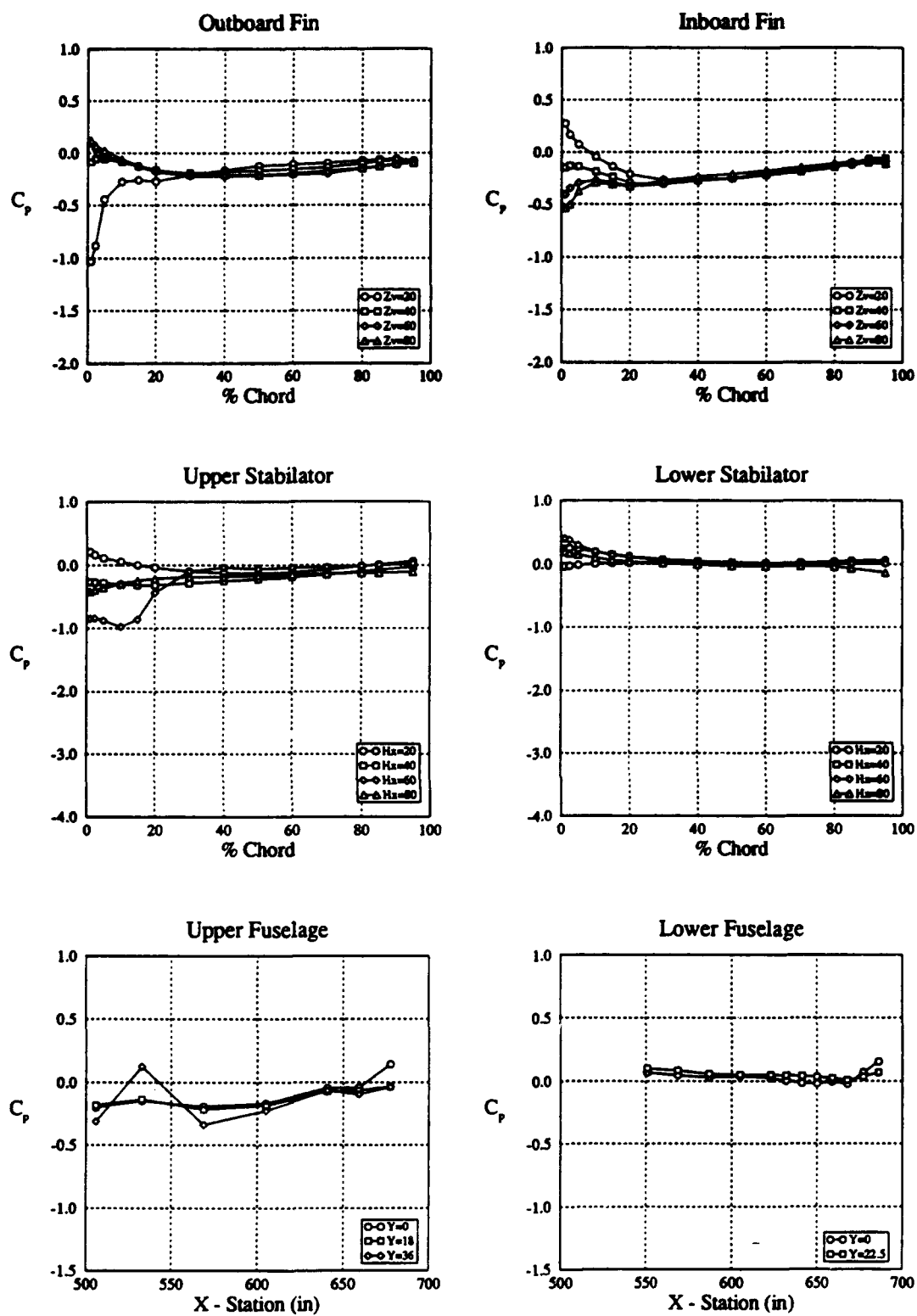
Figure 13 a :   Starboard Side Surface Pressure Distribution for Varying Stabilator Deflection
$\alpha = 10°, \beta = 0°, \delta = 5°$, LEF= 13.3°, TEF= 14.0°, LEX fence on
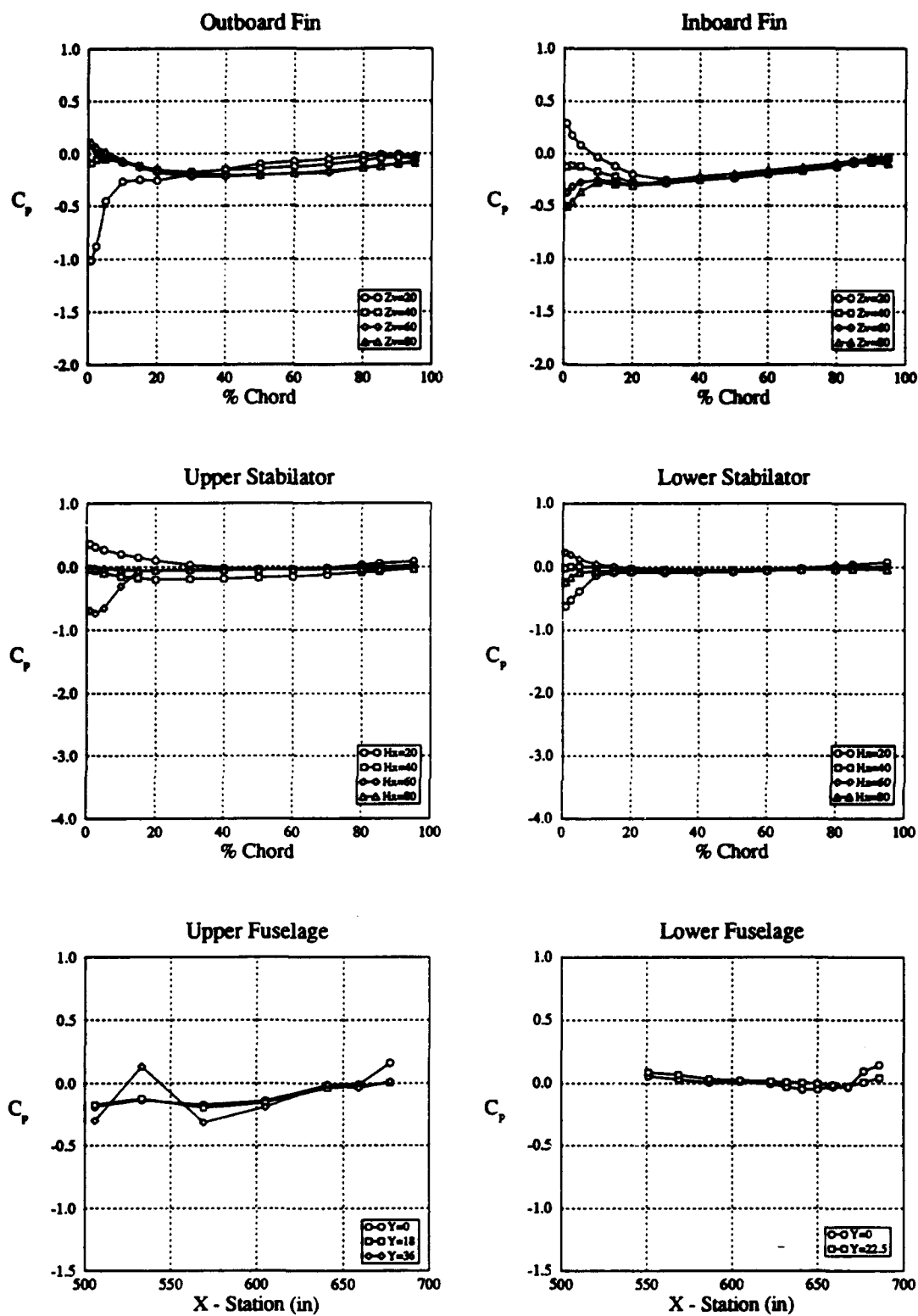
Figure 13 b : Starboard Side Surface Pressure Distribution for Varying Stabilator Deflection
$\alpha = 10°, \beta = 0°, \delta = 0°$, LEF= 13.3°, TEF= 14.0°, LEX fence on
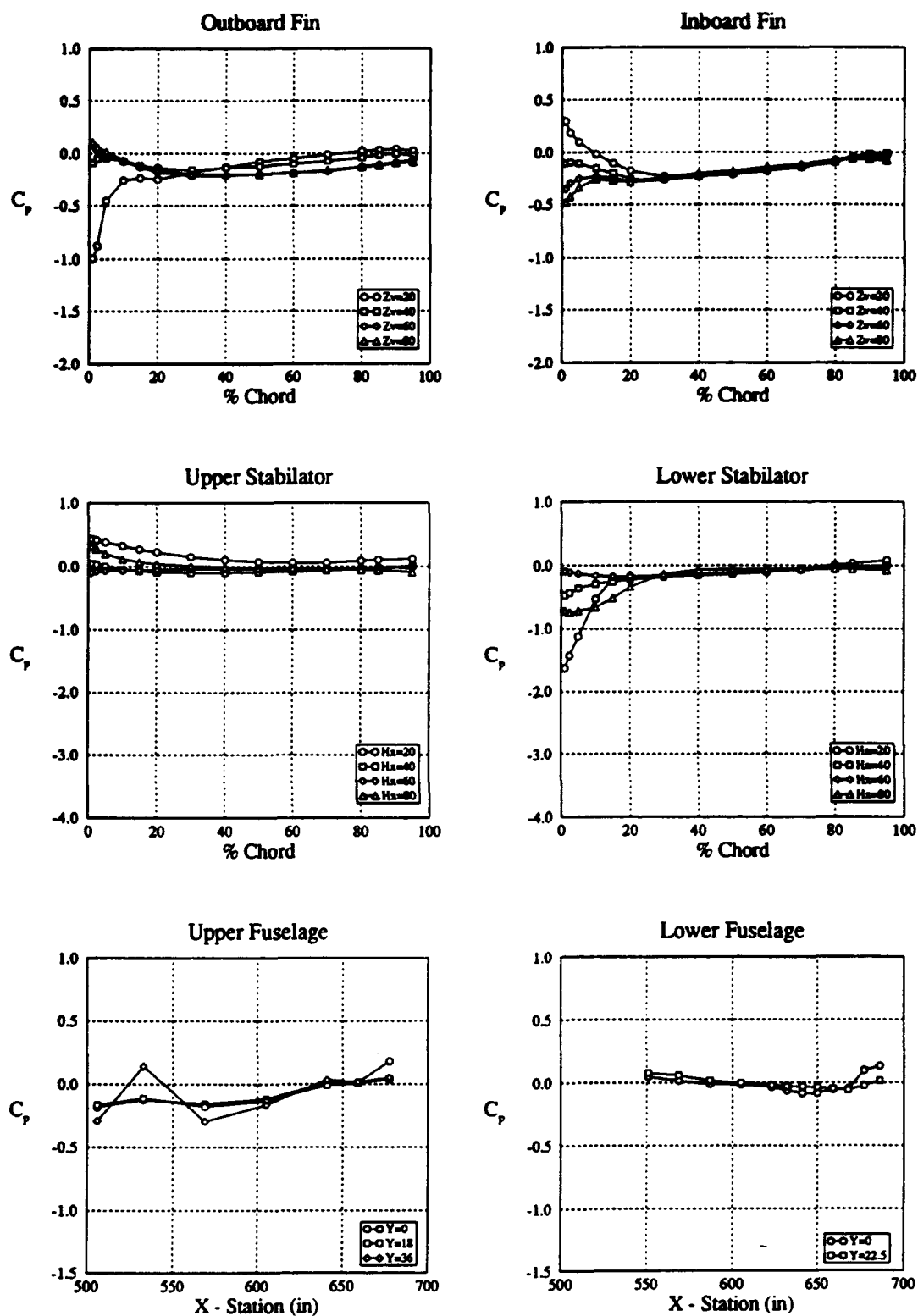
Figure 13 c :   Starboard Side Surface Pressure Distribution for Varying Stabilator Deflection
$\alpha = 10°, \beta = 0°, \delta = -5°$, LEF= 13.3°, TEF= 14.0°, LEX fence on

51
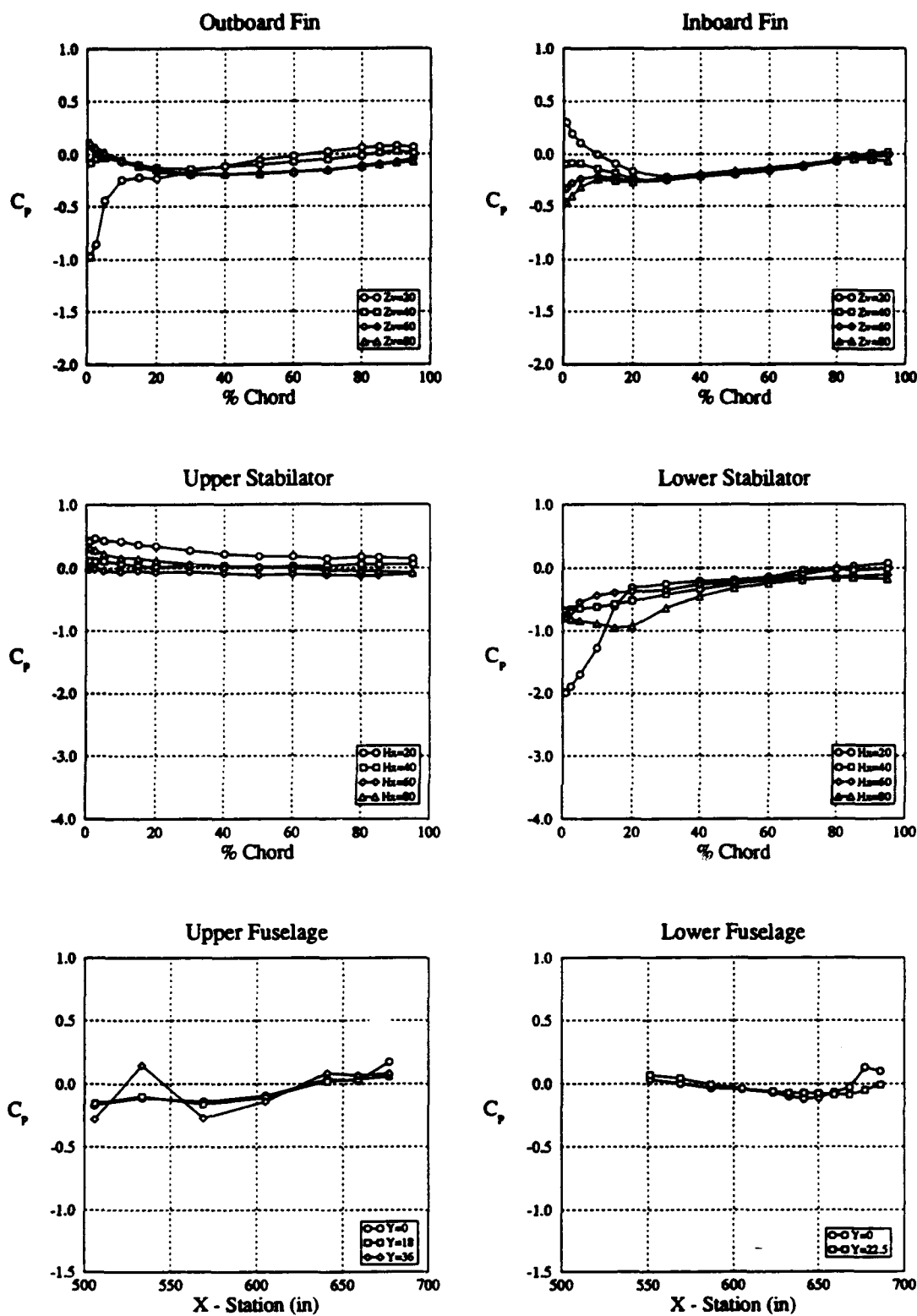
Figure 13 d : Starboard Side Surface Pressure Distribution for Varying Stabilator Deflection
$\alpha = 10°, \beta = 0°, \delta = -10°$, LEF= 13.3°, TEF= 14.0°, LEX fence on
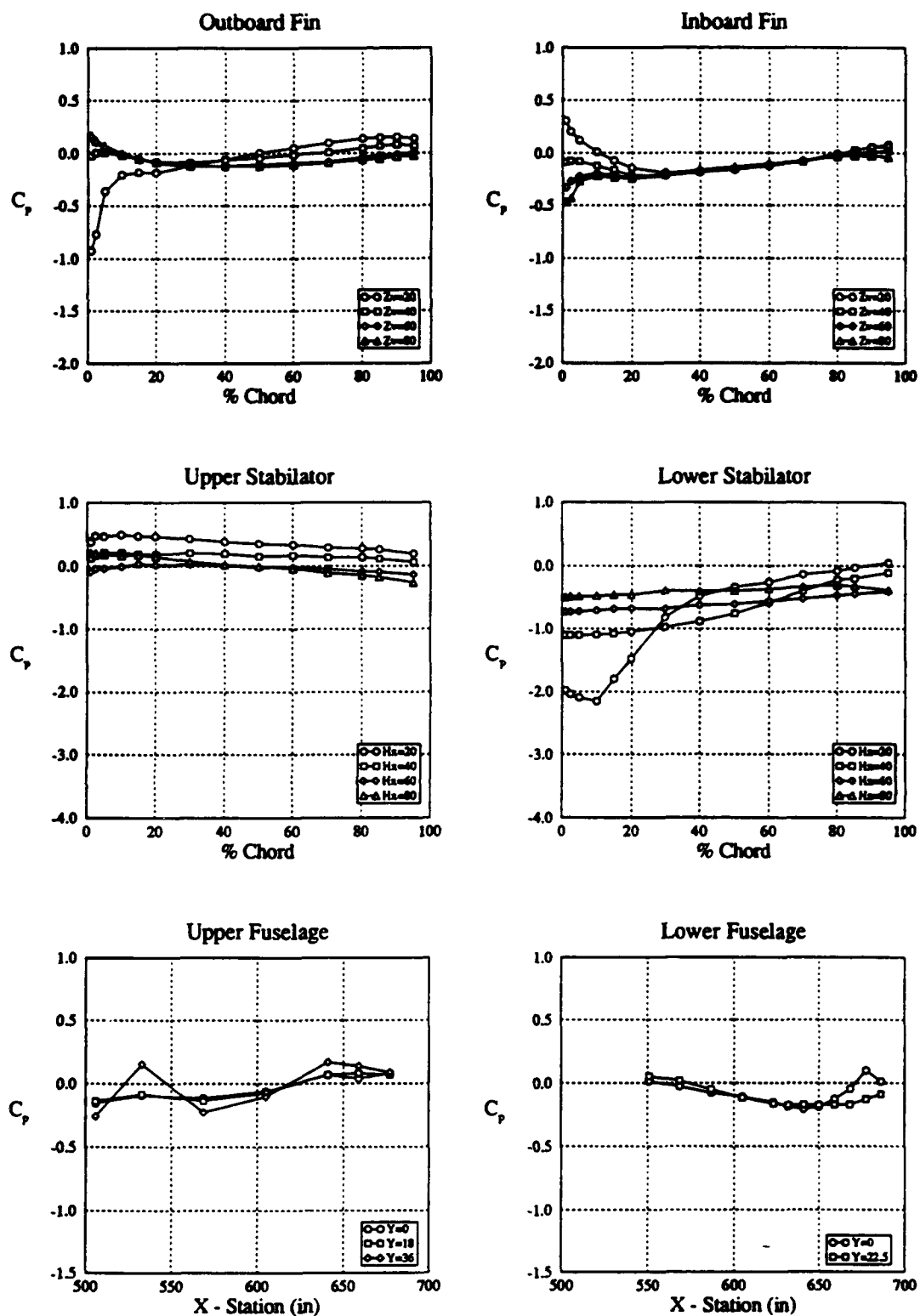
Figure 13 e : Starboard Side Surface Pressure Distribution for Varying Stabilator Deflection
$\alpha = 10°, \beta = 0°, \delta = -20°$, LEF= 13.3°, TEF= 14.0°, LEX fence on
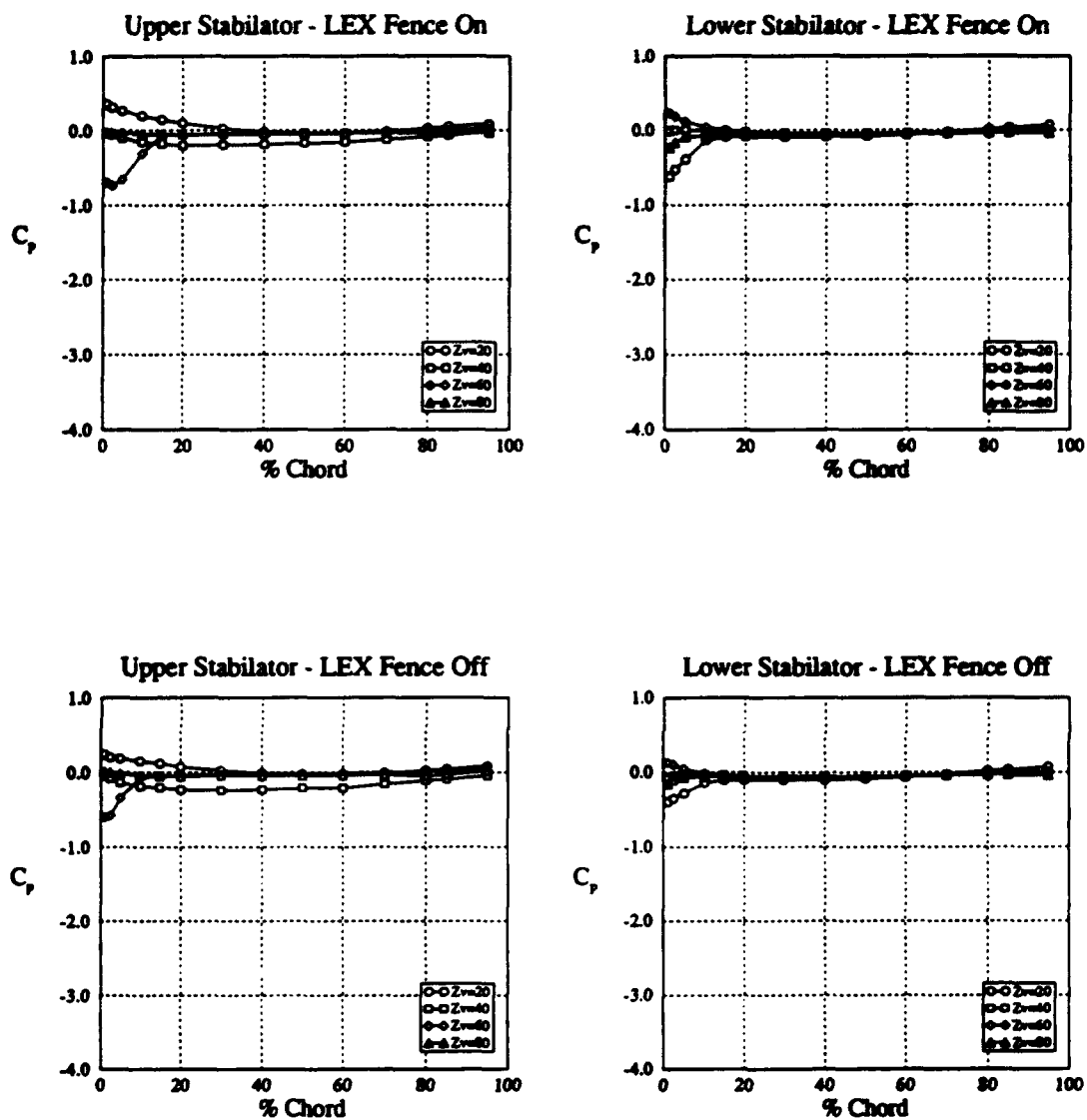
Figure 14 a :   Starboard Stabilator Surface Pressure Distribution for LEX Fence On and Off
$\alpha = 10°, \beta = 0°, \delta = 0°$, LEF= 13.3°, TEF= 14.0°
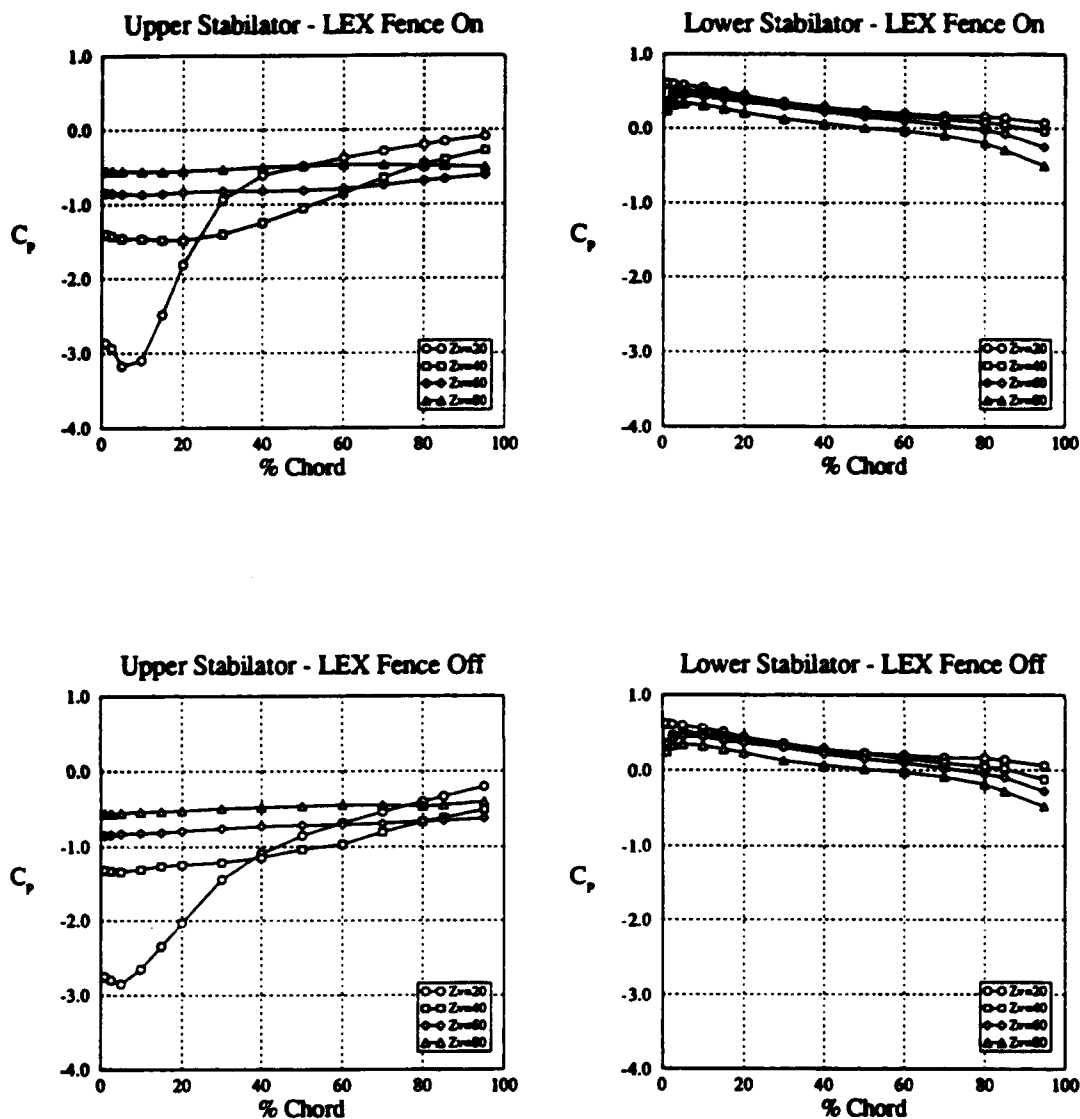
Figure 14 b : Starboard Stabilator Surface Pressure Distribution for LEX Fence On and Off
$\alpha = 25°, \beta = 0°, \delta = 0°$, LEF= 33.2°, TEF= 0.8°

55
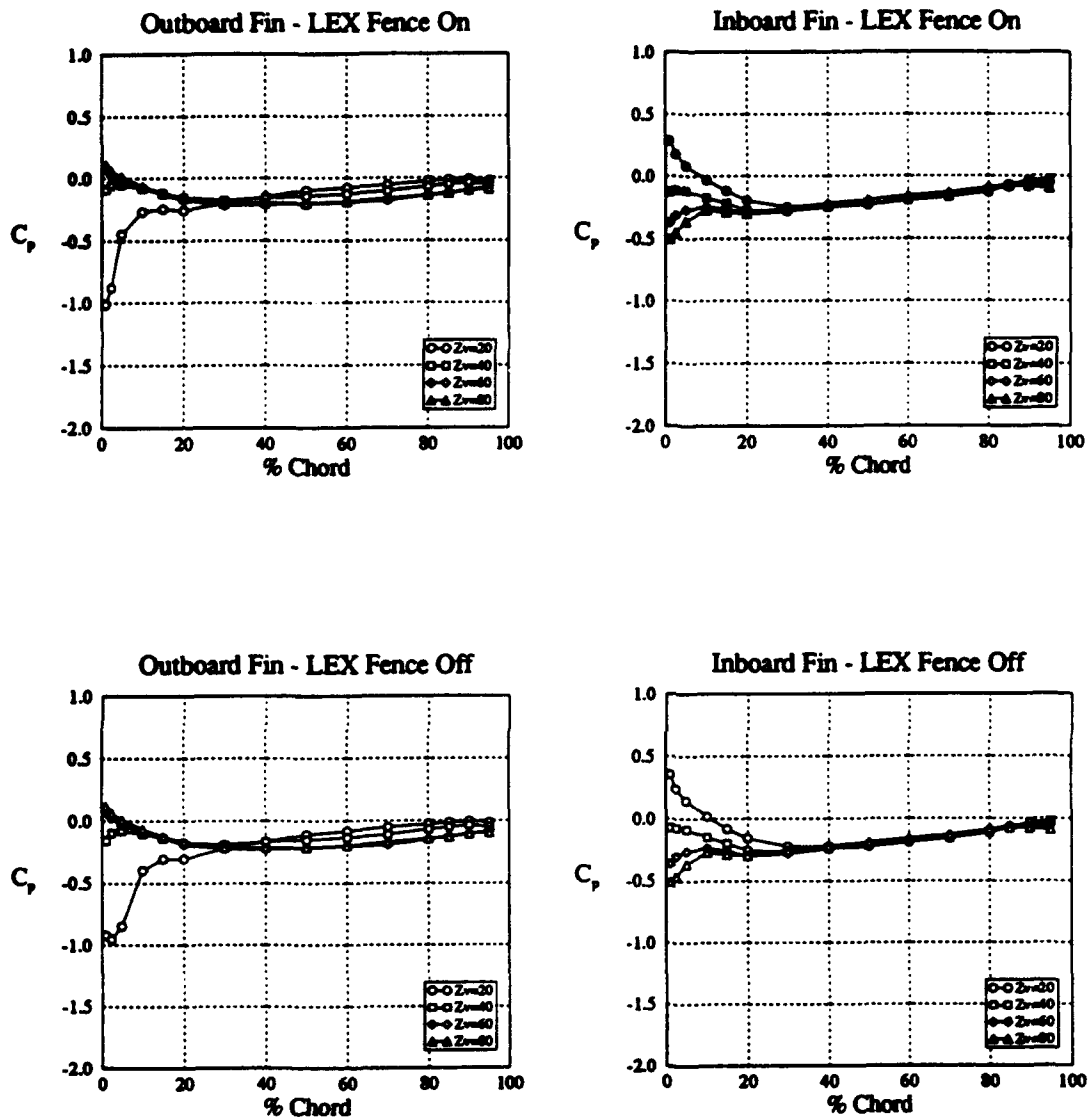
Figure 15 a :   Starboard Fin Surface Pressure Distribution for LEX Fence On and Off
$\alpha = 10°, \beta = 0°, \delta = 0°$, LEF= 13.3°, TEF= 14.0°
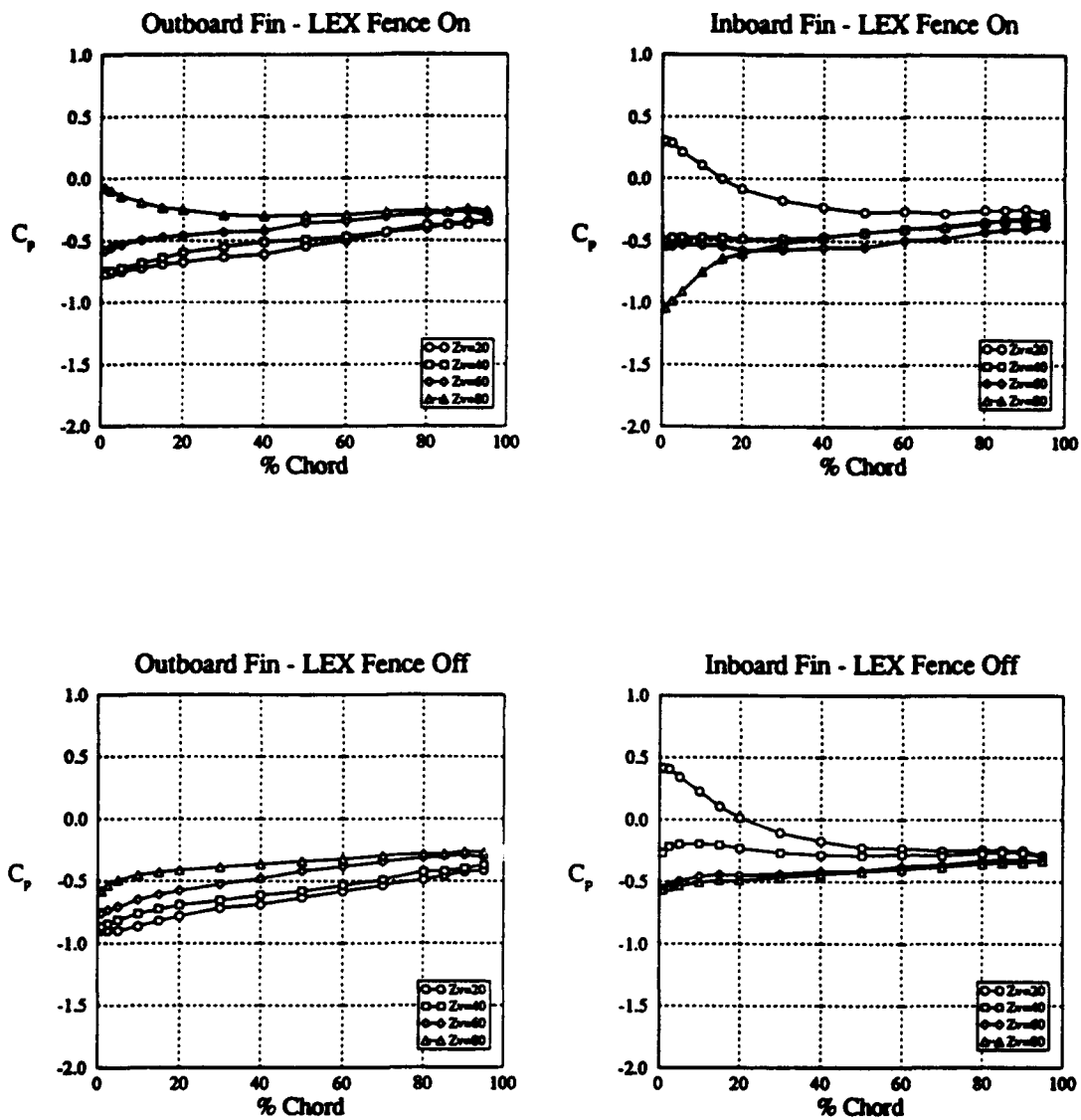
Figure 15 b :   Starboard Fin Surface Pressure Distribution for LEX Fence On and Off
$\alpha = 25°, \beta = 0°, \delta = 0°$. LEF= 33.2°, TEF= 0.8°
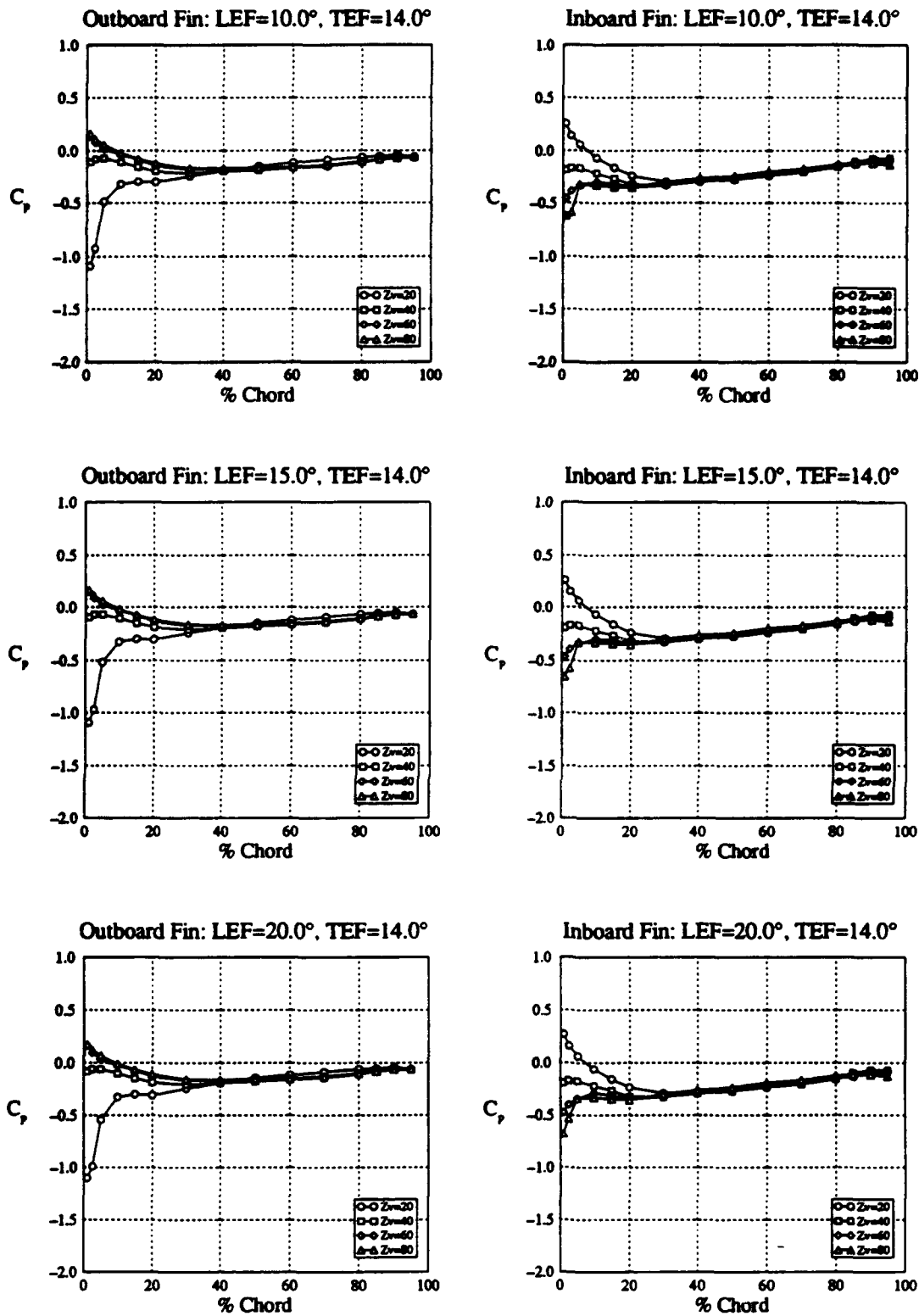
Figure 16 a :   Starboard Fin Surface Pressure Distribution
                 for Varying Leading Edge Flap Deflection
                 $\alpha = 10°, \beta = 0°, \delta = 0°$, TEF= 14.0°, LEX fence on
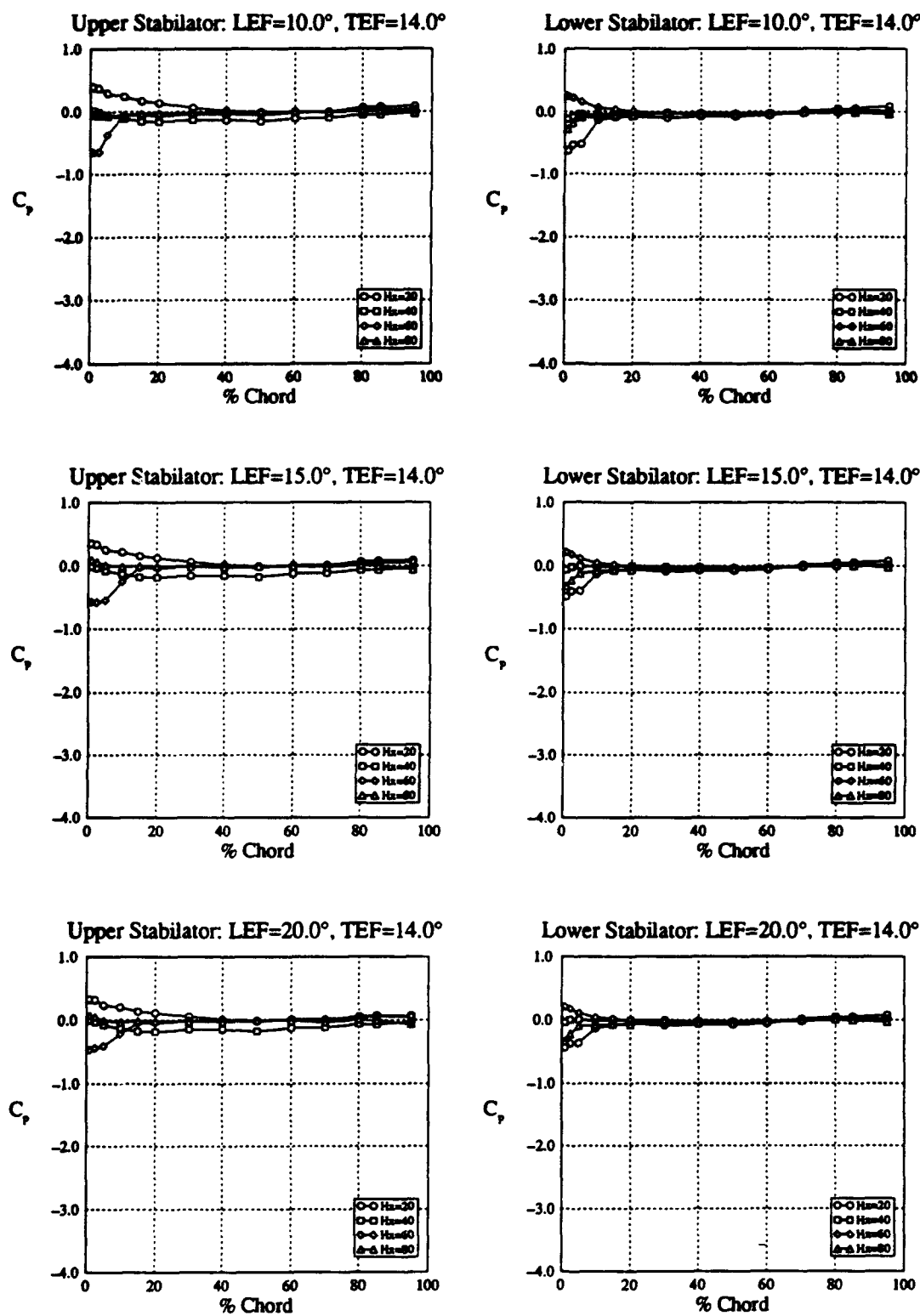
Figure 16 b : Starboard Stabilator Surface Pressure Distribution
for Varying Leading Edge Flap Deflection
$\alpha = 10°, \beta = 0°, \delta = 0°$, TEF= 14.0°. LEX fence on

59
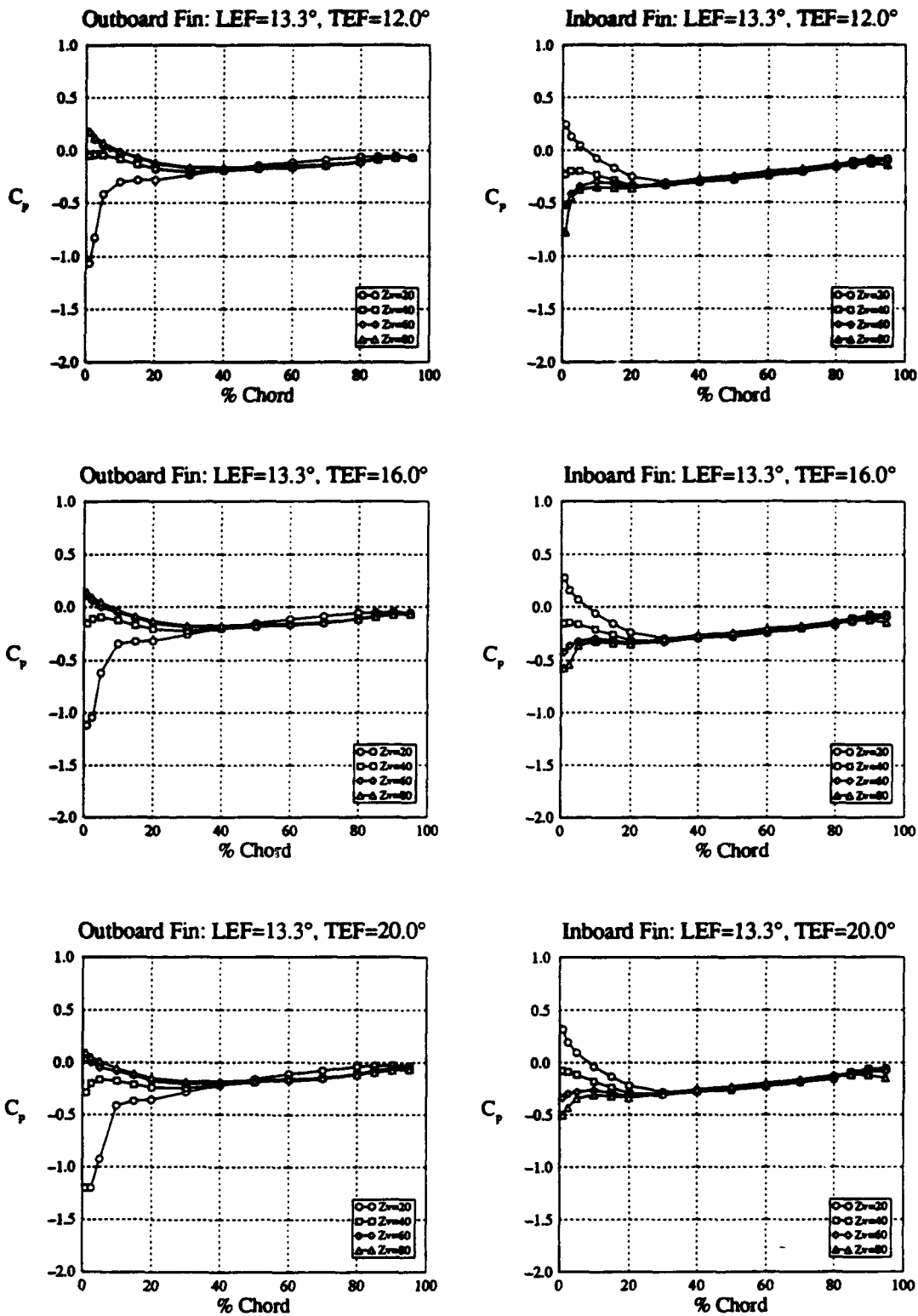
Figure 17 a : Starboard Fin Surface Pressure Distribution
for Varying Trailing Edge Flap Deflection
$\alpha = 10°, \beta = 0°, \delta = 0°$, LEF= 13.3°, LEX fence on

60
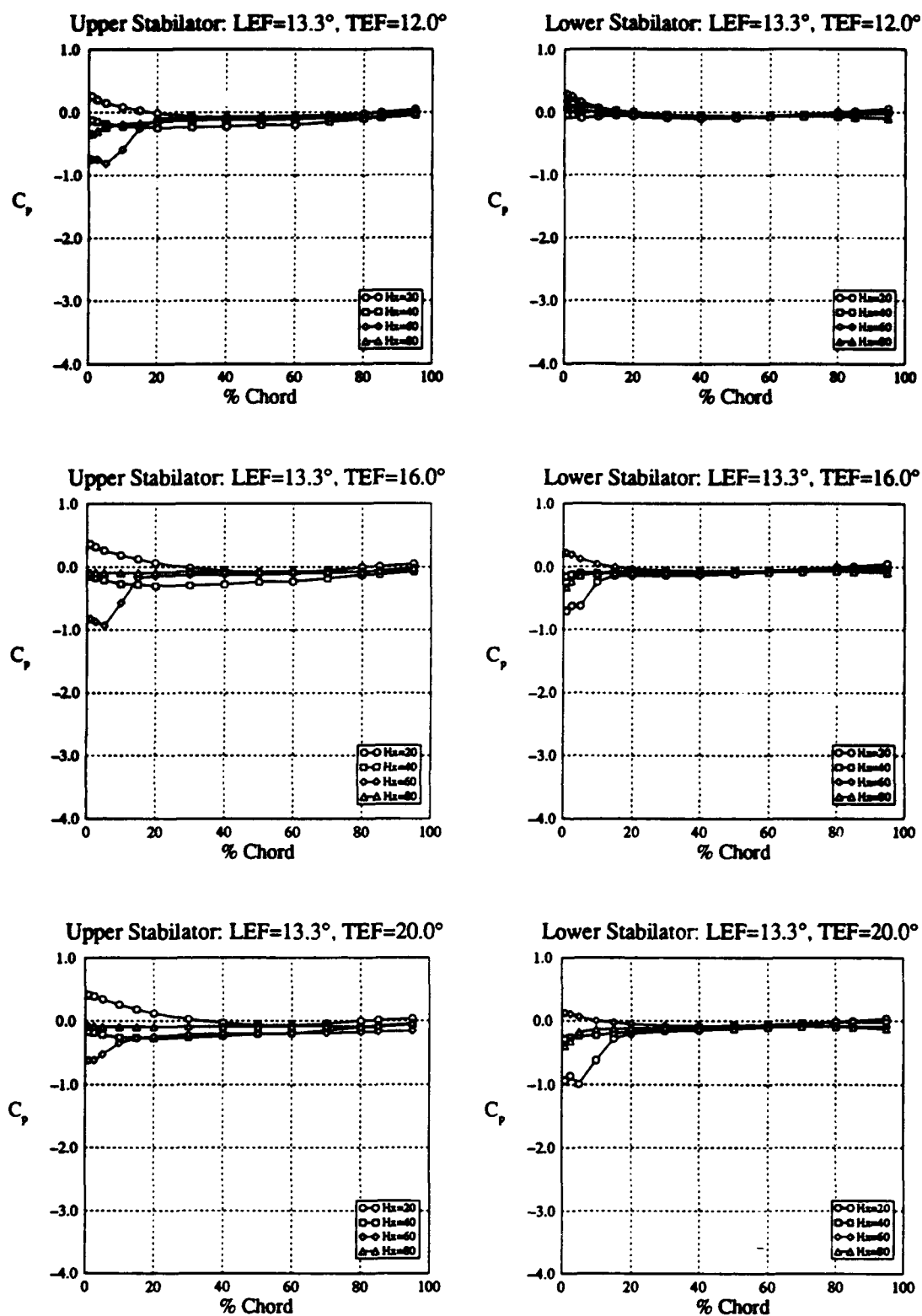
Figure 17 b :   Starboard Stabilator Surface Pressure Distribution
for Varying Trailing Edge Flap Deflection
$\alpha = 10°, \beta = 0°, \delta = 0°$, LEF= 13.3°, LEX fence on
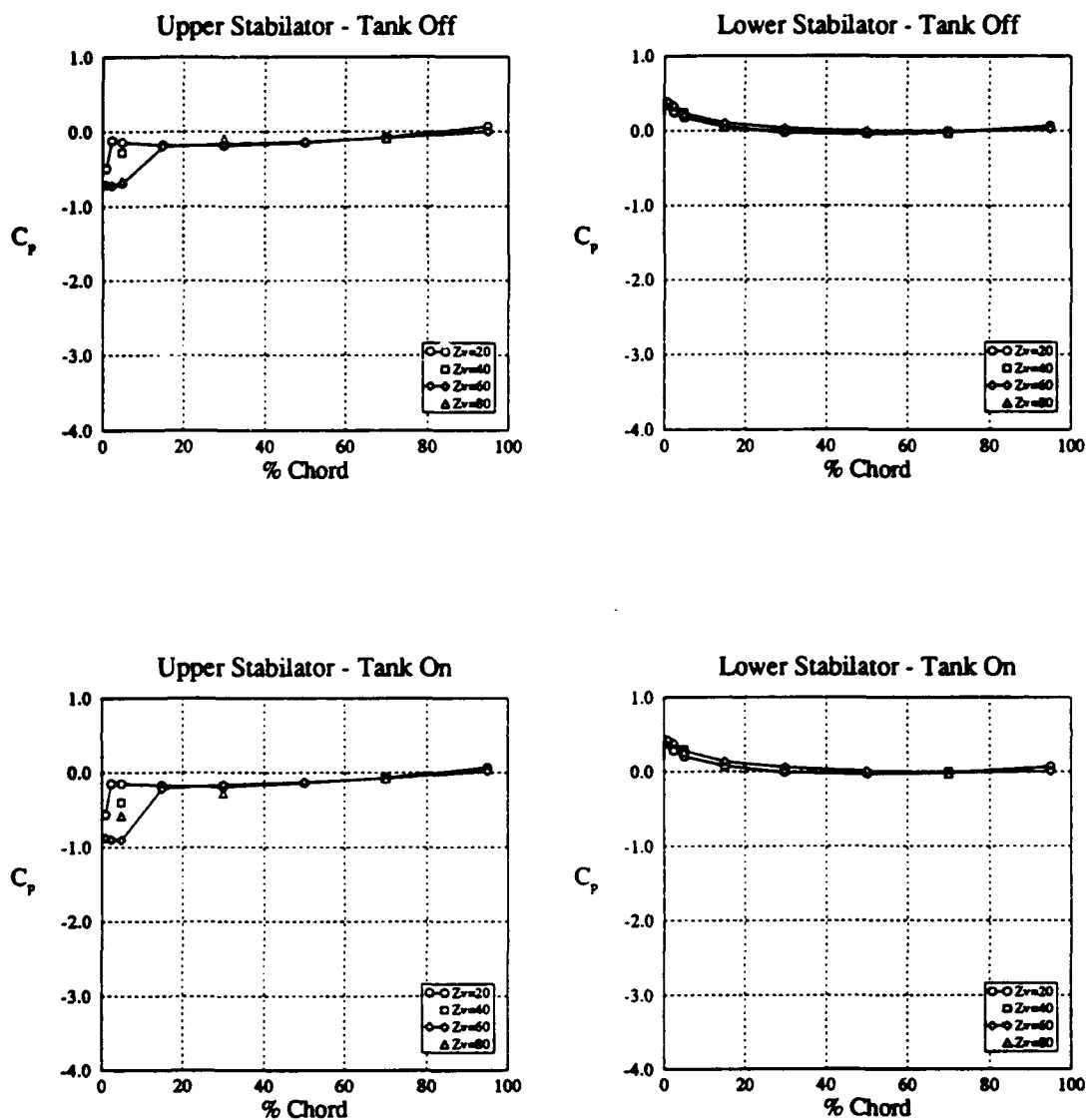
Figure 18 a :   Starboard Stabilator Surface Pressure Distribution for Wing Tank Off and On
$\alpha = 5°, \beta = 0°, \delta = 1°$, LEF= 6.6°, TEF= 7.0°, LEX fence on
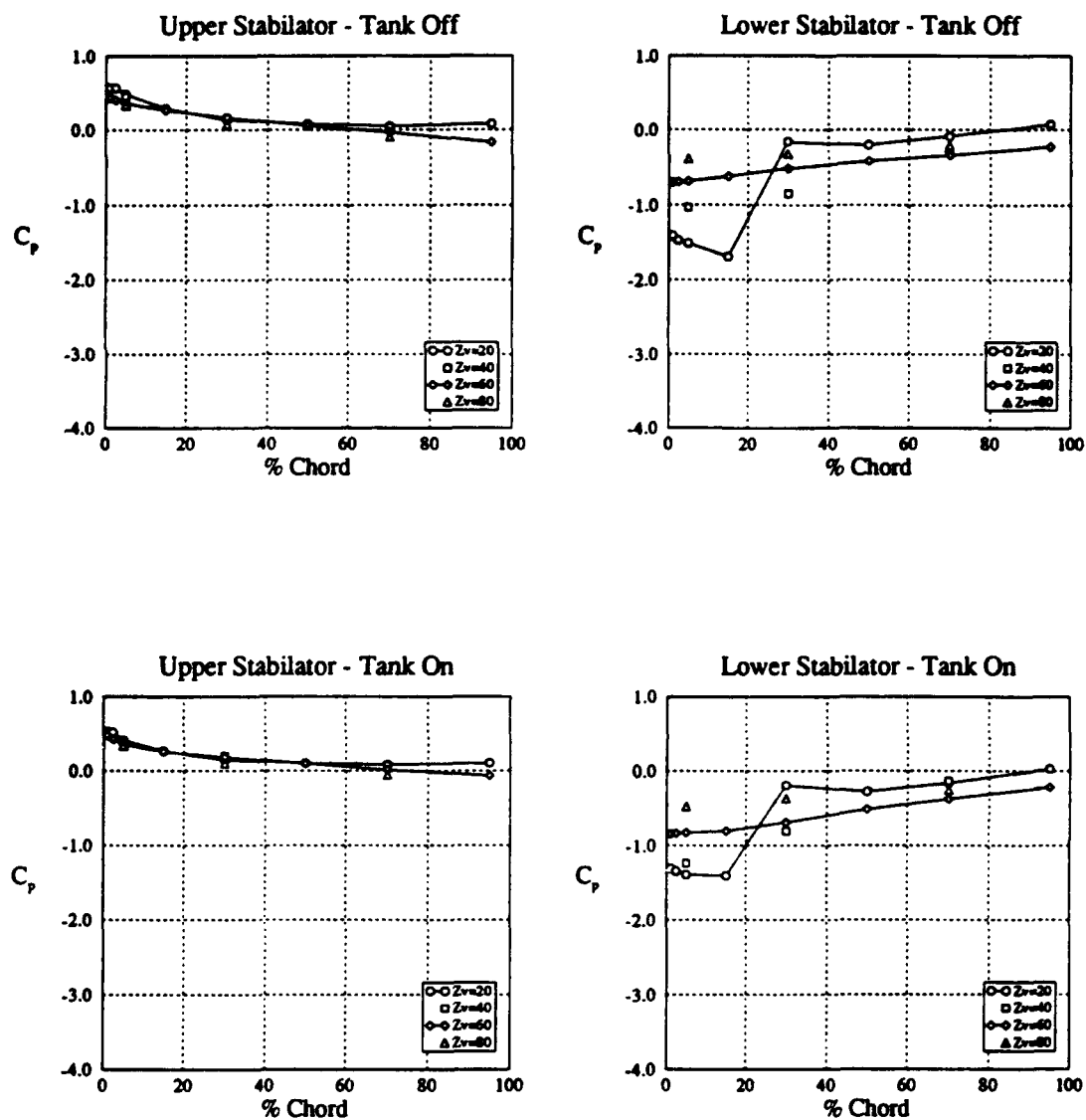
Figure 18 b :   Starboard Stabilator Surface Pressure Distribution for Wing Tank Off and On
$\alpha = 0°, \beta = 5°, \delta = -11°$, LEF= 0.0°, TEF= 0.0°, LEX fence on

Integrated Fin Loads, δ = 5 deg

Integrated Fin Loads, δ = 0 deg
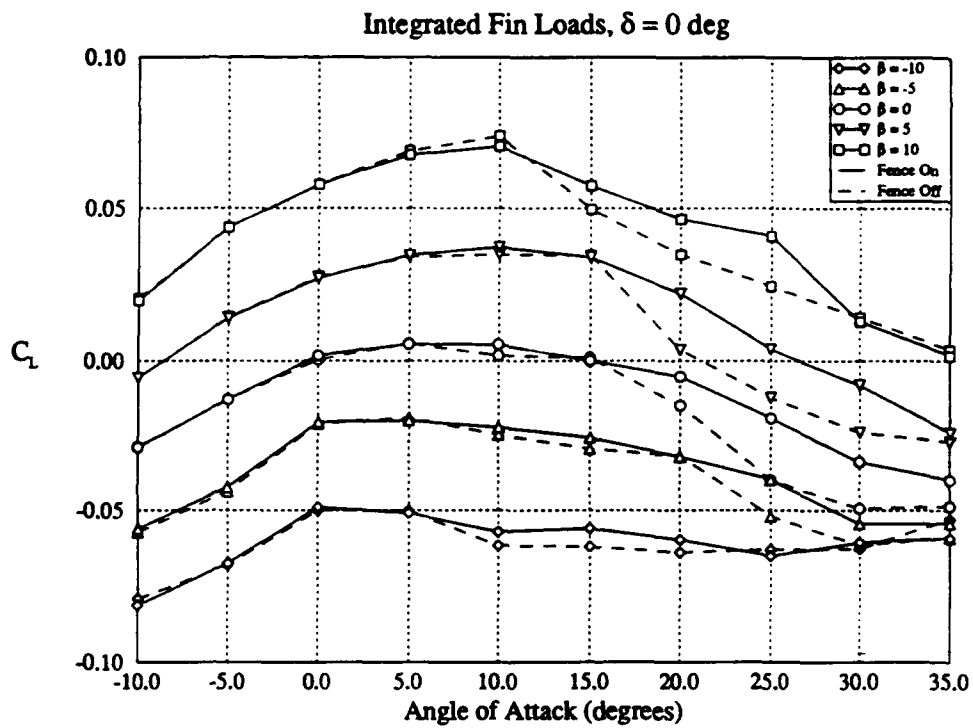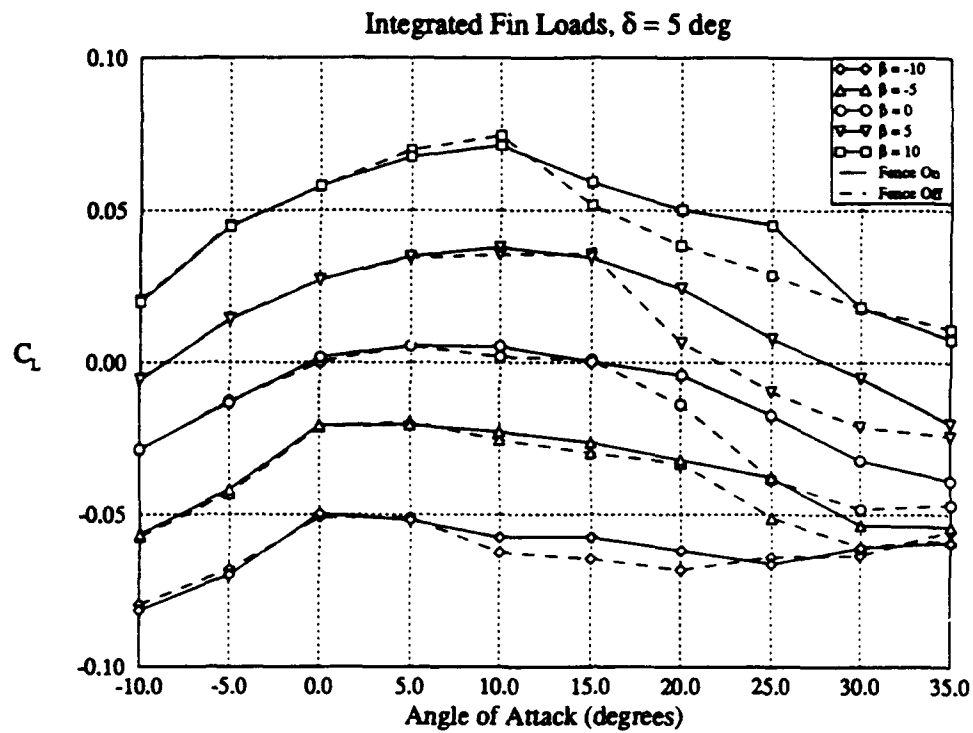
Figure 19 a & b : Normal Force on Starboard Fin as a Function of α, β, δ and LEX fence
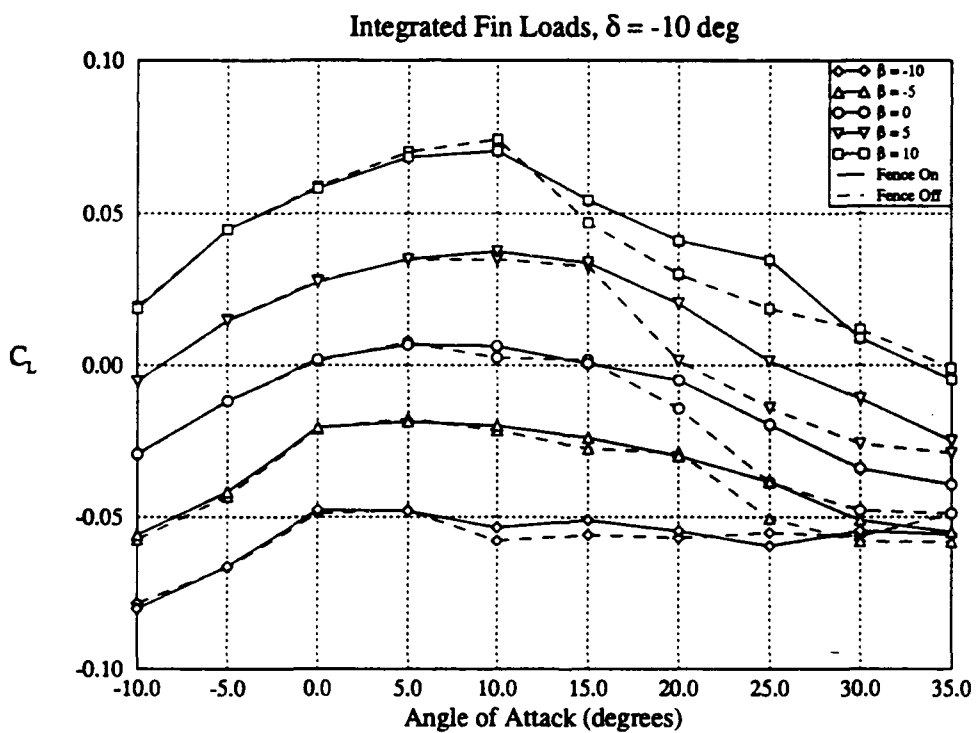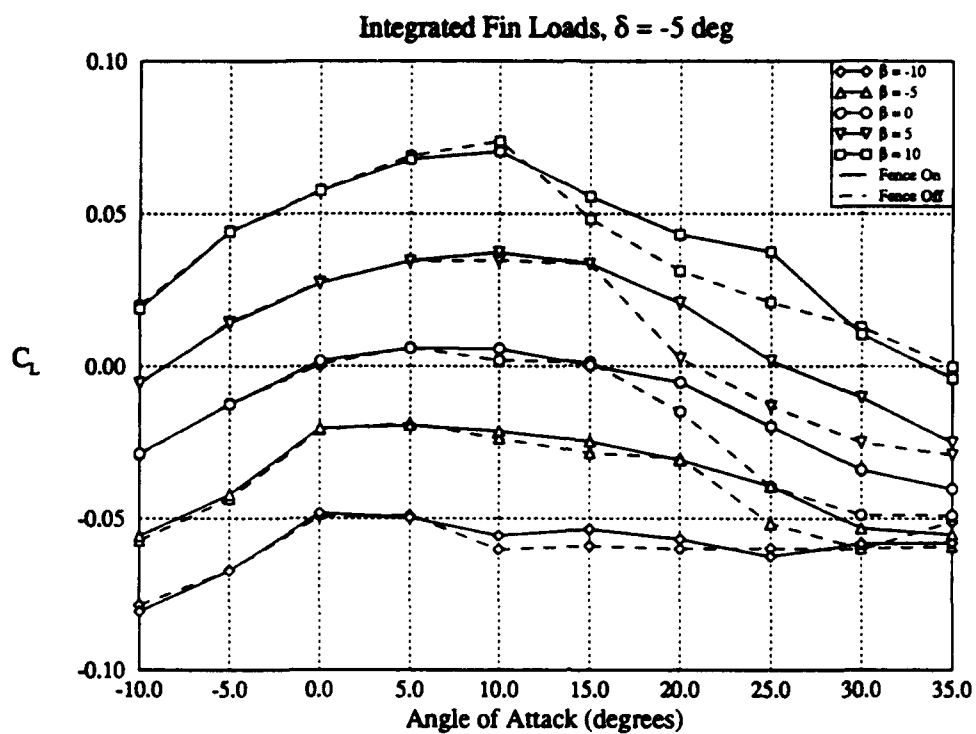
Figure 19 c & d :   Normal Force on Starboard Fin as a Function of α, β, δ and LEX fence
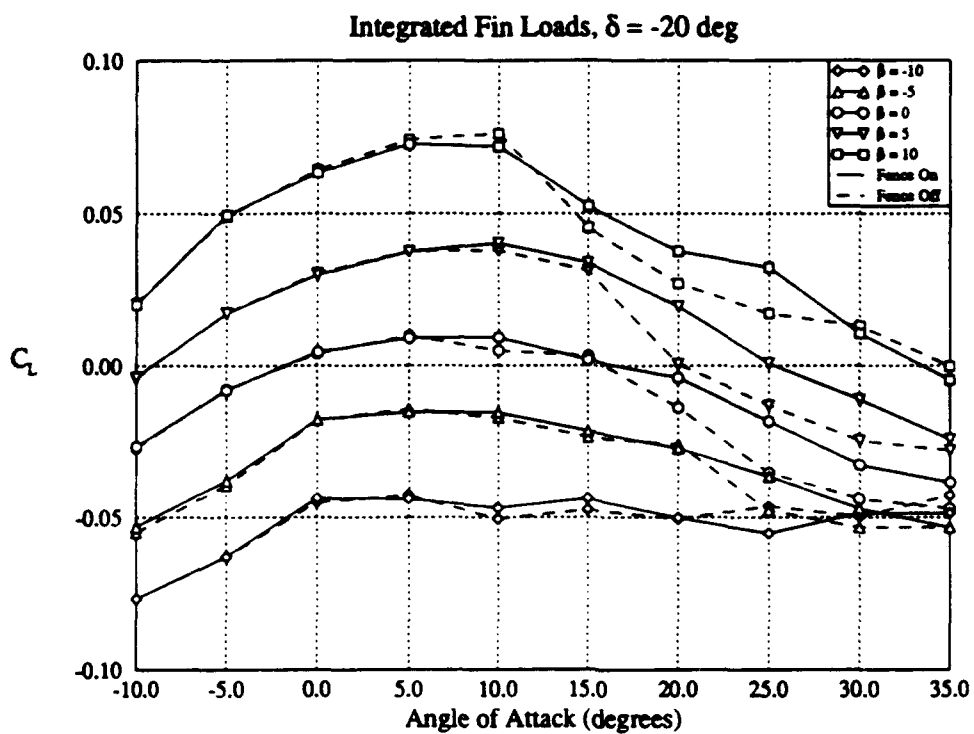
Figure 19 e : Normal Force on Starboard Fin as a Function of α, β, δ and LEX fence
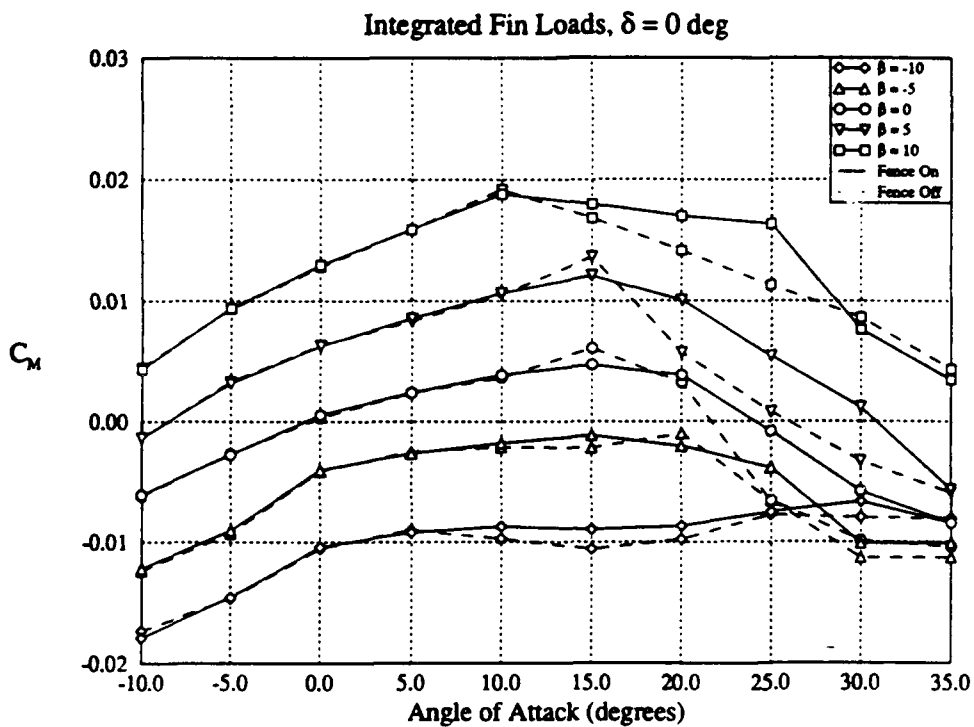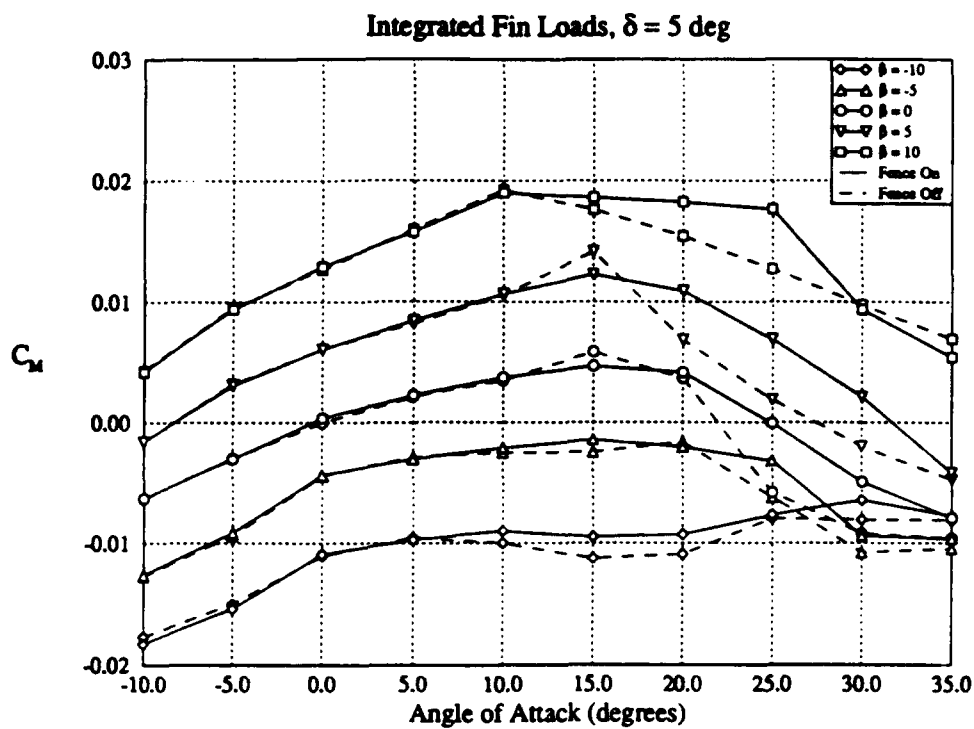
Figure 20 a & b : Pitching Moment on Starboard Fin as a Function of α, β, δ and LEX fence

Integrated Fin Loads, δ = -5 deg

Integrated Fin Loads, δ = -10 deg
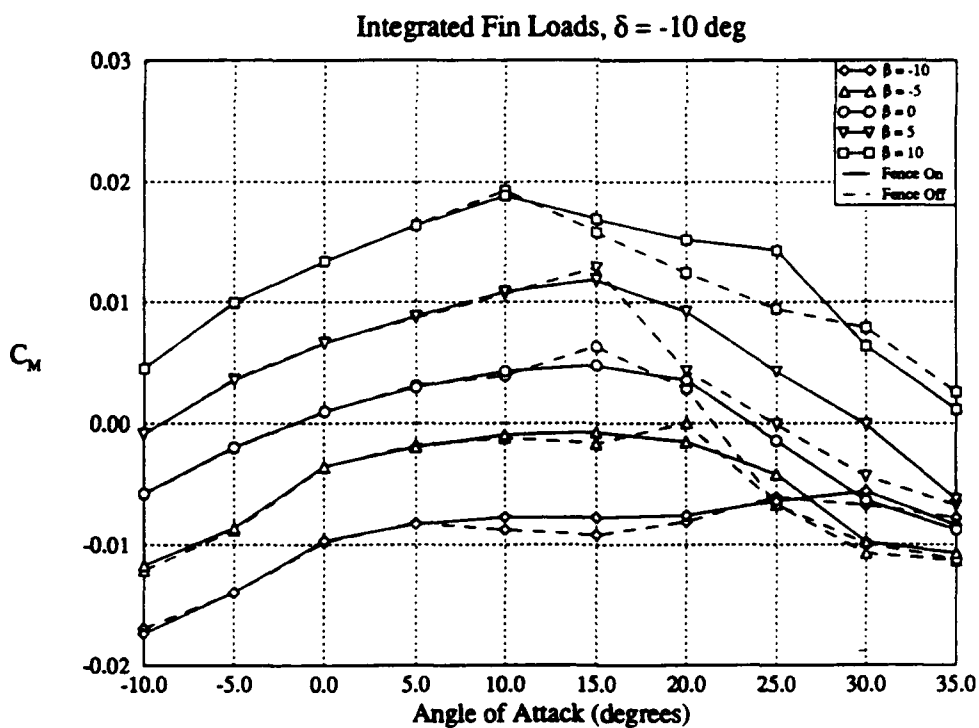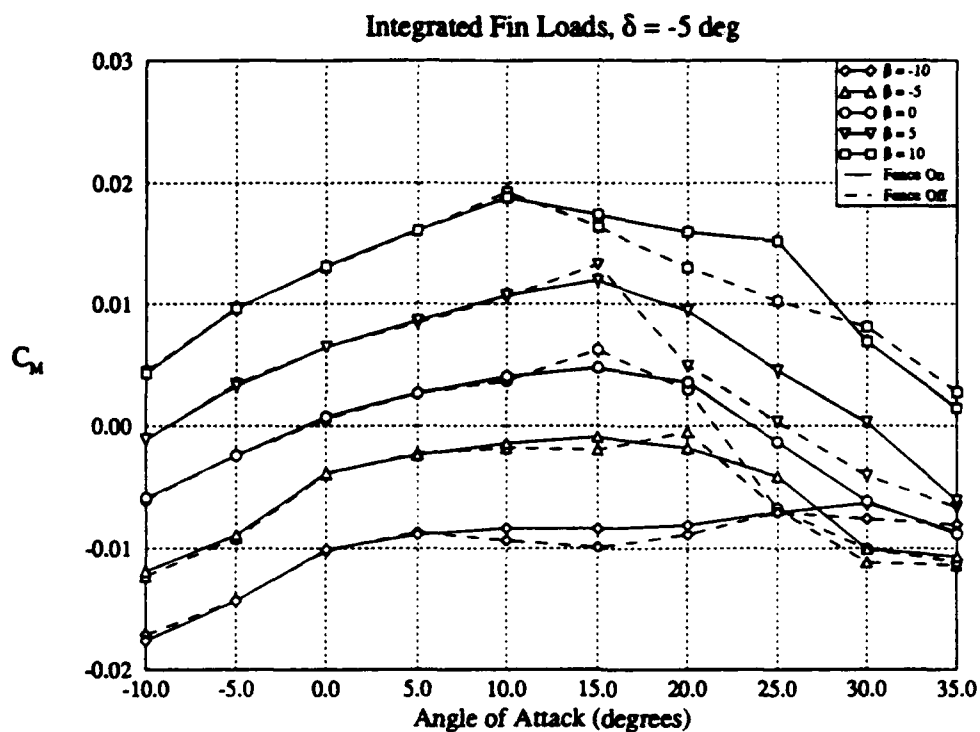
Figure 20 c & d :   Pitching Moment on Starboard Fin as a Function of α, β, δ and LEX fence

68
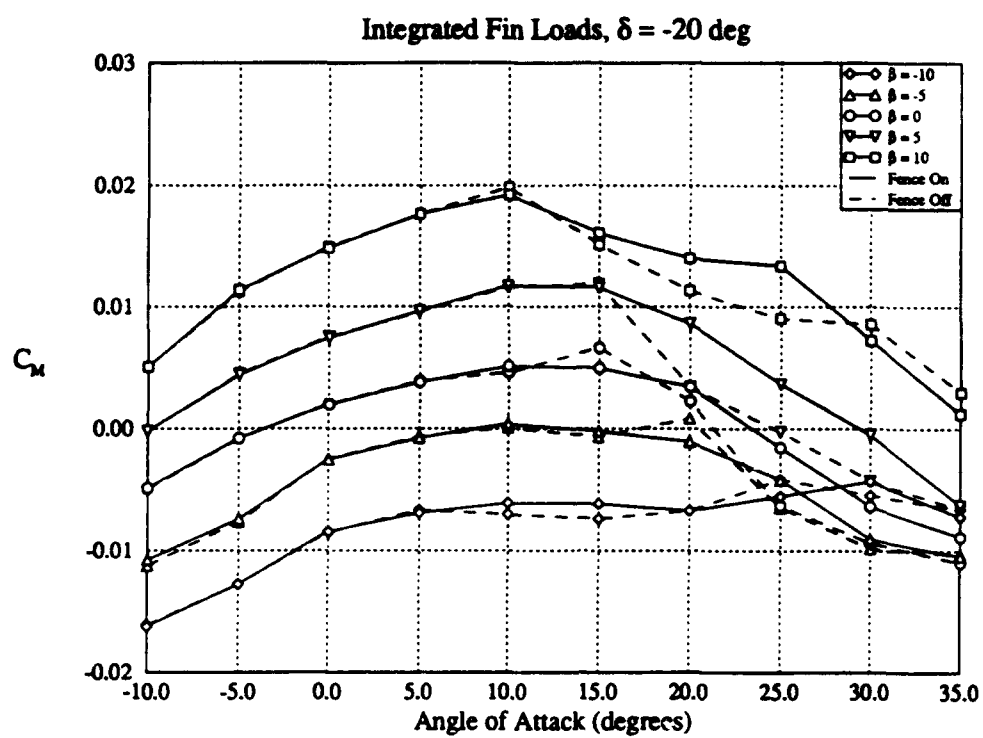
Figure 20 e : Pitching Moment on Starboard Fin as a Function of α, β, δ and LEX fence
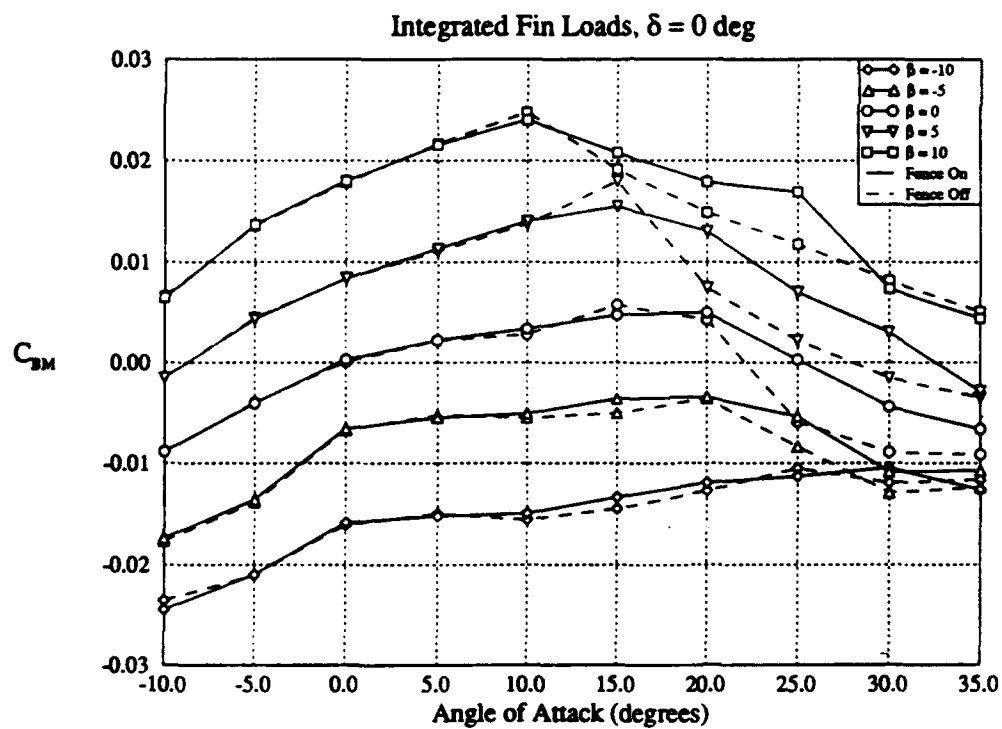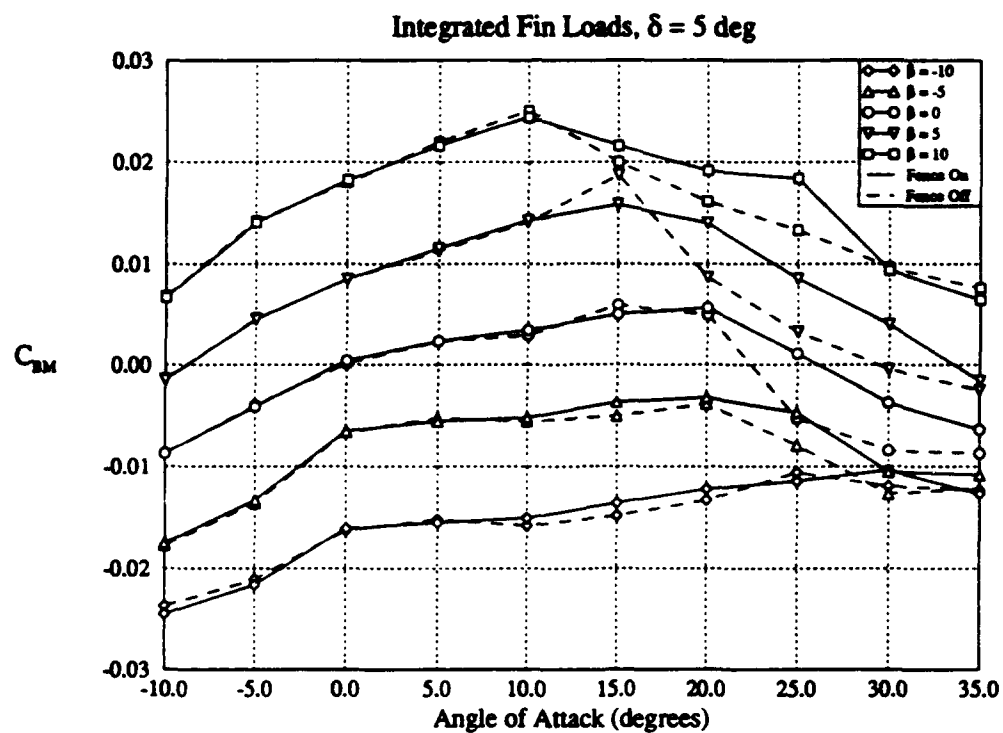
Figure 21 a & b :   Bending Moment on Starboard Fin as a Function of α, β, δ and LEX fence

70
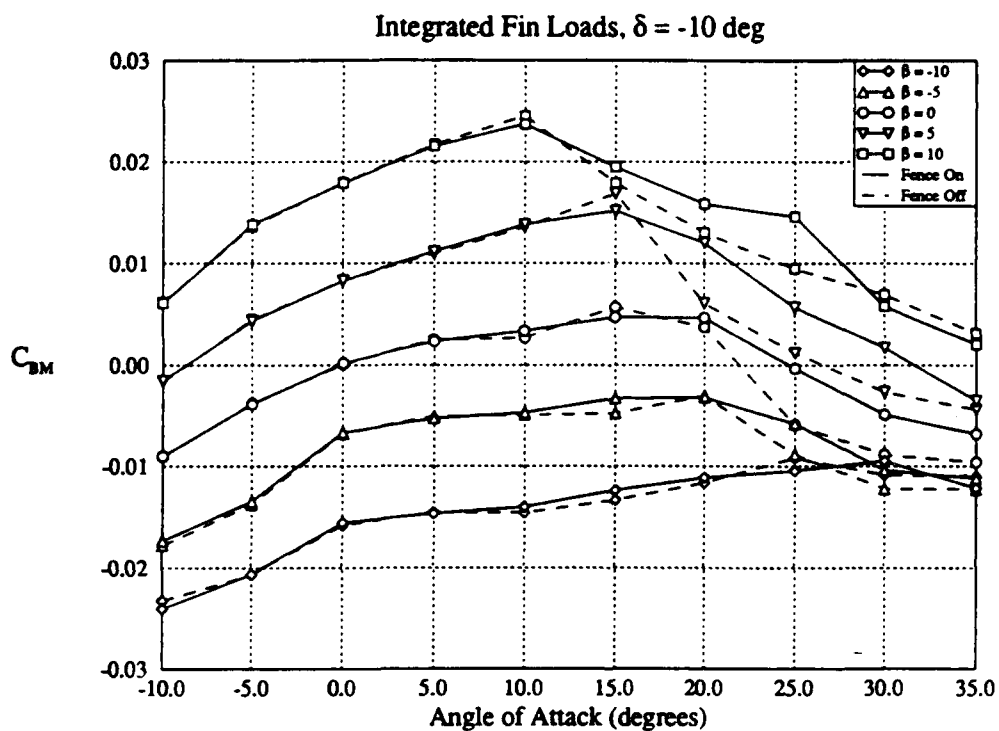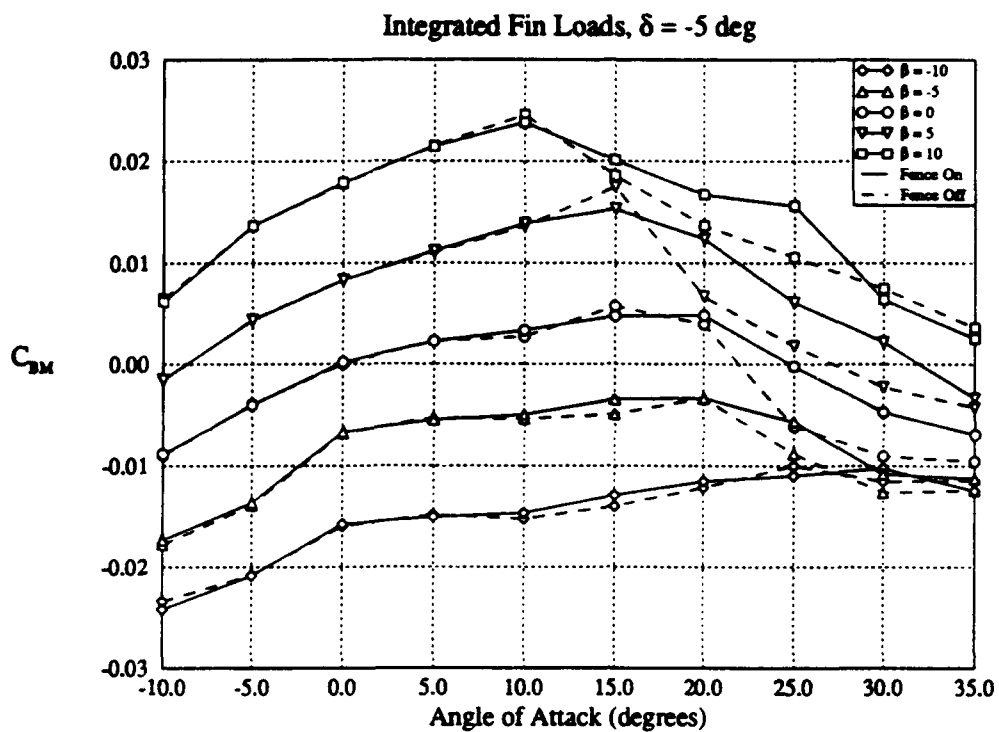
Figure 21 c & d : Bending Moment on Starboard Fin as a Function of α, β, δ and LEX fence
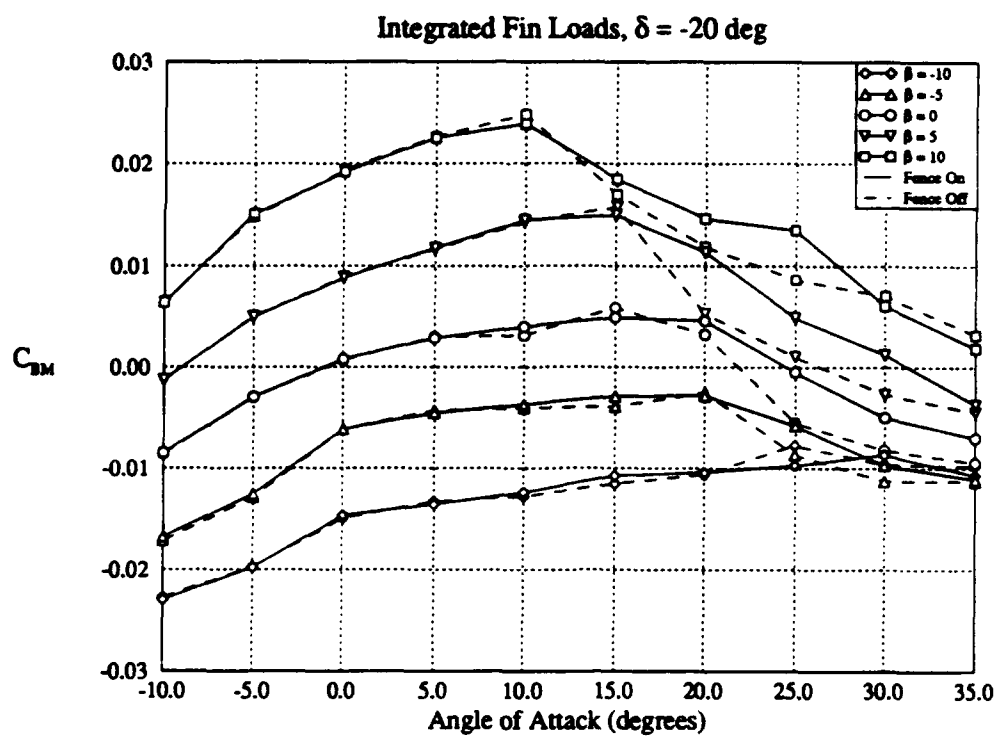
Figure 21 e : Bending Moment on Starboard Fin as a Function of α, β, δ and LEX fence
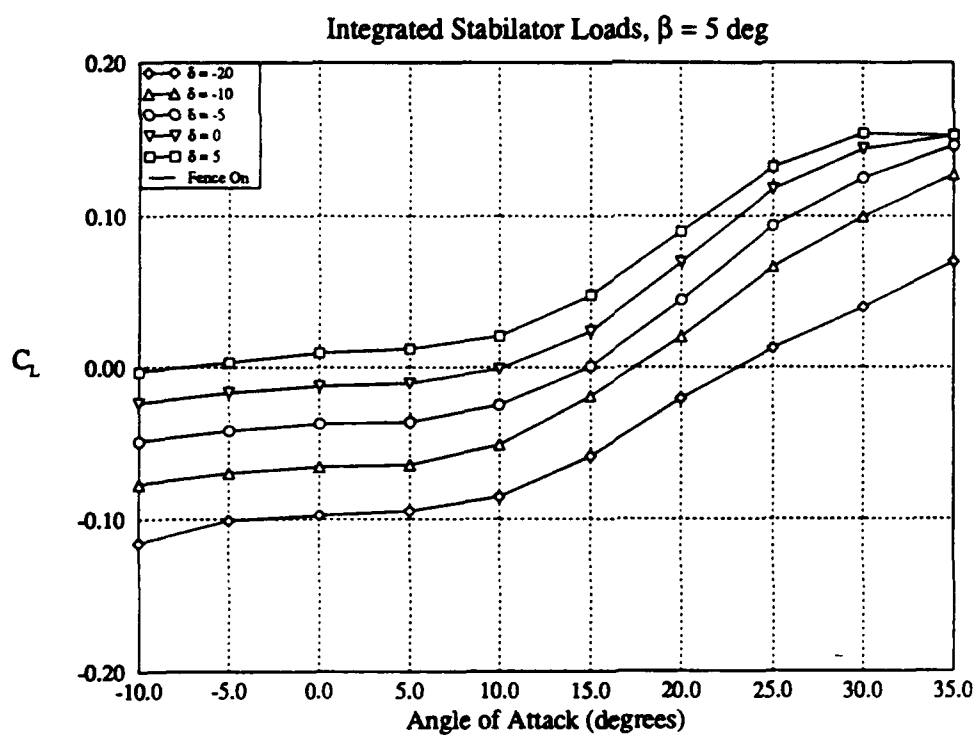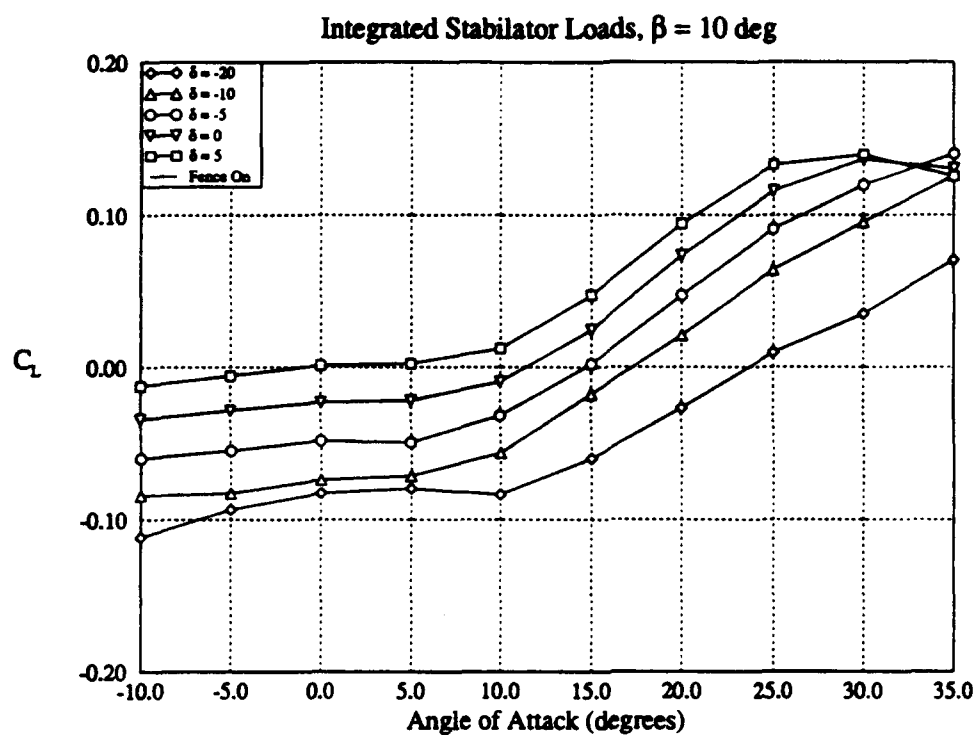
Figure 22 a & b :   Normal Force on Starboard Stabilator as a Function of α, β, δ and LEX fence

73

Integrated Stabilator Loads, β = 0 deg

Integrated Stabilator Loads, β = -5 deg
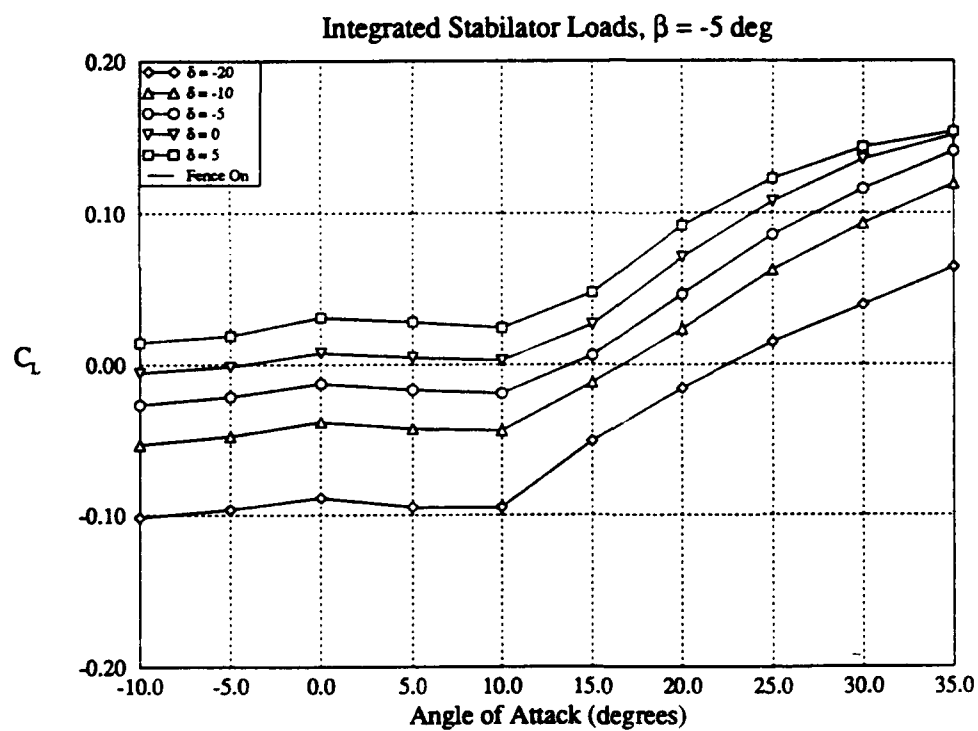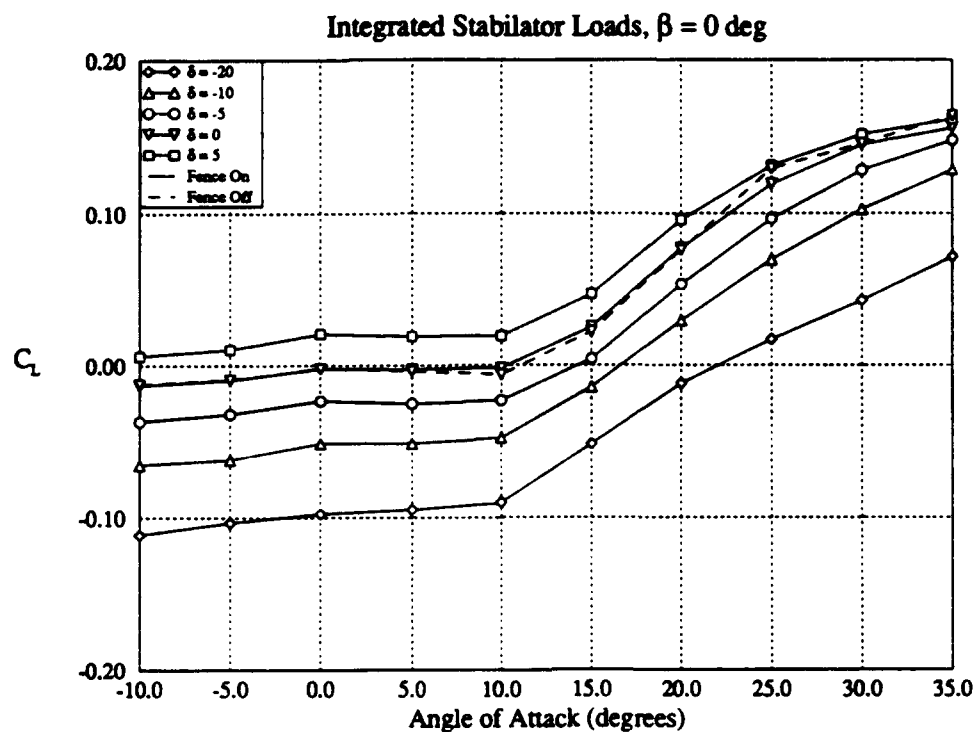
Figure 22 c & d :   Normal Force on Starboard Stabilator as a Function of α, β, δ and LEX fence

74
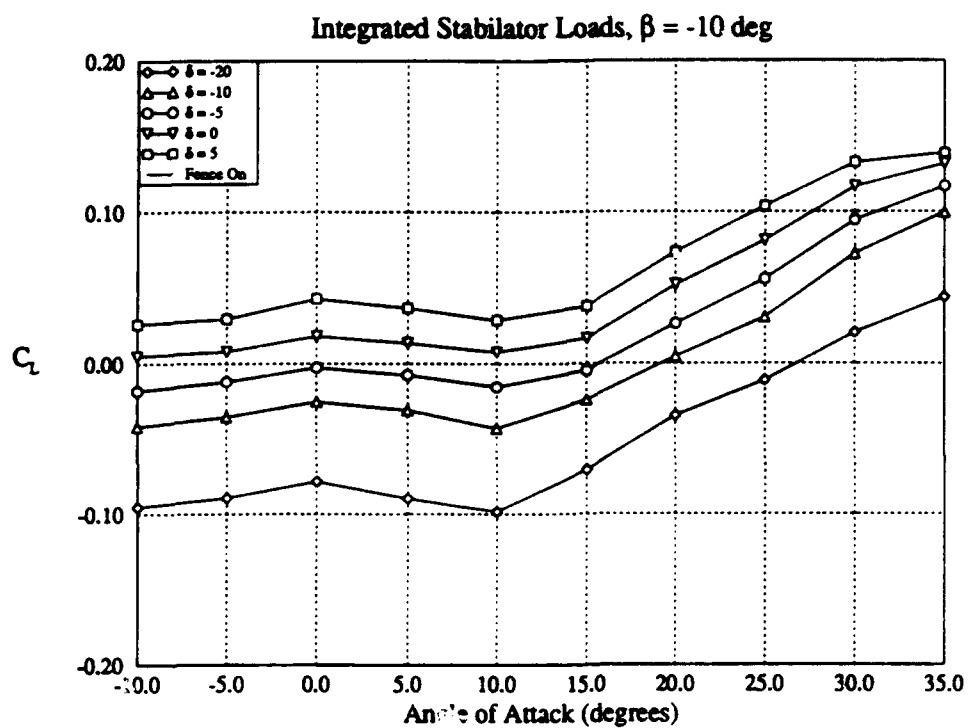
Figure 22 e : Normal Force on Starboard Stabilator as a Function of α, β, δ and LEX fence
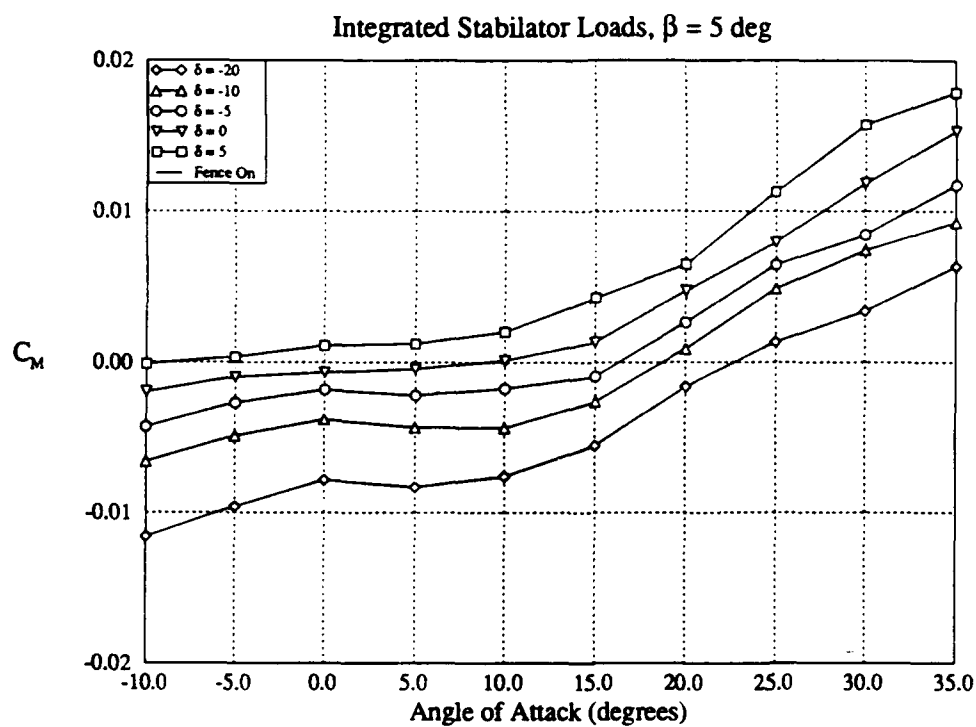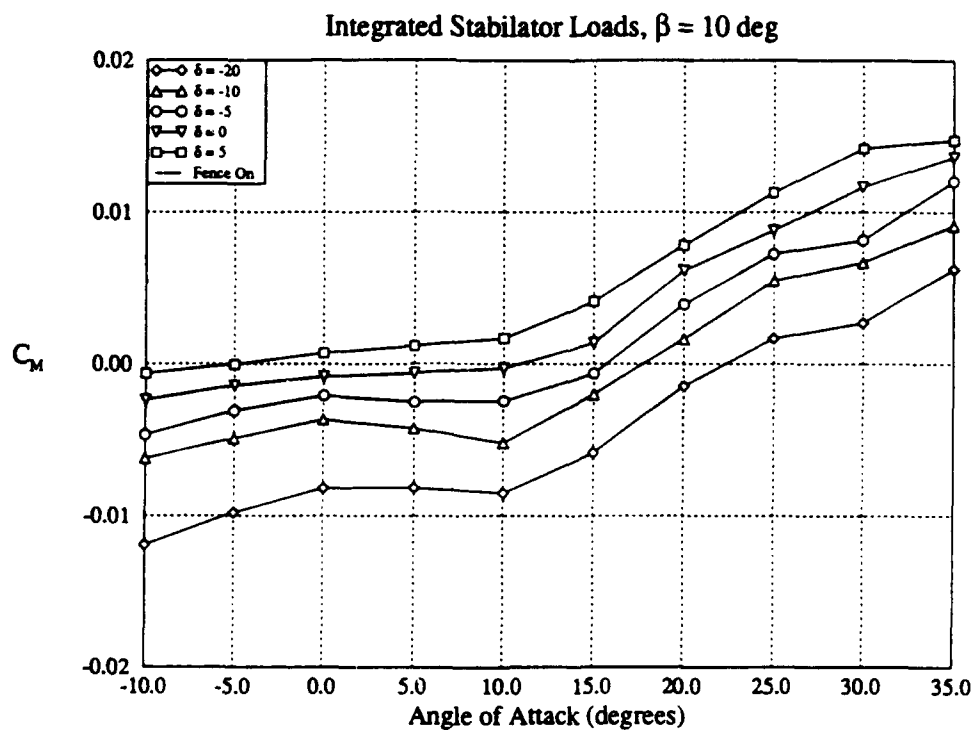
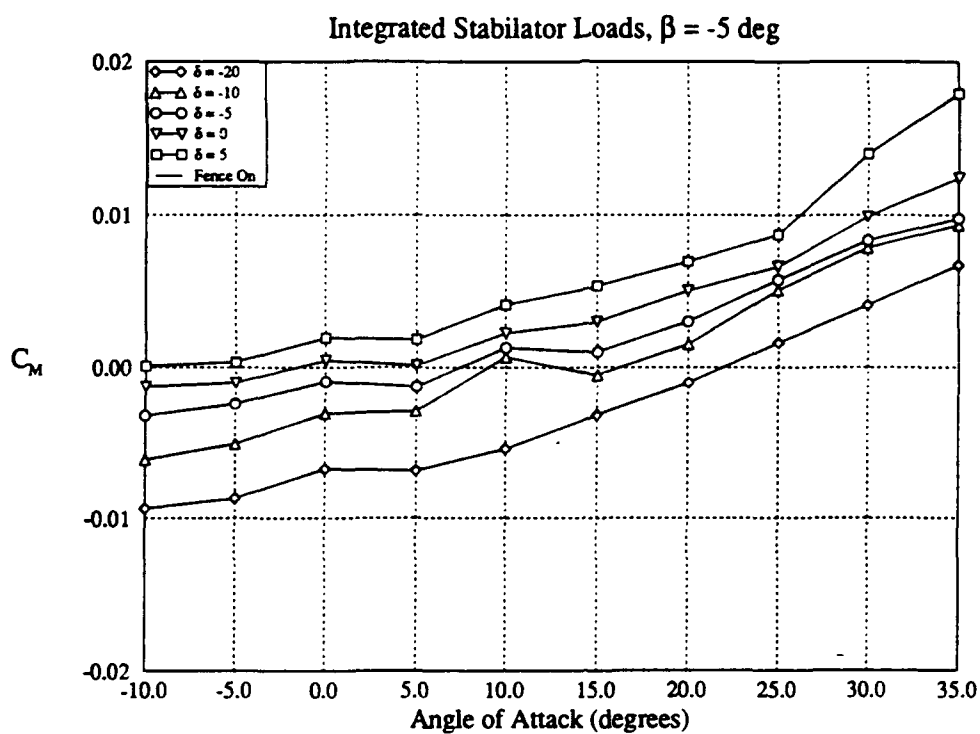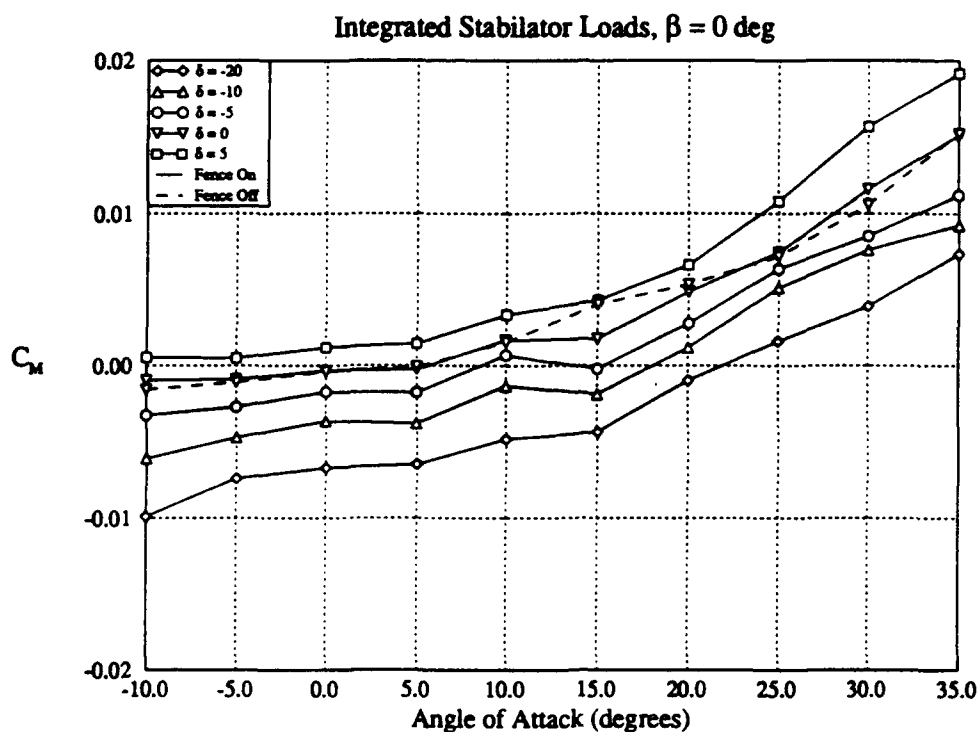Figure 23 a & b :   Pitching Moment on Starboard Stabilator as a Function of α, β, δ and LEX fence

Integrated Stabilator Loads, β = 0 deg

Integrated Stabilator Loads, β = -5 deg

Figure 23 c & d :   Pitching Moment on Starboard Stabilator as a Function of α, β, δ and LEX fence
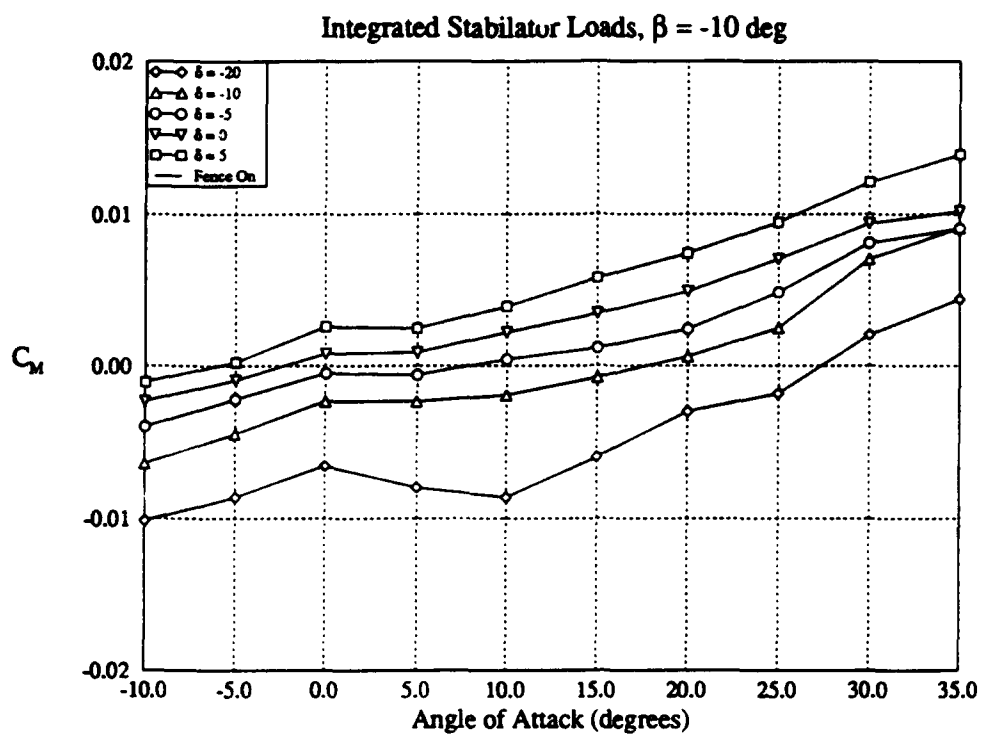
Figure 23 e :   Pitching Moment on Starboard Stabilator as a Function of α, β, δ and LEX fence
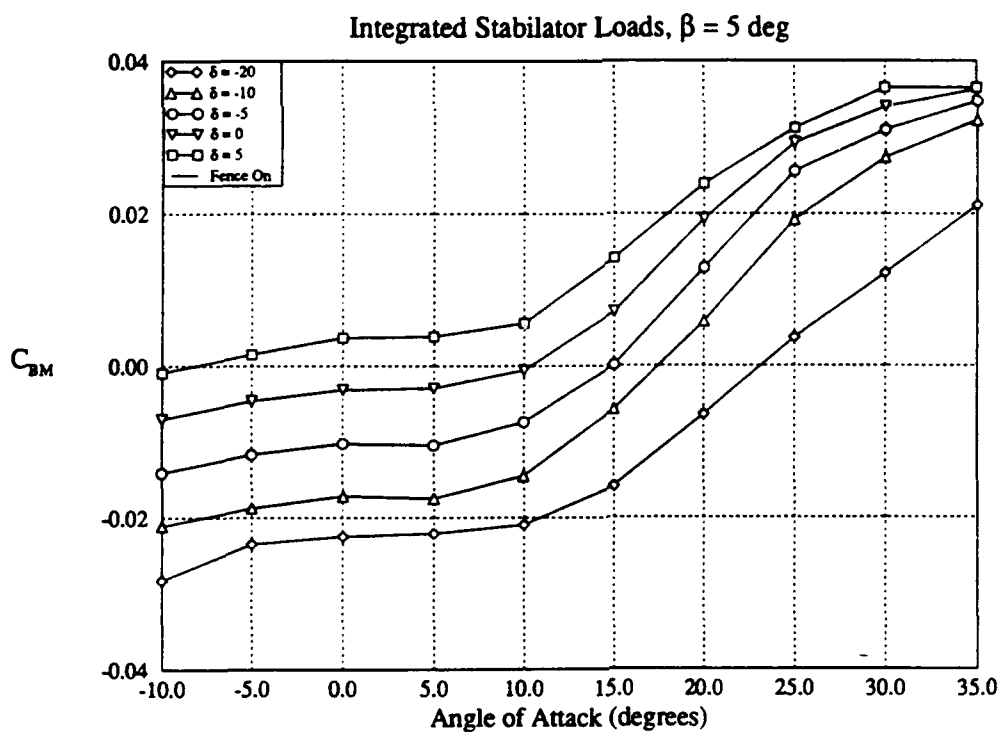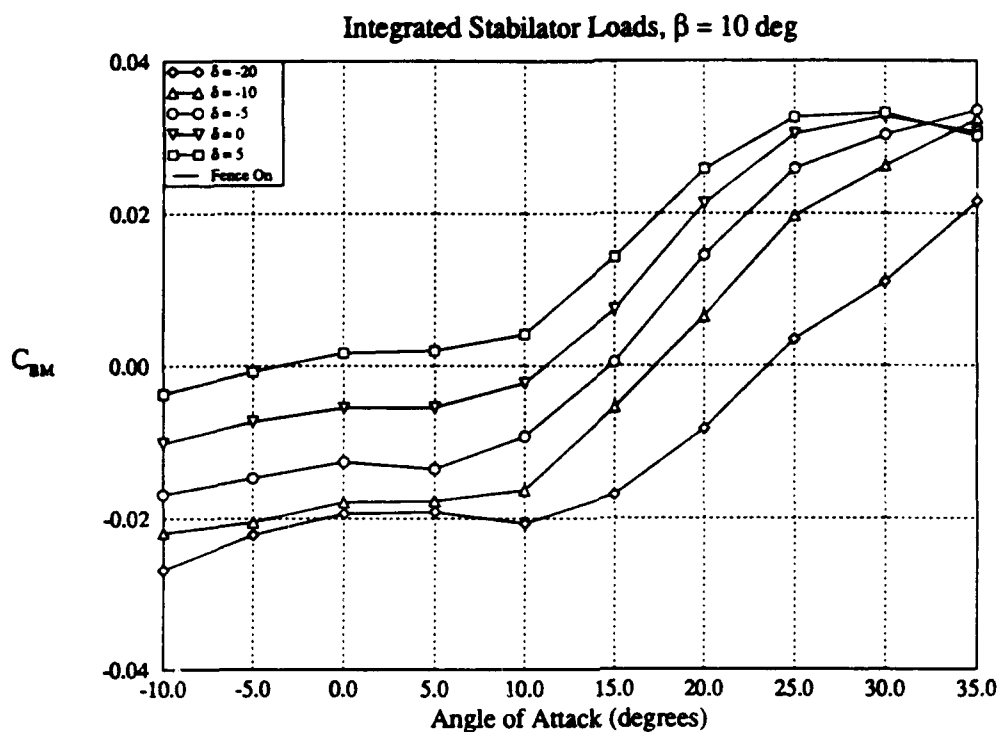
Figure 24 a & b :   Bending Moment on Starboard Stabilator as a Function of α, β, δ and LEX fence
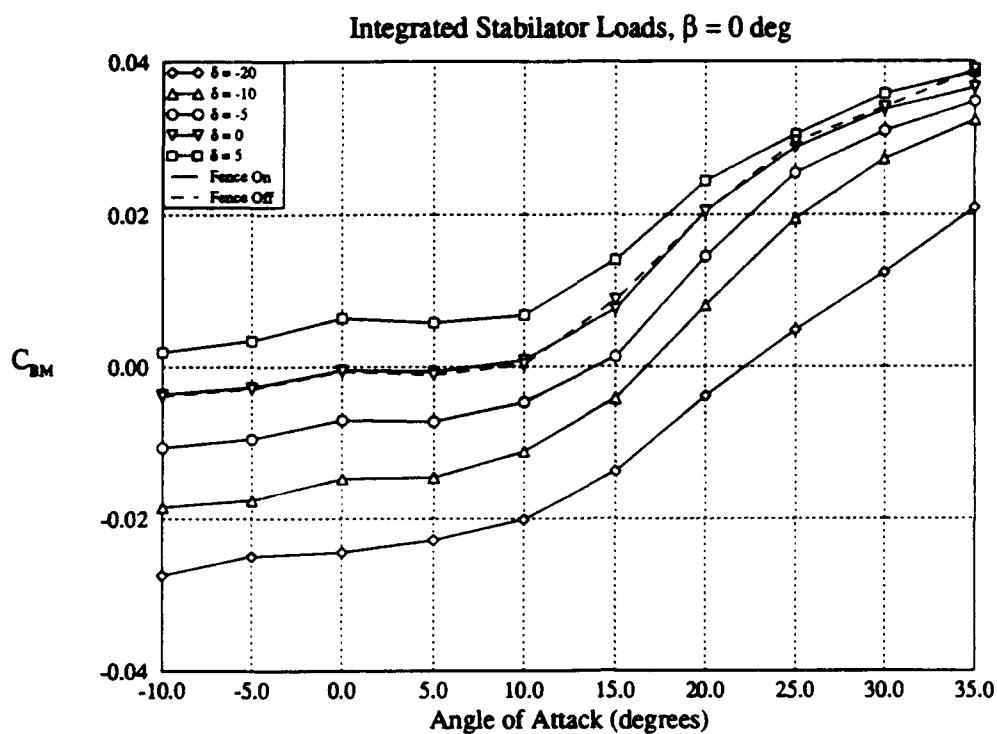
79
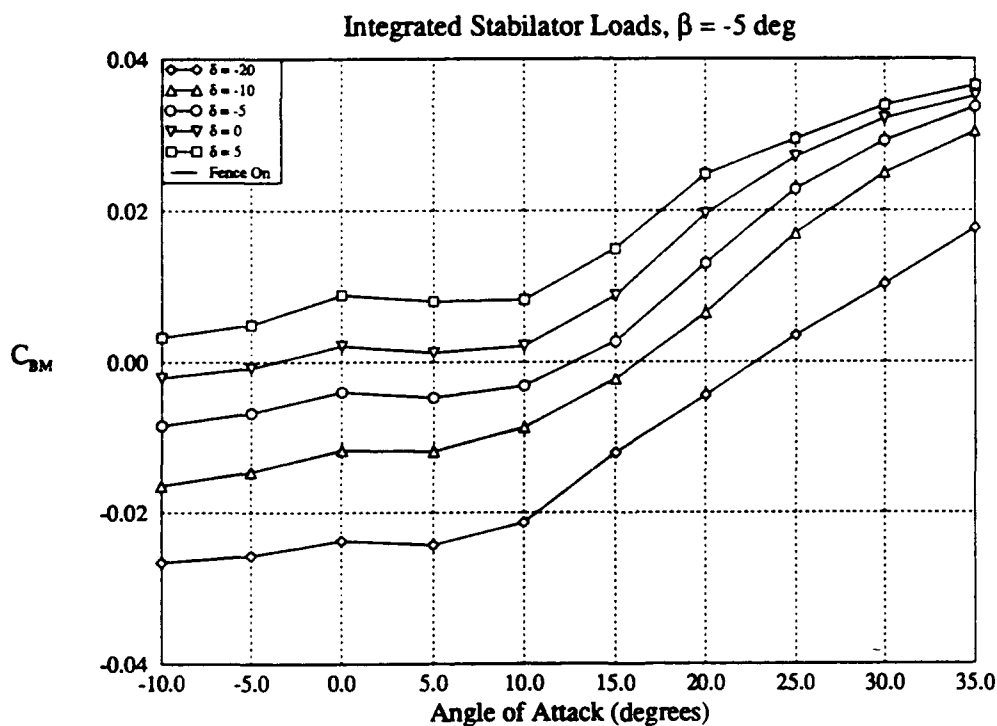
Figure 24 c & d : Bending Moment on Starboard Stabilator as a Function of α, β, δ and LEX fence
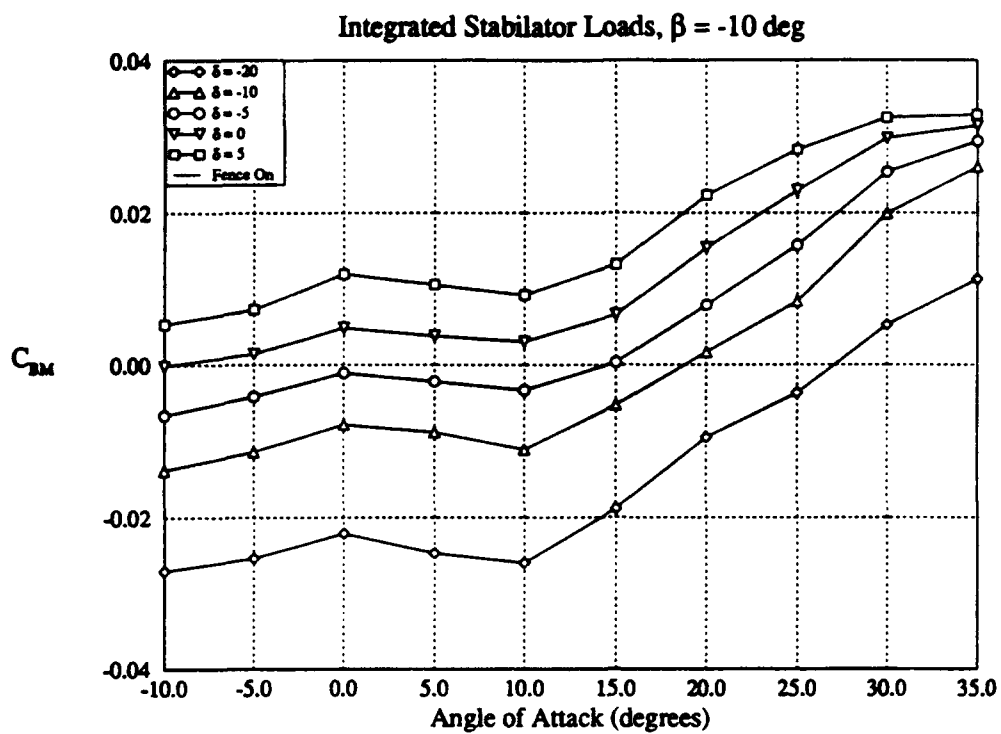
Figure 24 e : Bending Moment on Starboard Stabilator as a Function of α, β, δ and LEX fence

Integrated Fin Loads

Integrated Stabilator Loads

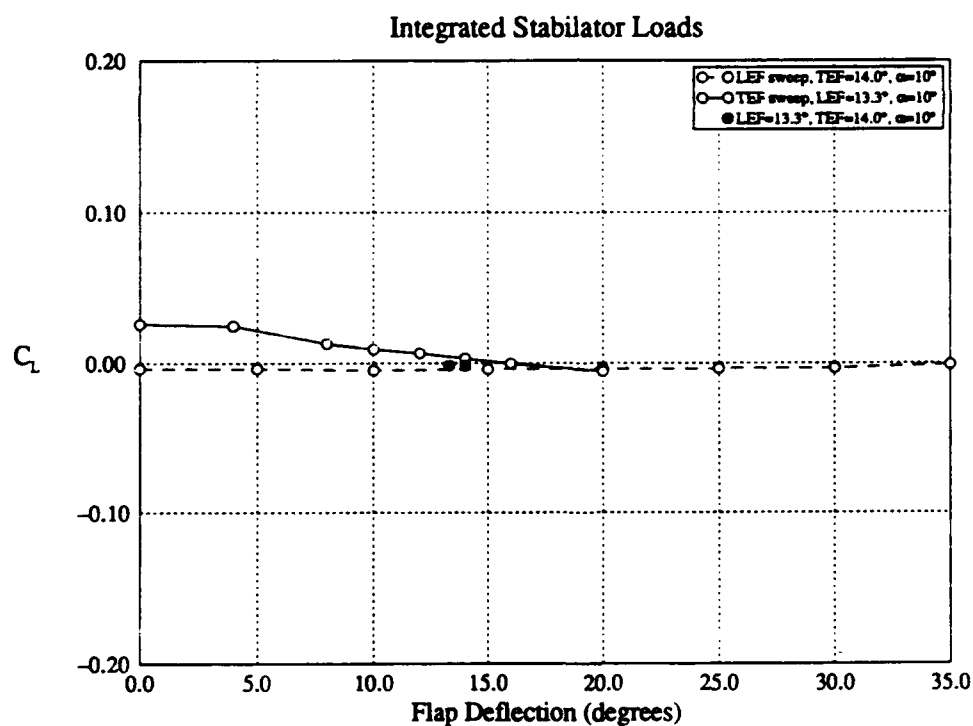Figure 25 :   Normal Force on Starboard Fin and Stabilator for
Varying Leading and Trailing Edge Flap Deflections
$\beta = 0°, \delta = 0°$, LEX fence on

82

Integrated Fin Loads

Integrated Stabilator Loads

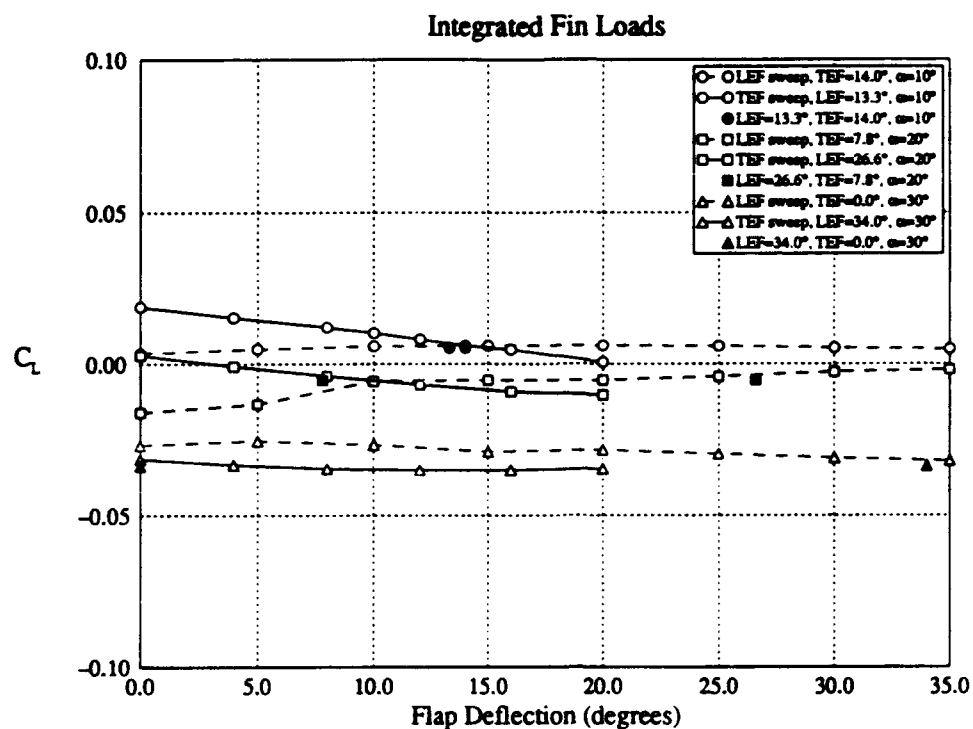Figure 26 : Pitching Moment on Starboard Fin and Stabilator for
Varying Leading and Trailing Edge Flap Deflections
$\beta = 0°, \delta = 0°$, LEX fence on

83

Integrated Fin Loads

Integrated Stabilator Loads

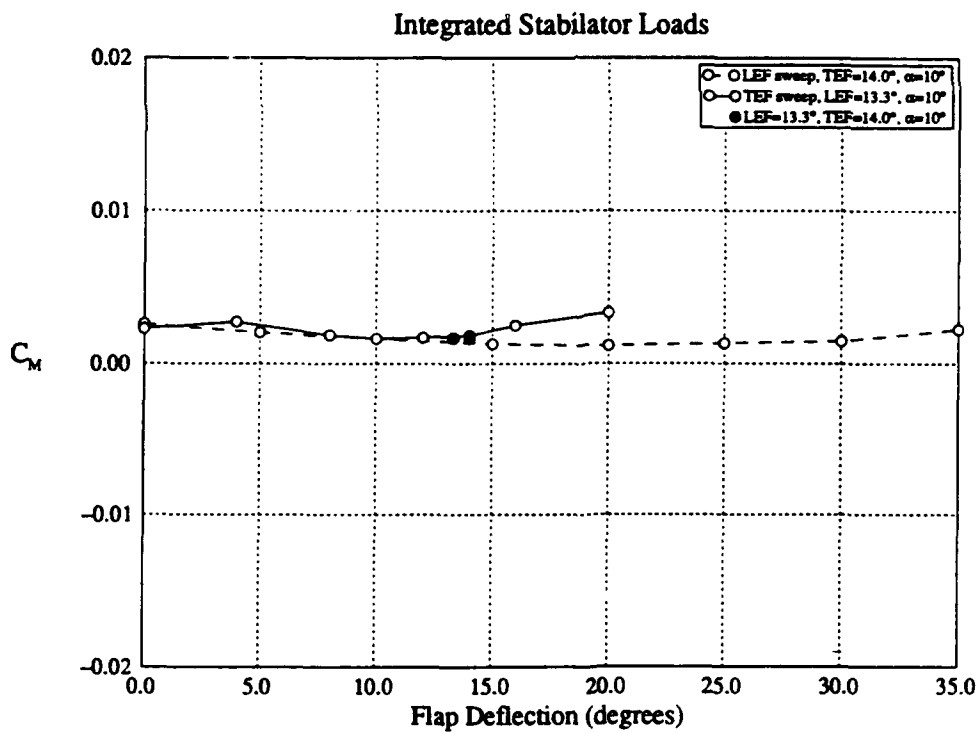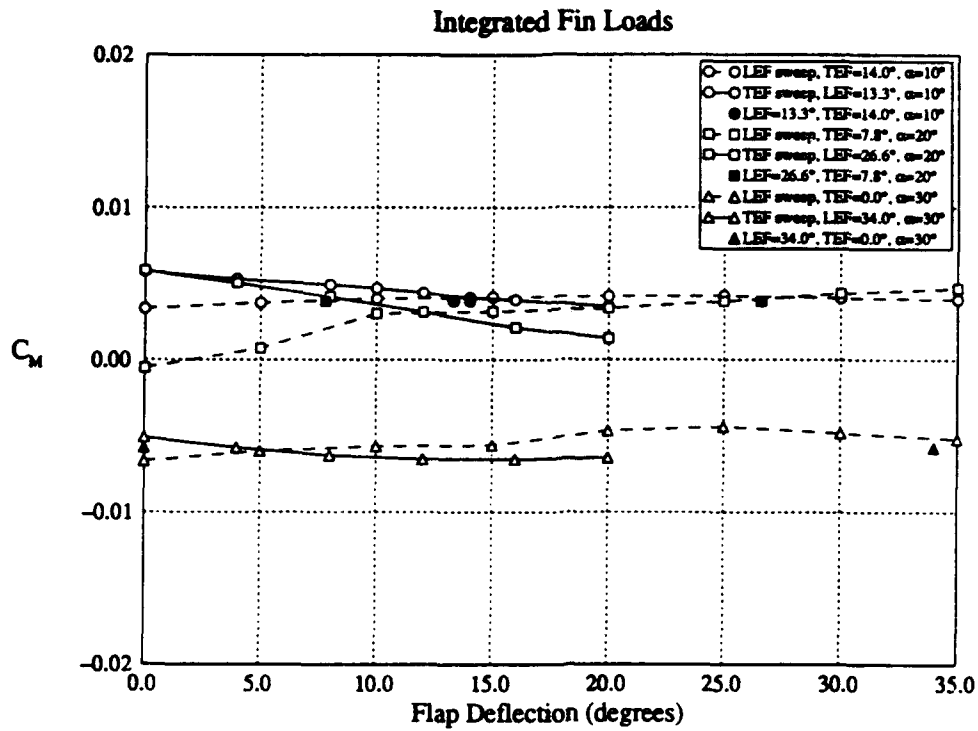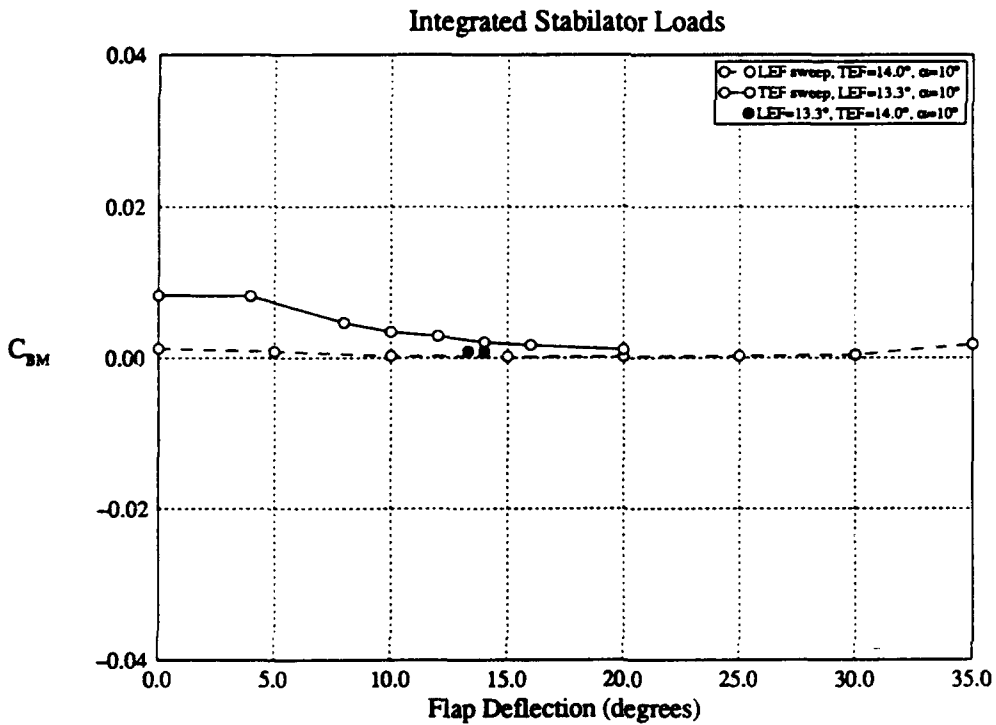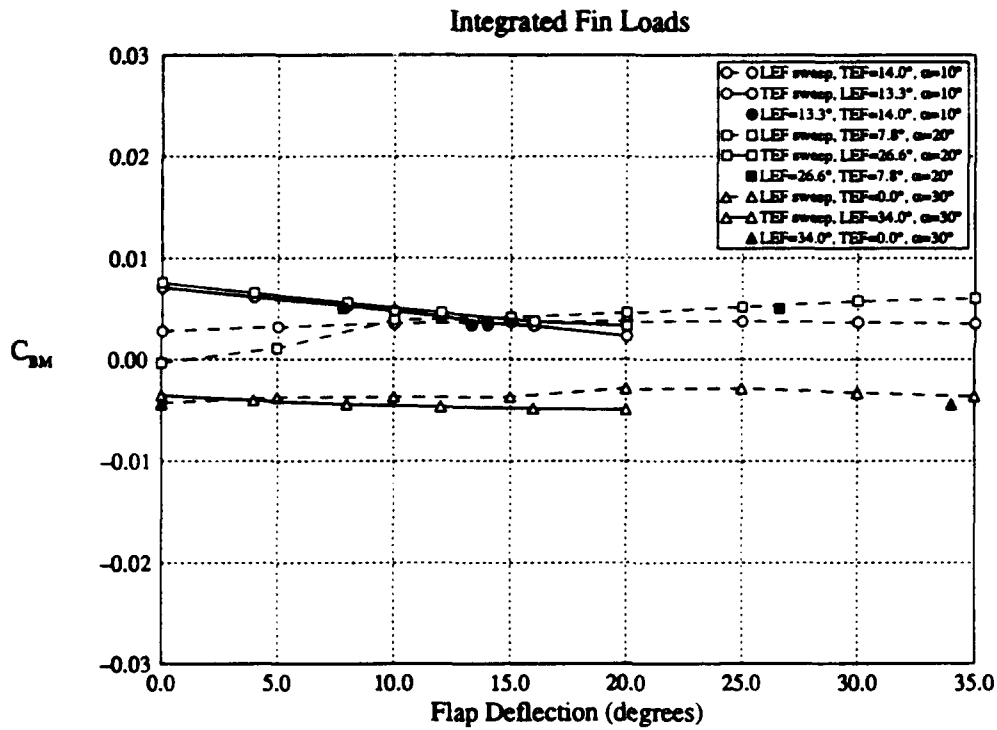Figure 27 : Bending Moment on Starboard Fin and Stabilator for
Varying Leading and Trailing Edge Flap Deflections
$\beta = 0°, \delta = 0°$, LEX fence on

84

DISTRIBUTION

AUSTRALIA

Defence Science and Technology Organisation

Chief Defence Scientist
FAS Science Policy } shared copy
AS Science Corporate Management
Counsellor Defence Science, London (Doc Data Sheet only)
Counsellor Defence Science, Washington (Doc Data Sheet only)
Senior Defence Scientific Adviser (Doc Data Sheet only)
Scientific Advisor Policy and Command (Doc Data Sheet only)
Navy Scientific Adviser (3 copies Doc Data Sheet only)
Scientific Adviser - Army (Doc Data Sheet only)
Air Force Scientific Adviser

Aeronautical Research Laboratory
    Director
    Library
    Chief Air Operations Division
    Chief Airframes and Engines Division
    Authors: L.D. MacLaren
                H.A. Quick

C.A. Martin	D. Graham
N. Pollock	P.D. White
N. Matheson	G. Habermann
M.K. Glaister	M.G.J. Higgs
B.D. Fairlie	A.J. Jakobovic
D.H. Thompson	L. Molent
J.S. Drobik	M. Stimson
S.D. Hill	P.A. Farrell
C.K. Rider	D. Symons
D.J. Sherman	M.F. Lee
W. Waldman	

W. Madley (CF Liaison Officer)
D. Conser (McDonnell-Douglas Liaison Officer)

Main Library - DSTO Salisbury

Electronics Research Laboratory
    GWD
        C. Jermey
        D.A. Pierens
        P. Nikoloff

Defence Central

OIC TRS, Defence Central Library
Document Exchange Centre, DIS (8 copies)
Defence Intelligence Organisation
Library, Defence Signals Directorate (Doc Data Sheet Only)

HQ ADF

Director General Force Development (Air)

Air Force

DGELS AIRREG4 HQLC
WGCDR T. Eames (TFP-IFOSTP-M)
Aircraft Research and Development Unit
    Scientific Flight Group
    C Flight Commander
    Library
TFLM SQN - Williamtown
OIC ATF ATS, RAAFSTT, WAGGA (2 copies)

UNIVERSITIES AND COLLEGES

Australian Defence Force Academy
    Library
    Head of Aerospace and Mechanical Engineering

    Sydney
        Engineering Library

    RMIT
        Library
        Aerospace Engineering

OTHER ORGANISATIONS

NASA (Canberra)
AGPS
ASTA Engineering, Document Control Office

CANADA

NRC, IAR
    Library
    B.H.K. Lee
    D. Simpson

CF
    Library
    DAS ENG 6-3 (2 copies)

CANADAIR
    Library
    J. Roussel
    C. Perron

UNITED STATES OF AMERICA

NASA Ames-Moffet Research Center
Library
L.A. Meyn

NASA Ames-Dryden Flight Research Facility
Chief Aeronautics Branch

McDonnell-Douglas
Library

SPARES (7 COPIES)

TOTAL (82 COPIES)

DOCUMENT CONTROL DATA

1a. AR NUMBER AR-008-367	1b. ESTABLISHMENT NUMBER ARL-RR-9	2. DOCUMENT DATE OCTOBER 1993	3. TASK NUMBER AIR 90/187

4. TITLE LOW-SPEED PRESSURE DISTRIBUTION MEASUREMENTS OVER THE AFT-FUSELAGE, FINS AND STABILATORS OF A 1/9th SCALE F/A-18 WIND-TUNNEL MODEL	5. SECURITY CLASSIFICATION (PLACE APPROPRIATE CLASSIFICATION IN BOX(S) IE. SECRET (S), CONF. (C) RESTRICTED (R), LIMITED (L), UNCLASSIFIED (U)). U (DOCUMENT) U (TITLE) U (ABSTRACT)	6. NO. PAGES 87 7. NO. REFS. 10

8. AUTHOR(S) L.D. MacLAREN H.A. QUICK	9. DOWNGRADING/DELIMITING INSTRUCTIONS Not applicable.

10. CORPORATE AUTHOR AND ADDRESS AERONAUTICAL RESEARCH LABORATORY AIR OPERATIONS DIVISION 506 LORIMER STREET FISHERMENS BEND VIC 3207	11. OFFICE/POSITION RESPONSIBLE FOR: RAAF - DSYSENGA SPONSOR _____ SECURITY _____ . DOWNGRADING _____ CAOD APPROVAL _____

12. SECONDARY DISTRIBUTION (OF THIS DOCUMENT)   Approved for public release.   OVERSEAS ENQUIRIES OUTSIDE STATED LIMITATIONS SHOULD BE REFERRED THROUGH DSTIC, ADMINISTRATIVE SERVICES BRANCH, DEPARTMENT OF DEFENCE, ANZAC PARK WEST OFFICES, ACT 2601

13a. THIS DOCUMENT MAY BE ANNOUNCED IN CATALOGUES AND AWARENESS SERVICES AVAILABLE TO ....   No limitations.

13b. CITATION FOR OTHER PURPOSES (IE. CASUAL ANNOUNCEMENT) MAY BE   [X] UNRESTRICTED OR   [ ] AS FOR 13a.

14. DESCRIPTORS F/A-18 aircraft Stabilators Wind tunnel models Aerodynamic loads Aft fuselages Pressure distribution Fins	15. DISCAT SUBJECT CATEGORIES 0101 010303

16. ABSTRACT

The steady-state aerodynamic pressure distribution over the aft fuselage, fin and stabilator of a 1/9th scale F/A-18 model has been measured for varying conditions at low speeds. Pressure distributions are presented in the form of a parametric study and the integration of the pressures to obtain total loads is included to indicate the overall effects of angle of attack, sideslip, stabilator deflection and the LEX fence. The results from these wind tunnel tests have illustrated the degree to which vortical flow dominates the conditions over the aft end of the aircraft, due to the presence of the primary LEX vortex and to local separations from sharp edged surfaces.

THIS PAGE IS TO BE USED TO RECORD INFORMATION WHICH IS REQUIRED BY THE ESTABLISHMENT FOR ITS OWN USE BUT WHICH WILL NOT BE ADDED TO THE DISTIS DATA UNLESS SPECIFICALLY REQUESTED.

16. ABSTRACT (CONT).

17. IMPRINT

AERONAUTICAL RESEARCH LABORATORY, MELBOURNE

18. DOCUMENT SERIES AND NUMBER	19. WA NUMBER	20. TYPE OF REPORT AND PERIOD COVERED
Research Report 9	52 515D	

21. COMPUTER PROGRAMS USED

22. ESTABLISHMENT FILE REF.(S)

23. ADDITIONAL INFORMATION (AS REQUIRED)

END